UMTA-NJ-06-0014-01

U.S. Department
of Transportation

**Urban Mass
Transportation
Administration**

Wheel/Rail Force Prediction and Measurement for Three Transit Trucks Operating at PATCO

George Mekosh, Jr.

**The Budd Company
Technical Center
Fort Washington,PA 19034**

**November 1985
Final Report**

This document is available to the public through the National Technical Information Service, Springfield, Virginia 22161.

Technical Report Documentation Page

1. Report No.	2. Government Accession No.	3. Recipient's Catalog No.
UMTA-NJ-06-0014-86-1		

4. Title and Subtitle

Wheel/Rail Force Prediction and Measurement for Three Transit Trucks Operating at PATCO

5. Report Date
November 1985

6. Performing Organization Code

8. Performing Organization Report No.

7. Author(s)
George Mekosh, Jr.

9. Performing Organization Name and Address
The Budd Company
Technical Center
300 Commerce Drive
Fort Washington, PA 19034

10. Work Unit No. (TRAIS)
NJ-06-0014

11. Contract or Grant No.
NJ-06-0014

13. Type of Report and Period Covered
Final Report
Jan. 1984 - Nov. 1985

12. Sponsoring Agency Name and Address
U.S. Department of Transportation
Urban Mass Transportation Administration
400 Seventh Street, S.W.
Washington, DC 20590

14. Sponsoring Agency Code
URT-11

15. Supplementary Notes
Grant Managers
Paul R. Spencer - (202) 425-0090
Charles O. Phillips - (617) 494-2568

16. Abstract Wheel/rail curving force predictions and measurements were made for three different transit truck configurations operating at PATCO. The configurations included the Budd P-III trucks operating at PATCO since delivery in 1968 and referenced as the baseline, two experimental steerable axle trucks operating in revenue service since January 1982 and two standard P-III trucks equipped with prototype soft suspension bushings operating in revenue service since April 1982.

The computer predictions were made prior to the vehicle testing, using the Budd non-linear rail vehicle dynamic simulation model and were in close agreement with the average wheel/rail forces measured using an instrumented wheelset. Data from an 800 foot radius curve showed that the average lateral force for the lead outer wheel is about 5300 lbs. for the baseline truck, 2600 lbs. for the soft bushing truck, and 1500 lbs. for the steerable truck. These are significant reductions which should result in reduced wheel flange wear, reduced rail gauge face wear, reduced energy requirements, and reduced noise levels in curves.

The measured wheel/rail force data showed that both the lateral and vertical forces oscillate between peaks and valleys and at various frequencies. The peak lateral force values can be two and, occasionally three times the average value for a particular curve. The vertical force excursions are considerably lower and well within a ±25% range.

Using a modified friction versus creepage characteristic at the wheel/rail contact patch, the Budd computer model was able to simulate to some degree the lateral force oscillations. However, these results are preliminary and require further investigation.

17. Key Words	18. Distribution Statement
Curve negotiation; Rapid Transit; Steerable Trucks; Soft Suspension Bushings; PATCO; Wheel/Rail Force Measurement; Wheel/Rail Wear	Available to the Public through the National Technical Information Service, Springfield, Virginia 22161.

19. Security Classif. (of this report)	20. Security Classif. (of this page)	21. No. of Pages	22. Price
Unclassified	Unclassified	128	

PREFACE

The Office of Systems Engineering of the Urban Mass Transportation Administration (UMTA), through the Transportation Systems Center (TSC) is conducting analytical and experimental studies to relate transit truck design characteristics to wheel/rail forces and wheel/rail wear ratio. The results of these studies are expected to provide rail transit systems with options for reducing the wheel/rail wear rates while maintaining or improving equipment performance.

In the past decade, significant efforts have been made toward developing steerable truck configurations employing direct connections between axles and supplemental linkages connecting the axles to the carbody. In addition, improved primary suspension elements have been developed as direct replacements for certain suspension systems currently used on existing transit equipment. These new configurations improve curving performance while maintaining high speed stability margins and ride quality levels.

Under an earlier contract with the U.S. Department of Transportation, Transportation Systems Center (Contract No. DOT-TSC-1740), The Budd Company Technical Center conducted design feasibility studies for the retrofit of an existing truck design to a linkaged steered configuration. The Budd Company Technical Center subsequently built two prototype steerable axle trucks for field testing on the PATCO system, which is operated by the Port Authority Transit Corporation.

The Budd Company Technical Center field tested the prototype steerable axle trucks in cooperation with PATCO under an UMTA funded, Section 6 Research, Development and Demonstration Grant (Contract No. UMTA-NJ-06-0014). Upon the successful completion of this test program, the prototype steerable axle trucks were placed into revenue service.

The Budd Company Technical Center also developed a prototype soft primary suspension bushing as an intermediate solution to the curving performance problems of conventional transit truck designs. A carset of soft bushings were also placed into revenue service.

With three distinctively different truck design configurations operating in daily revenue service, PATCO represented a unique opportunity to quantify the curving performance differences between the various designs. Therefore, an extension to the initial program was proposed in March 1983. This report describes the work that was conducted by The Budd Company Technical Center under amended Contract No. UMTA-NJ-06-0014-01 during the period January 1984 thru November 1985.

EXECUTIVE SUMMARY

The principal objectives of this program were to first predict and then measure wheel/rail curving forces for three different transit truck design configurations in operation at PATCO. The design configurations included the standard Budd-Pioneer III trucks operating at PATCO since delivery in 1968 and referenced at the baseline for comparison, two experimental steerable axle trucks operating in revenue service since January 1982, and two standard P-III trucks equipped with prototype soft suspension bushings operating in revenue service since April 1982.

Secondary objectives included measuring groundborne vibration levels at selected sites along the right-of-way, measuring axle and truck frame accelerations, and evaluating ride quality for the three different truck configurations.

The Budd computer predictions of wheel/rail curving forces for the three configurations were presented to PATCO and TSC personnel prior to testing. These predictions were based on a PATCO 800 foot radius curve balanced for a 40 mph scheduled speed. The steady state curving forces predicted by the Budd model were in close agreement with the average curving forces measured by the instrumented wheelset. The measured data taken on the 800 foot radius curve indicates that the average lateral force level between the lead outer wheel and rail is about 5,300 lbs. for the baseline truck, 2,600 lbs. for the soft bushing truck and 1,500 lbs. for the steerable truck. These values represent force reductions on the order of 51% for the soft bushing truck and 72% for the steerable truck. These are significant reductions that should result in reduced wheel flange wear, reduced rail gauge face wear in curves, reduced energy requirements during curving and reduced noise levels during curving.

The measured wheel/rail force data also indicates that both the lateral and vertical forces oscillate between peaks and valleys and at various frequencies. The peak values of the lateral force oscillations, for example, can be as high as two and occasionally, three times the average value for a particular curve. The vertical force excursions are considerably lower, typically well within a ±25% range.

The computer model was unable to simulate the force oscillations using standard wheel/rail friction versus creepage characteristics. However, the Budd non-linear model was able to simulate lateral force oscillations by inputting a modified friction versus creepage characteristic. The modified characteristic is represented by a friction versus creepage curve which rises according to classical Kalker theory, reaches a maximum value, and then drops off at various rates. Recent laboratory research has indicated that this characteristic is

not only possible, but quite probable. Several preliminary sensitivity studies were made. These preliminary results indicated that the lateral force oscillations are affected by variations in the following parameters which include the longitudinal and lateral primary truck suspension spring rates, truck wheelbase, the lateral track support system spring rate, the longtudinal and lateral micro slip characteristic of the wheel/rail material combination and wheel/rail profile geometry.

The measured wheel/rail force data taken on curves equipped with restraining rail shows that the differences between individual curve conditions are greater than the differences between the truck configurations. However, in general, the soft bushing equipped truck showed significant reductions in restraining rail-wheel force when compared to the baseline truck; while the steerable truck showed only slight reductions. The major reason for this outcome is that the lateral primary suspension spring rate of the soft bushing truck is considerably lower than the standard truck and the steerable truck.

Both analytical studies and test data suggest that an entire fleet of steerable axle trucks would eliminate the need for restraining rail and rail lubrication.

The wheelset and side frame acceleration data indicates that the soft suspension bushings reduce the truck frame vibration environment. The improved environment can prolong the service life of frame mounted equipment.

Carbody ride quality was essentially the same for all three truck configurations as indicated by accelerations measured inside the carbody. This result was expected since ride quality is primarily a function of the secondary suspension system performance in trucks with this range of primary spring rates.

The groundborne vibration data collected at various sites along the PATCO right-of-way indicates that the different truck configurations do influence wayside vibration levels, and in general, the soft bushing truck produced lower vibration levels.

ACKNOWLEDGEMENTS

The author would like to express appreciation and sincere gratitude to the following individuals without whose support a fruitful completion of this test program would not have been possible.

R. G. Schwab, General Manager of PATCO, for his willingness to participate in this joint PATCO/UMTA/Budd effort.

J. William Vigrass, Assistant General Manager at PATCO, who served as Contract Administrator, for his cooperation, direction, and general support.

R. C. Berk, Superintendent of Equipment at PATCO, and PATCO shop foreman, Howard W. Ross and Vince Bucci, for their cooperation, support, and patience during the preparation of all test configurations.

Earl Hughes, Superintendent of Way and Power at PATCO, for the information provided concerning track layout and operation.

Patrick L. Boyd, of ENSCO, who was responsible for the instrumented wheelset, for his general support during the testing and guidance in interpreting the data.

Charles O. Phillips, of TSC, who served as Technical Monitor for the Design Feasibility Phase and both phases of field testing, for providing support and guidance throughout all programs.

Dr. Herbert Weinstock of TSC, who provided a cross-check for the computer predictions.

And last, but certainly not least, my very special thanks to Budd Tech Center test crew members, Herb Kiser, Test Engineer, Joe Landue, Instrumentation Specialist, and Chris Franz, Truck Designer, for their effort during the entire program.

TABLE OF CONTENTS

LIST OF FIGURES

LIST OF TABLES

1.0 Introduction and Background

Most of us have ridden rapid transit cars around sharp curves and are painfully aware of the ear-splitting screech and squeal caused by the steel wheel flanges rubbing against the sides of dry rails. While this is annoying to passengers and to those who live and work in close proximity to the curved track, it is an extremely costly problem for transit system operators in terms of high wheel flange wear, high rail wear, excess energy consumption and noise pollution.

The squeal noise and most of the wheel flange wear and rail gauge wear experienced with conventional parallel axle trucks are due to the non-radial running position of the leading axle in sharp curves. The non-radial running position results in a tracking error that is defined as the angle-of-attack between the wheel and rail. It is the combination of the wheel/rail angle-of-attack and the slipping action between the wheel and rail or creep that cause the noise, wear, and an unnecessarily high lateral force between the wheel flange and the rail.

In response to this important problem, The Budd Company Technical Center began development of a steerable axle truck in 1978. The design starting point was Budd's highly successful Pioneer-III truck used on passenger railcars throughout the world. The specific design configuration selected for study was the P-III truck used on the Port Authority Transit Corporation (PATCO) high speed line between downtown Philadelphia and Lindenwold, New Jersey.

Approximately one-half of the preliminary design and analysis performed by Budd, was funded by the Urban Mass Transportation Administration's (UMTA), Office of Technology Development and Deployment. This effort resulted in a report (report no. DOT-TSC-UM104-PM-80-49), dated December 1980 and titled **"Design Feasibility Study for Modifying an Existing Heavy Rapid Rail Truck to a Steerable Configuration"**. This report concluded that it was technically feasible to modify a conventional truck to a steerable configuration with significantly improved curving performance while maintaining its high critical speed characteristics and ride quality levels.

The Budd Company then built three experimental steerable axle truck frame assemblies; two for field testing and evaluation at PATCO and one for fatigue testing at the Budd laboratory. The two field test trucks were fitted with existing truck bolsters, propulsion and braking equipment provided by PATCO and installed under Car #114 in March 1981. Preliminary field testing was conducted on curved track outside the PATCO shops. In May 1981, the fatigue test truck successfully completed its two million cycle fatigue test, thereby establishing its structural design integrity. PATCO then released Car #114 for mainline testing during off peak hours.

The initial mainline testing of the two experimental

steerable axle trucks, now referred to as Phase I, was largely funded by a Section 6 Research, Development and Demonstration Grant (Contract No. NJ-06-0014) from the Urban Mass Transportation Administration to PATCO with Budd acting as prime contractor. Phase I testing lasted nearly six months and was essentially completed by December 1981. These tests clearly demonstrated that the steerable axle trucks significantly improved curving performance while maintaining the necessary high speed stability margins and ride quality levels. The steerable axle trucks were able to negotiate PATCO's sharpest curves (28° or 207 ft. radius) essentially noise free.

Based on the positive results of the fatigue test and road tests, the steerable axle trucks were placed in high mileage revenue service to establish long term wheel wear characteristics and maintenance requirements. These trucks have been operating in revenue service under Car #114 since January 1982.

It was also around this time frame that The Budd Company Technical Center developed a soft primary suspension bushing design that offered an intermediate solution to the curving performance problems of conventional parallel axle rapid transit trucks. And by April 1982, Budd designed, built, and placed into revenue service at PATCO one carset of prototype soft suspension bushings. These trucks are still in revenue service and have also demonstrated improved curving performance.

With three distinctively different truck design configurations operating in daily revenue service, PATCO represented a unique opportunity to quantify the curving performance differences between the various designs. This information would be helpful to transit properties considering new vehicles or upgrading existing fleets. Therefore, an extension to the initial test program (Phase I) was proposed in March 1983. The following sections of this report describe the Phase II test program which started in January 1984 with procurement of an instrumented wheelset and finished vehicle testing in November 1984. The data analysis was completed in July 1985.

2.0 Scope and Objectives

The principal objectives of this test program were to predict and measure the wheel/rail curving forces for three distinctively different rapid transit truck design configurations in revenue service at PATCO. The design configurations included the standard Budd P-III trucks referenced as the baseline for comparison, the experimental steerable axle trucks, and the standard P-III trucks equipped with prototype soft suspension bushings.

The wheel/rail force predictions were made using Budd's proprietary non-linear rail vehicle dynamic simulation model. Budd used updated versions of the steerable truck and conventional truck models that were developed for design feasibility studies (1). The input data was updated where more recent component test data was available.

The wheel/rail force measurements were made using an instrumented wheelset that provided real time analog traces of lateral and vertical forces on both wheels. ENSCO was subcontracted to instrument the wheelset, monitor the output during testing, and provide support in data reduction.

Secondary objectives included measuring groundborne vibration levels at selected sites along the PATCO right-of-way, measuring axle and truck frame vibration levels, and evaluating ride quality for all three truck configurations.

Budd provided the necessary instrumentation to monitor certain data on strip chart recorders and record all data on magnetic tape for post processing and permanent record. In addition, Budd provided a video system that was used to monitor the wheel/rail interface of both wheels on the instrumented wheelset during testing. The video proved invaluable in the data reduction and in better understanding curving mechanics.

TSC provided personnel and equipment for measuring geometry and wear characteristics of the 800 ft. radius curve at PATCO. The wheel/rail force predictions were based on this curve so that a comparison could be made with force levels measured at other properties of similar curvatures.

3.0 PATCO Vehicle Description

The rail cars currently operated by PATCO consist of 75 cars built by The Budd Company in 1968 and 46 cars built by Vickers Canada in 1980. The Budd and Vickers cars are virtually identical. They are both of stainless steel construction. Figure 3-1 shows a picture of a PATCO car. The married pair cars have seating for 80 passengers; while the single cars have seating capacity for 72 passengers. Table 3-1 gives various dimensions and weights of the PATCO vehicles. The Budd Company built the trucks for both the Budd cars and the Vickers cars. These trucks are referred to as the standard Budd Pioneer III (P-III) truck.

PATCO has been operating a carset of experimental steerable axle trucks under Car #114 since January 1982 and also a carset of standard P-III trucks equipped with soft primary suspension bushings since April 1982. The soft bushing equipped trucks were initially installed under Car #284, which is married to Car #283. Car #283 was equipped with standard P-III trucks and served as a baseline for comparative analysis.

The three truck configurations were all tested separately under the same test vehicle (Car #114), which was operated as a single car. The three truck configurations are described in the following sections.

3.1 Standard Budd P-III Truck

The standard Budd P-III truck in use at PATCO is shown in the next two figures. Figure 3-2 is a plan view and side elevation view of the truck assembly. Figure 3-3 is an exploded isometric sketch showing the major truck parts. Table 3-2 gives the truck weight breakdown and Table 3-3 gives the primary and secondary suspension parameters. Additional information, including center-of-gravity locations and mass-moments-of-inertia are presented in Section 5.2.

The basic P-III truck frame is a fabricated three piece inboard bearing design consisting of two side frames and a bolster. The side frames are independent of one another in the pitch direction and provide very good equalizaton characteristics.

The bolster has a center yaw pivot which fits between the two side frames and is free to rotate as well as move up and down a controlled distance. The center yaw pivot has a small diametrical clearance which limits the relative longitudinal and lateral movement between the bolster yaw pivot and the side frames. The connection of the two side frames to the yaw pivot is called the "spider". The "spider" to yaw pivot connection is very stiff in the longitudinal direction, preventing lozenging of the side frames in plan view, and it is also quite stiff in the lateral direction. This connection transmits the longitudinal loads (acceleration and braking) and the lateral

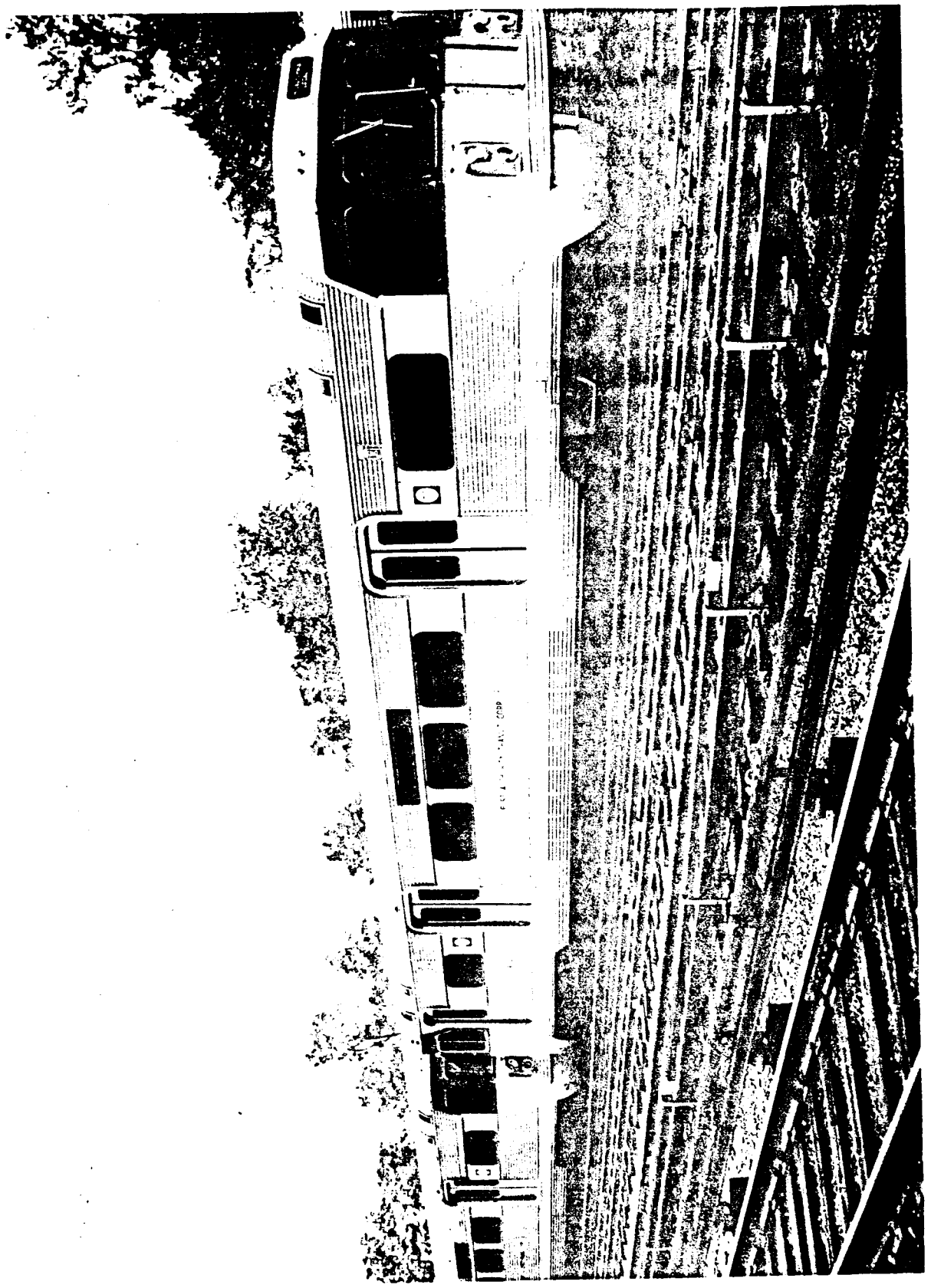

Figure 3-1: PATCO VEHICLE

TABLE 3-1: PATCO VEHICLE PARAMETERS

Maximum Scheduled Speed	75 MPH
Length of car over anticlimbers at the centerline of car	67' 6"
Length of car over coupler faces	67' 10"
Distance center to center of trucks	47' 6"
Maximum width of carbody over threshold	10' 0"
Height rail to top of floor, new wheels	3' 10 1/2"
Maximum height rail to top of roof, new wheels, empty car	12' 4"
Height of high level station platform above top rail	3' 10"
Centerline of track to edge of high level platform	5' 3"
Coupler height above rail	28 1/2"
Maximum number of cars in train	8
Maximum superelevation	10"
Minimum horizontal curve radius - with cars coupled	
Minimum vertical curve radius	
Length of minimum radius vertical curve	
Wheel diameter	
Track gauge	
Wheel gauge	
Truck wheelbase	
Vehicle weights	
Carbody	52,680#
Standard truck (without handbrake)	12,760#
Ready to run	78,200#
Full seated (80 passengers @ 155#)	90,600#
Normal maximum (125 @ 155#)	97,575#
Crush load (195 @ 155#)	108,425#

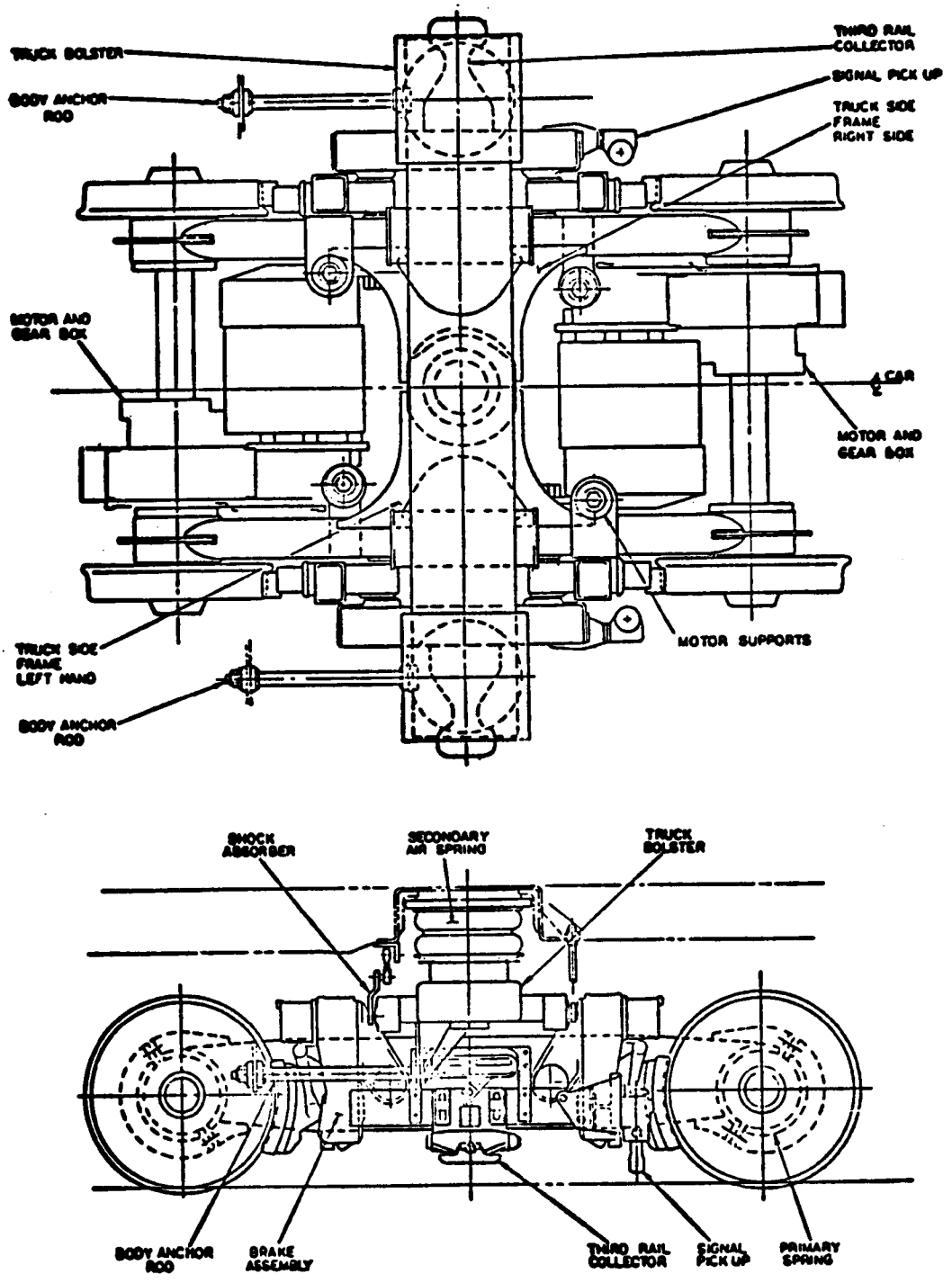

Figure 3-2: STANDARD P-III TRUCK

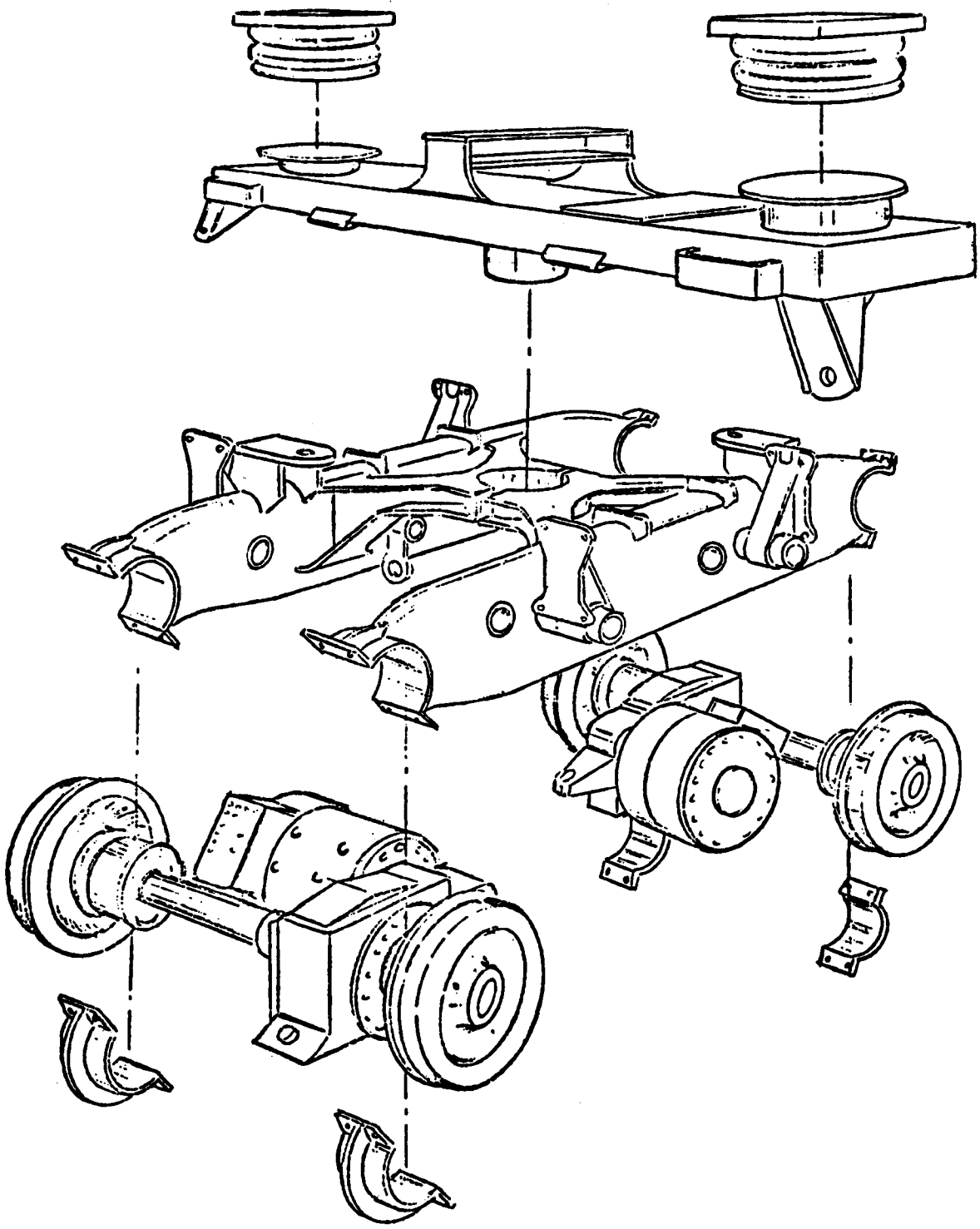

Figure 3-3: STANDARD P-III TRUCK

loads between the side frames and bolster. The bolster rests on the side bearings which are located on the side frame centerlines. All vertical loads are transferred between the bolster and side frames via the side bearings, sometimes referred to as the "side bearers". In curves, truck rotation occurs between the bolster and the side frames at the center yaw pivot and at the side bearings. The rotational resistance or yaw resistance of the P-III truck design is primarily a function of the spacing of the side bearings and their frictional force characteristics. The yaw pivot has minimal contribution to the net yaw resistance.

The side bearings, as originally supplied by The Budd Company, consisted of teflon fabric held in place by a phenolic resin base material system. The teflon fabric provided a controlled friction surface which resulted in a relatively constant truck yaw resistance for empty and loaded car conditions. PATCO has been replacing the original side bearings, on an as-required-basis, with a ultra high molecular weight polyethelene side bearing. The performance of the replacement side bearing is similar to the original material and this was verified during this test program by instrumenting the carbody anchor rods. The carbody anchor rods, also called "radius rods", prevent the bolster from moving longitudinally and from rotating with respect to the carbody.

The secondary suspension is contained within the bolster assembly. This system is primarily responsible for the ride quality of the carbody as it determines the vertical, lateral, and roll suspension parameters of the carbody. Because of the independence and light weight of the side frames, the natural frequencies of the side frames on the primary suspension can be kept comfortably above those of the secondary suspension. This means that the secondary suspension parameters do not have to be compromised to accommodate heavy parts vibrating at intermediate frequencies.

The secondary suspension consists of two air springs, located at the ends of the bolster. The bolster acts as an air reservoir, connected through orifices to the air springs. Orifice resistance to the transfer of air between the air springs and the reservoir provides vertical damping. In addition to orifice damping and reservoirs, vertical hydraulic shock absorbers are used. The carbody is permitted to move laterally by the distortion of the air springs. Lateral hydraulic shock absorbers are used to dampen this motion. The maximum lateral movement is limited by rubber bump stops. The secondary suspension parameters are given in Table 3-3.

The primary suspension is provided by rubber rings located between the axle bearing assemblies and the side frames. The rubber elements are relatively stiff in all three directions. The stiffness values are given in Table 3-3. Holes molded in the rubber ring top and bottom account for the fact that the vertical stiffness rate is less than the longitudinal rate.

TABLE 3-2: PATCO P-III TRUCK WEIGHT BREAKDOWN

DESCRIPTION	QTY./TRUCK	WEIGHT (LBS.)
WHEELSET	2	1750
GEAR UNIT	2	1020
MOTOR	2	1320
SIDE FRAME ASSEMBLY	2	1460
BOLSTER ASSEMBLY	1	1660
	TOTAL TRUCK WEIGHT	**12760**

TABLE 3-3: PATCO P-III TRUCK SUSPENSION PARAMETERS

	STIFFNESS X 1000 (LBS./IN./TRUCK)			SPRING LOCATION (INCHES)		
	VERTICAL	LATERAL	LONG.	VERTICAL	LATERAL	LONG.
PRIMARY	640	2000	1180	14	-23	-45
SECONDARY	5	2	50	40.4	-44.5	0

The wheelset uses inboard bearings and solid 28 inch diameter wheels with the standard AAR 1 in 20 profile. The axles on the PATCO trucks are hollow.

The PATCO P-III truck has two separate traction motor/gear unit assemblies with the motor parallel to the axles. Each gear unit is supported from the axle at one end and by a vertical resilient hanger to the side frame at the other end. Each traction motor is resiliently mounted to its gear unit at one end and by a vertical and longitudinal resilient hanger system at the other end. Dynamic movement between the traction motor and gear unit is small.

The PATCO trucks are equipped with dynamic brakes and tread brakes. The tread brake actuators are mounted from the side frames for precise alignment with the wheels. The third rail power shoe collectors are also mounted from the side frames.

3.2 Soft Bushing P-III Truck

The P-III trucks operating at PATCO with the soft primary suspension bushings are identical to the standard PATCO trucks in every way, except for the soft bushings. The soft bushings were designed by The Budd Company to be a direct replacement for the standard rubber shock ring, as shown in Figure 3-4. Figure 3-5 shows a picture of the upper and lower bushing halves. This proprietary design is a bonded construction sandwiching urethane between inner and outer steel sleeves. The upper and lower bushing halves are sculptured to provide the desired stiffness rates in all three directions.

The stiffness rates of the soft bushings are given in Table 3-4. The longitudinal rate was made sufficiently soft to improve the axle steering characteristics while maintaining high speed stability margins at 75 mph operation with severely worn wheels. The vertical rate was lowered to reduce the truck frame vibration environment and also reduce the groundborne vibrations transmitted to surrounding structures along the railroad right-of-way. The truck frame vibration levels that were measured are discussed in Section 6.4. The groundborne vibration levels that were measured are discussed in Section 7.0. The soft bushing lateral stiffness rate is much lower than the standard unbonded rubber ring construction.

PATCO has ordered from The Budd Company ten carsets of soft bushings under Contract No. 4292-1, which is a Section 3(a)(1)(C) Grant partially funded by UMTA Project No. NJ-03-3001. Delivery was made during October 1985.

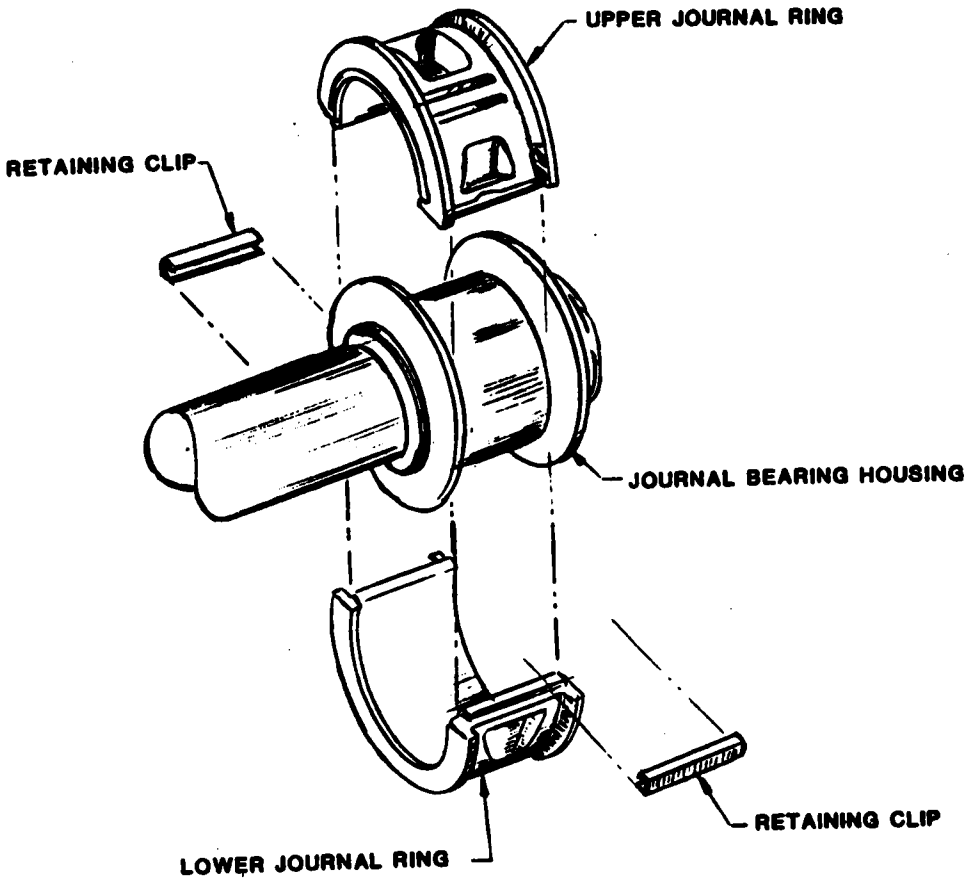

Figure 3-4 SOFT SUSPENSION BUSHING INSTALLATION

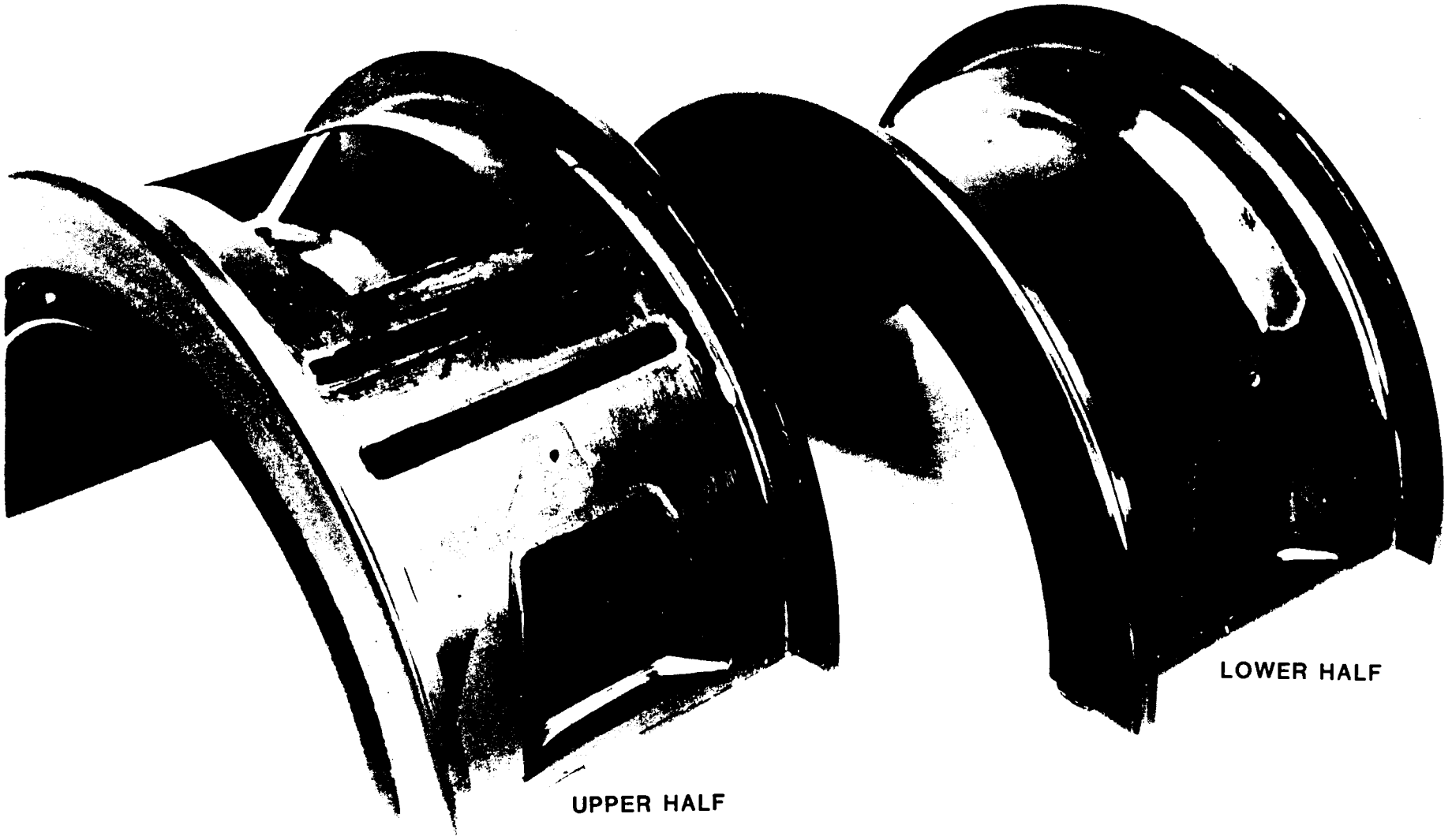

Figure 3-5: SOFT SUSPENSION BUSHING

TABLE 3-4: SOFT BUSHING TRUCK PRIMARY SUSPENSION PARAMETERS

	STIFFNESS X 1000 LBS./IN./TRUCK
VERTICAL	192
LATERAL	400
LONGITUDINAL	144

3.3 Steerable P-III Truck

The prototype steerable axle truck design configuration that is currently operating in revenue service at PATCO is shown in the following three figures. Figure 3-6 is a plan view and side elevation view of the steerable truck assembly, Figure 3-7 is a drawing of the steering arm controls, and Figure 3-8 is an exploded isometric sketch showing the major truck parts. Table 3-5 gives the truck weight breakdown and Table 3-6 gives the primary and secondary suspension parameters. Additional information, including center-of-gravity locations and mass-moments-of-inertia are presented in Section 5.3.

The steerable truck is quite similar to the standard P-III truck with modifications to the side frames and the addition of steering arms. The steerable truck was designed to accommodate the existing truck bolster, wheel axle assemblies, propulsion units, and tread brake units.

The steering arms are C shaped structures that provide a structural mounting base for the motors, axles and gear units. The steering arms are connected together at the center of the truck by a Metalastic bushing. This connection insures equal but opposite yaw motion of the two steering arms. This connection also transfers longitudinal and vertical loads between the steering arms and insures equal but opposite pitching motions as well. The steering arms are attached to the wheel axle assemblies by a clamping arrangement that engages the standard unbonded rubber shock ring around the axle journal bearing.

The propulsion unit and wheelset assemblies were not modified in any way. The three support links that connect the motor and gear unit to the truck frames, on the standard P-III truck, are connected instead to the steering arms using the same

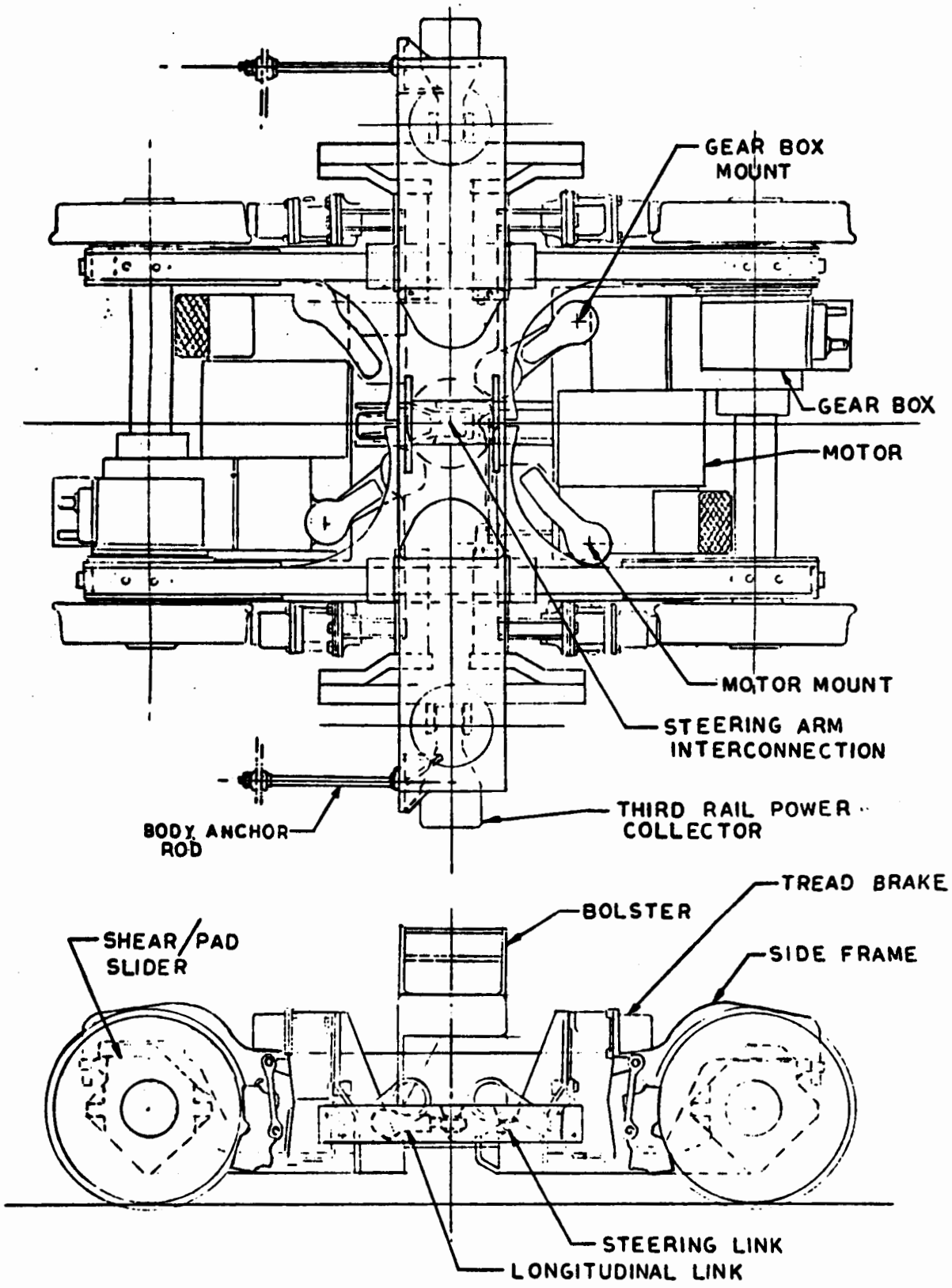

Figure 3-6: STEERABLE TRUCK

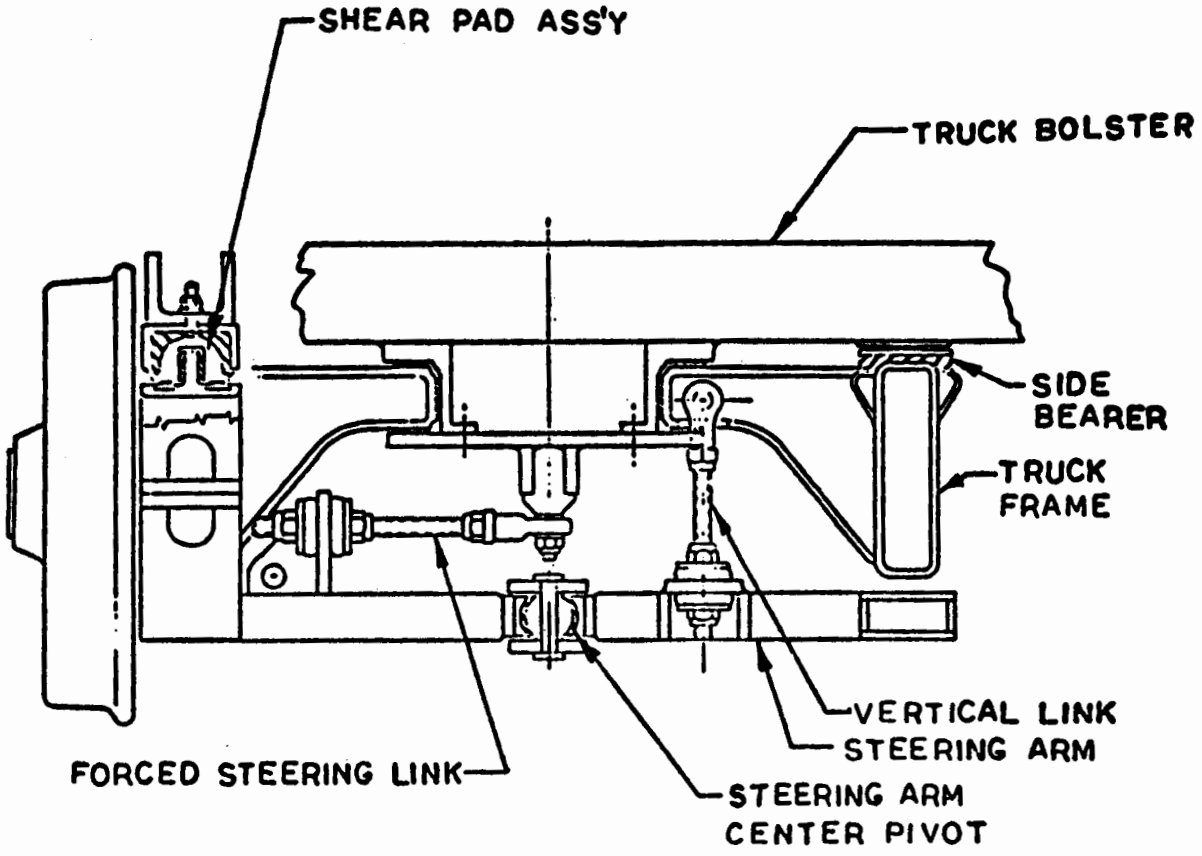

Figure 3-7: STEERING ARM CONTROLS

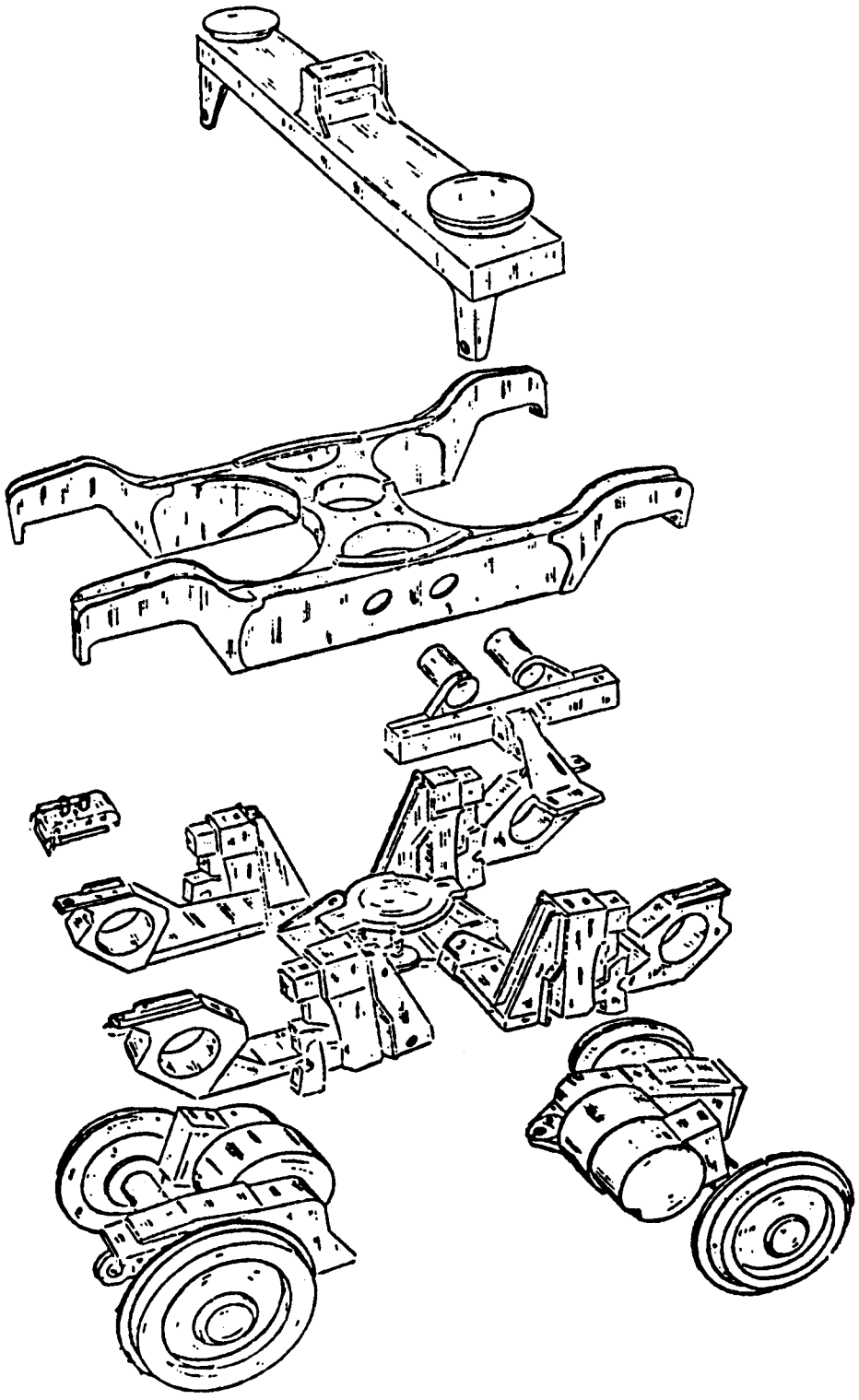

Figure 3-8: STEERABLE TRUCK

TABLE 3-5: STEERABLE TRUCK WEIGHT BREAKDOWN

DESCRIPTION	QTY./TRUCK	WEIGHT (LBS.)
WHEELSET	2	1,750
GEAR UNIT	2	1,020
MOTOR	2	1,320
STEERING ARM ASSEMBLY	2	1,110
SIDE FRAME ASSEMBLY	2	1,720
BOLSTER ASSEMBLY	1	1,700
	TOTAL TRUCK WEIGHT	**15,540**

TABLE 3-6: PATCO STEERABLE TRUCK SUSPENSION PARAMETERS

	STIFFNESS X 1000 (LBS./IN./TRUCK)			SPRING LOCATION (INCHES)		
	VERTICAL	LATERAL	LONG.	VERTICAL	LATERAL	LONG.
PRIMARY	640	2000	1180	14	-23.0	-45.0
SHEAR PAD	1000	400	*120	22	-23.0	-45.0
SECONDARY	5	2	50	40.4	-44.5	0

*The shear pad longitudinal stiffness is in series with a friction force slider that breaks away between 1000 to 1500 lbs.

resilient links and hardware. This was done so that the propulsion units would remain interchangeable with all PATCO trucks. This was a desirable approach when retrofitting two trucks. However, if a large number of trucks were to be retrofitted, a simpler propulsion unit/steering arm interface design could be provided by supporting the propulsion assembly from below.

The steering arms interface with the side frames at the four corners of the truck through shear pad/slider assemblies. The shear pad portion of the assembly provides spring stiffness in all directions. The longitudinal stiffness satisfies the high speed lateral stability and steering requirements of the truck. The primary suspension parameters, including the shear pad, are given in Table 3-6.

The slider portion of the shear pad/slider assembly was designed to limit the longitudinal forces associated with large yaw motions of the axles in sharp curves. Figure 3-9 shows the axle yaw displacements required for radial positioning in curves. For the best possible steering performance, the slider coefficient of friction should be low in comparison with the wheel/rail creep coefficient. On the other hand, the slider friction must be high enough to prevent sliding for small yaw displacements so that the longitudinal spring rate of the shear pad can make its contribution to high speed stability. The slider friction material was designed to provide the necessary breakaway force level with sufficient coulomb damping.

Under normal conditions, the axles operate in a self-steering mode. The steering action is the result of wheel/rail creep forces acting in combination with the inter-axle parameters designed into the truck. The self-steering action is backed by a positive steering arrangement that will prevent large values for the wheel/rail angle of attack under any operating condition no matter how adverse it might be.

The positive steering arrangement consists of a lateral link between the bolster pivot and the steering arms for the outside axle. The positive steering action is generated by the lateral motion of the link attachment point on the bolster relative to the side frame when the truck swivels relative to the bolster. The amount of this lateral motion depends on the longitudinal eccentricity of the steering link from the center of truck and the degree of truck swivel. The longitudinal eccentricity is chosen to give radial axle positioning in circular curves. The amount of eccentricity required to do this is a function of truck wheel base and truck center spacing.

The lateral link is attached to the bolster with a ball joint. At this location, angular motion can be as high as several degrees. The other end of the link, where angular motion is much less, is attached to the steering arm with a threaded connection and rubber bushings so that the effective length can be adjusted for a parallel axle positioning on

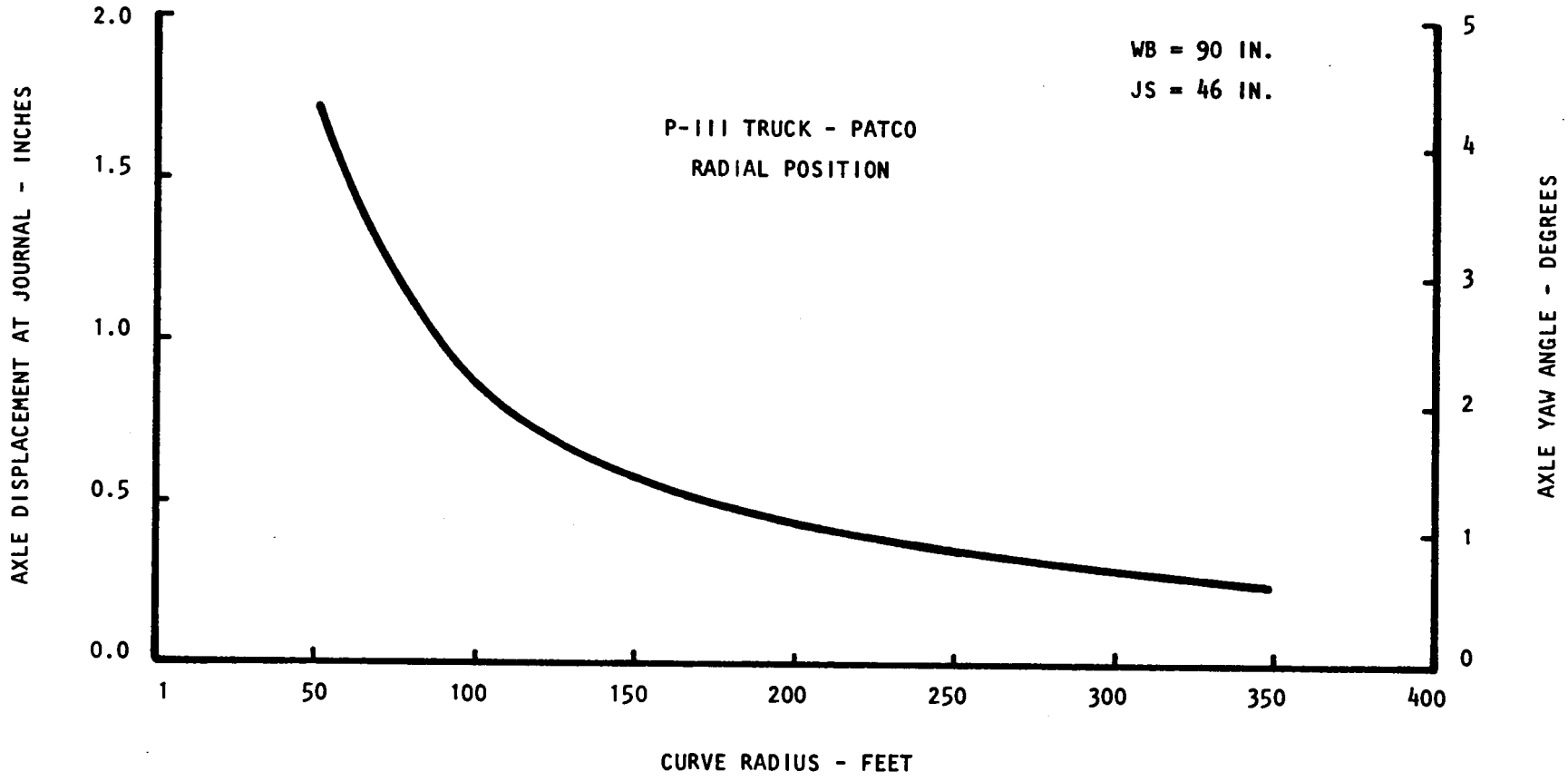

Figure 3-9: RADIAL POSITION REQUIREMENTS

straight track. An adjustable free zone for the positive steering restraint is also provided.

There is also a longitudinal link between the bolster pivot and the inner steering arm to transfer normal longitudinal loads associated with propulsion and braking. The crash longitudinal loads would be carried through safety stops provided between the steering arm and the side frames, and then to the bolster as is the case with the standard truck design.

Most of the steering arm pitching moments associated with normal propulsion and braking are balanced out between the two steering arms by an exchange of vertical forces at the steering arm interconnection. Any unbalance of these pitching moments and the weight of the steering arms are supported by vertical hangers to the side frames.

The side frame end of the vertical hanger is a ball joint and the steering arm end is a threaded bolt attachment with rubber bushings. The vertical hangers will give the steering arms a certain amount of restoring moment due to a pendulum effect.

The steering arms also incorporate mounting brackets for the existing tread brake units. Because the brake units are mounted on the steering arms, they are always properly positioned with respect to the axle and will not interfere with normal steering operation.

The side frames are modified at the four corners to interface with the shear pad/slider assembly as described previously. The side frames were fabricated from rectangular tube measuring 14 inches x 6 inches with a wall thickness of 1/2 inch. Stiffening ribs were added to the truck frame corners. Each shear pad/slider assembly is attached to the side frame by three threaded fasteners and two guide pins. The side frame to bolster interface are the same as on the standard P-III truck. The third rail power shoe collector is mounted from the side frame, quite similar to the standard design configuration.

The bolster remains unchanged with respect to the secondary suspension and its interfaces with the side frames. (See description of standard P-III truck for more information about secondary suspension.) However, there is a modification to the bolster center pivot bottom plate and safety strap arrangement. The bolster pivot bottom plate provides a vertical up stop between the bolster and side frame. The bottom plate is also attached to the carbody through safety straps. The safety straps provide a safety connection between the trucks and the carbody in the event of a derailment. All operational loads are transferred from the axles through the steering arms and the longitudinal drag link into the bolster, using the bottom plate connection. The loads are then transferred into the carbody using the longitudinal anchor rods between the bolster and the carbody. The positive steering input position is generated by

truck swivel and is transferred from the bolster bottom plate to the steering arms using the lateral steering link.

The prototype steerable truck design does weigh more than the standard P-III truck. Table 3-5 gives the actual weights of the major steerable truck parts. The weight increase is primarily due to the steering arms themselves. The side frame modifications also increased the total truck weight somewhat. As was mentioned earlier, the steerable truck was designed to accommodate the existing PATCO bolster, wheel axle assemblies, propulsion units and tread brake units. It is quite possible that a new design that is not required to mate with existing equipment could produce significant weight savings. The primary area for potential weight savings is a simpler propulsion unit/steering arm interface. It is also possible that additional weight could be saved by designing a different steering arm support configuration.

4.0 PATCO System Description

The PATCO System, known locally as the Lindenwold High Speed Line, runs between downtown Philadelphia and Lindenwold, New Jersey. The line is 14.5 miles long and is shown schematically in Figure 4-1. A condensed alignment profile chart is given in Appendix A.

In Philadelphia, the line runs east and west under Locust Street utilizing a tunnel constructed many years before the line went into service. There is a very sharp 28° curve where the route turns north under 8th Street to the 8th and Market Streets station. From here to City Hall, Camden, the route has been in use for many years--the service having been known as the "Bridge Line". There are additional sharp curves and a grade as the line comes up to cross the Delaware River on the Benjamin Franklin Bridge. In Camden, the route is again underground with several sharp curves.

Just beyond Camden City Hall, there is new construction connecting the old "Bridge" route with an existing railroad right-of-way. From here to Lindenwold, the curves are gradual and the line is generally elevated. Even though the stations are relatively close together, the cars often reach 75 mph in this area.

This line includes a wide variety of operating conditions from sharp curves with restraining rail in the tunnels to a long section along a railroad alignment with gentle curves. The majority of the curves are in the 2° range; however, there are several curves in the tunnels which are in the 20° to 28° range. Note that restraining rail is used on all curves sharper than 8° in curvature.

Operating with 121 vehicles, the PATCO system accumulated 4,055,895 car-miles and serviced 10,211,589 passengers during 1984. The total traffic has been estimated at 6 million gross tons per year past any given point along the system.

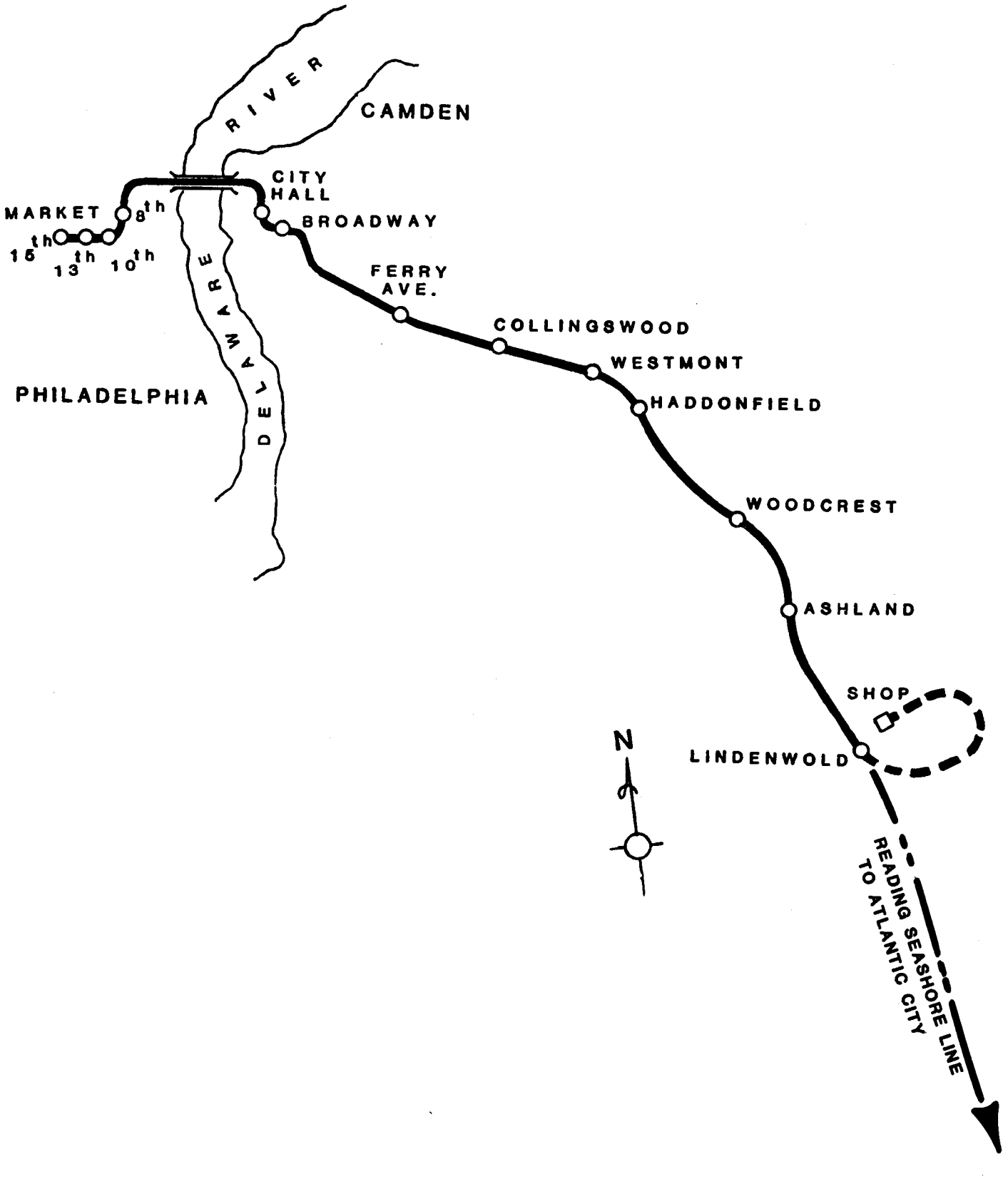

Figure 4-1: PATCO HI-SPEED LINE

5.0 Computer Predictions of Wheel/Rail Forces

Since the credibility of theoretical work can be greatly enhanced by corroboration with data resulting from controlled experiments, part of this program was dedicated to predicting the wheel/rail force levels before the actual measurements were made. Predictions were made for all three truck configurations., i.e., standard P-III, soft bushing, and steerable. The computer model simulated operation through the 7°10' (800 ft. radius) curve on the westbound track approaching the Camden Subway. (See Track Chart in Appendix A for specific location.) This curve, with its eight inches of superelevation is balanced for 40 mph operation, which is the scheduled track speed. This curve was specifically selected for computer modeling because it is the only PATCO curve in the moderate curvature range and it is also one of the few curves without restraining rail. The modeled curve parameters are shown in Figure 5-1.

The computer program that was used for modeling is the Budd non-linear rail vehicle dynamic simulation model and it is briefly described below in Section 5.1. Program input data for the standard P-III truck and soft bushing truck models is described in Section 5.2. The input data for the steerable truck model is described in Section 5.3. The special case of the wheel/rail interface, including tread profile and creep characteristics, is described in Section 5.4 with the predictions reported in Section 5.5.

5.1 Non Linear Rail Vehicle Dynamic Simulation Model

The non-linear model is a digital computer program that is set up to simulate the dynamics of rail vehicles. The dynamic input is generated by vehicle speed and various track features, such as tangent track, entry and exit spirals, constant radius curvature, superelevation, track twist, and track defects, which may be either lateral and/or vertical. The program computes the dynamic response of the major truck components being modeled and the forces and torques acting at various points where these parts are interconnected. Each part that is modeled has all six degrees-of-freedom. The 10 part models used have 60 degrees-of-freedom.

The equations of motion are solved by numerical integration so that the many non-linearities of the wheel/rail interface and the usual non-linearities of the interconnections between truck parts can be realistically represented. The program has built-in error criteria which permit large integration time steps during periods of steady state operation and very small time steps during transient conditions.

MODELED CURVE PARAMETERS

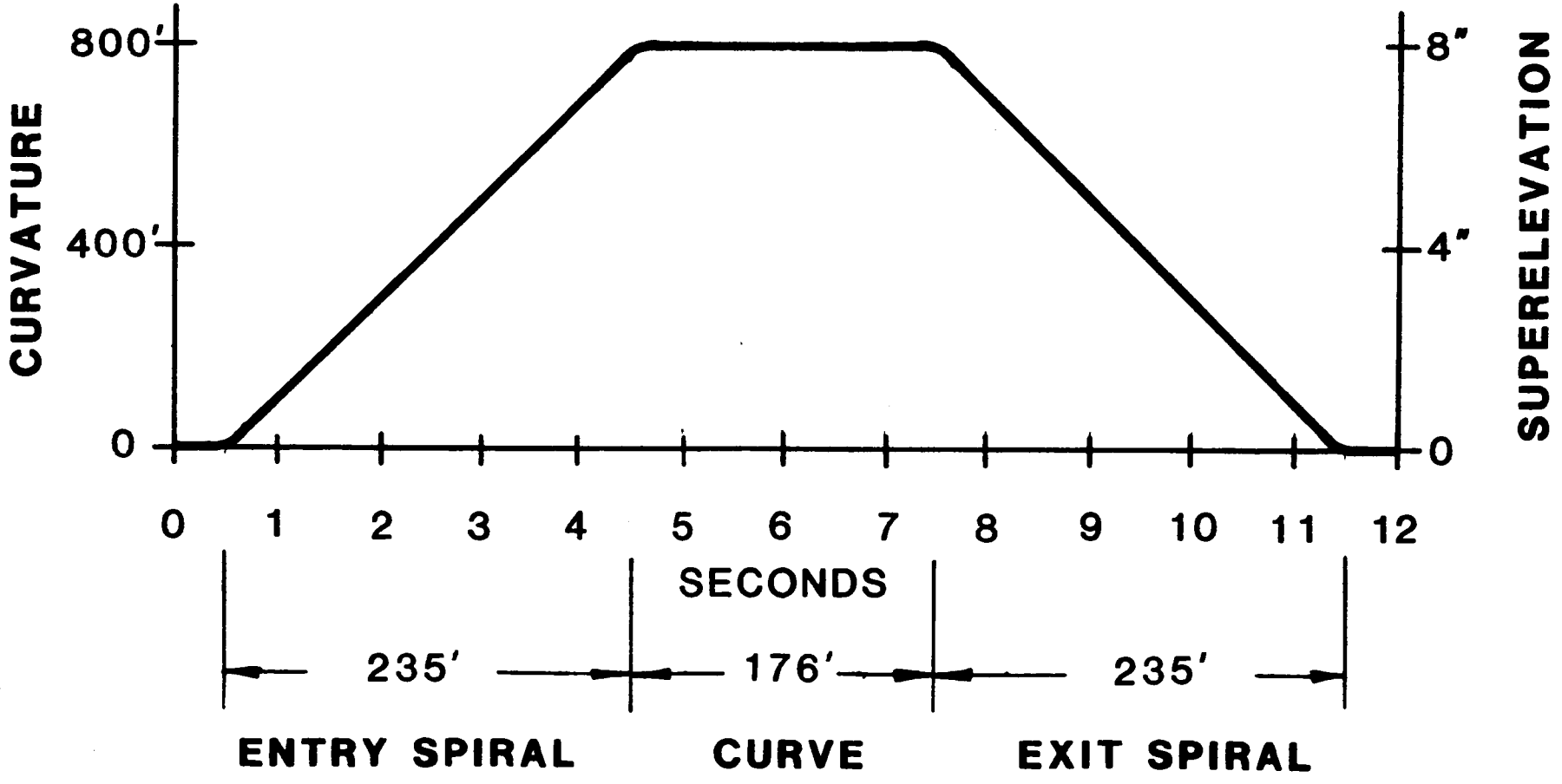

Figure 5-1: MODELED CURVE PARAMETERS

5.2 Standard P-III Truck and Soft Bushing Truck Model Description

The model configurations and input data are essentially updated versions of those used for establishing "Design Feasibility" (1) in 1980. The relative locations of centers-of-gravity and interconnections for the standard P-III truck model and the soft bushing truck model are shown in plan view in Figure 5-2 and in side elevation in Figure 5-3. Note that the parts modeled are shown numbered inside hexagons and the interfaces modeled are shown numbered inside circles . A similar set of schematics were made for the steerable truck model. The characteristics of the parts modeled are given in Table 5-1. The characteristics include mass, moments-of-inertia, and center-of-gravity locations. Also note that a more detailed breakdown of truck weights was given previously in Section 3.1.

The interfaces that were modeled for the standard P-III truck and the soft bushing truck are listed in Table 5-2, along with their locations. The stiffness and damping values that were modeled at each interface are cross-referenced to Table 5-3 by the Spring/Damper Set Number.

Table 5-3 gives the actual stiffness (K) and damping (C) values that were modeled for various directions. All six degress-of-freedom are available; however, only those used are listed. If the interface were modeled linearly, only one value for stiffness and/or damping is given. However, if a non-linear device were modeled, the stiffness and damping values are given as K_1, K_2, C_1, and C_2. Figure 5-4 shows examples of piecewise linear stiffness and damping representation. The values K_2 and C_2 are starred * in Table 5-3 and are related to deflections (d) and velocities (v), which specify the breakpoints. This modeling technique can be used to represent coulomb friction or springs in series with damper elements.

Appendix B shows the computer printout of the input data used for a typical standard P-III truck simulation.

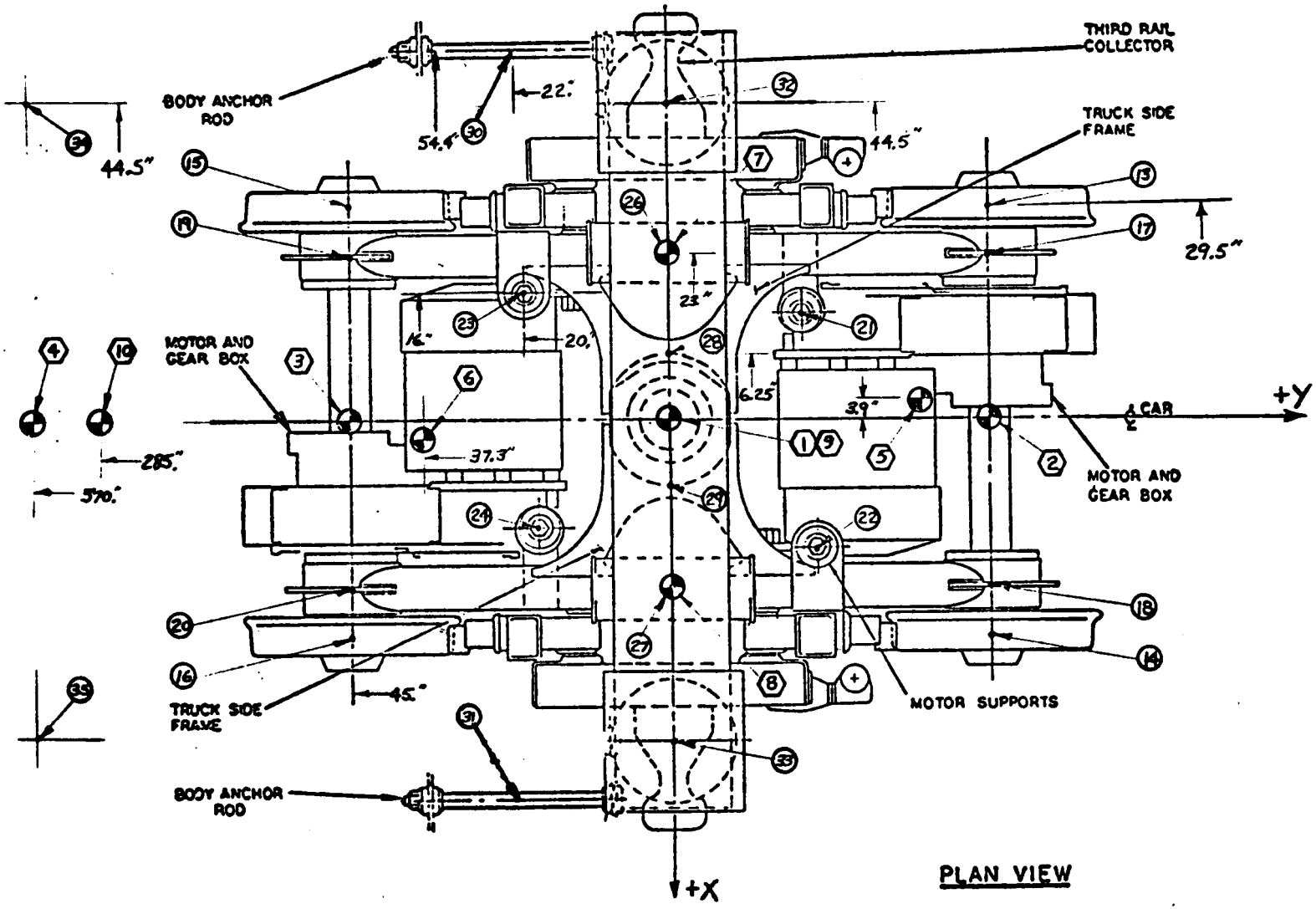

Figure 5-2: STANDARD PIII TRUCK MODEL

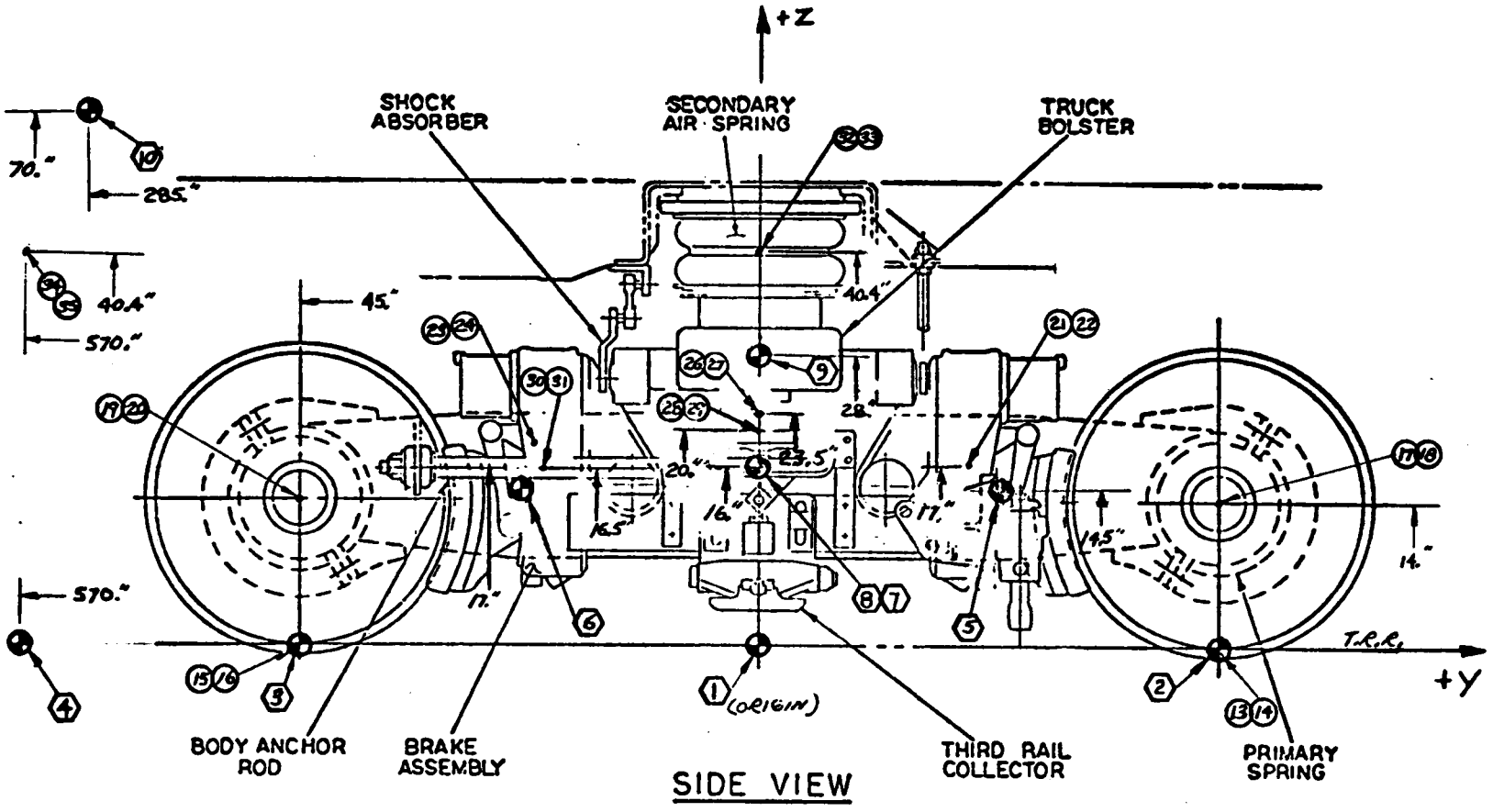

Figure 5-3: STANDARD PIII TRUCK MODEL

PART NO	DESCRIPTION	MASS (LB-SEC^2) IN	MOMENTS-OF-INERTIA (IN-SEC-LB^2) YAW	ROLL	PITCH	C.G. LOCATION (IN) LAT	LONG	VERT
1	Master Coordinate System	--	--	--	--	0	0	0
2	Leading Track Part	--	--	--	--	0	45.	0
3	Trailing Track Part	--	--	--	--	0	-45.	0
4	End of Car Track Part	--	--	--	--	0	-570.	0
5	Leading Motor/Axle Assy	10.57	4760	4540	1570	-3.9	37.3	14.5
6	Trailing Motor/Axle Assy	10.57	4760	4540	1570	3.9	-37.3	14.5
7	Left Side Frame Assy	3.78	5410	850	3410	-23.	0	16.
8	Right Side Frame Assy	3.78	5410	850	3410	23.	0	16.
9	Bolster Assy	4.28	4310	5010	110	0	0	28.
10	Carbody	140.5	7.9×10^6	2.9×10^5	7.85×10^6	0	-285.	70.

TABLE 5-1: PARTS MODELED FOR STANDARD P-III TRUCK AND SOFT BUSHING TRUCK

TABLE 5-2: INTERFACES MODELED FOR STANDARD P-III TRUCK AND SOFT BUSHING TRUCK

INTER-FACE NO.	DESCRIPTION	SPRING/ DAMPER SET NO.	LOCATION FROM ORIGIN (IN) LAT	LONG	VERT
1-6	Gravity force on real parts 5-10	--	--	--	--
7-12	Centrifugal force on real parts 5-10	--	--	--	--
13	Left-lead wheel/rail contact patch	1	-29.5	45.	0
14	Right-lead wheel/rail contact patch	1	29.5	45.	0
15	Left-trail wheel/rail contact patch	1	-29.5	-45.	0
16	Right-trail wheel/rail contact patch	1	29.5	-45.	0
17	Left-lead primary suspension	2	-23.	45.	14.
18	Right-lead primary suspension	2	23.	45.	14.
19	Left-trail primary suspension	2	-23.	-45.	14.
20	Right-trail primary suspension	2	23.	-45.	14.
21	Lead gear box to frame support	3	-16.	20.	17.
22	Lead motor to frame support	3	16.	20.	17.
23	Trail motor to frame support	3	-16.	-20.	17.
24	Trail gear box to frame support	3	16.	-20.	17.
25	Spare (not used)	--	--	--	--
26	Left side bearer	5	-23.	0	23.5
27	Right side bearer	5	23.	0	23.5
28	Left side frame spider	6	- 6.3	0	20.
29	Right side frame spider	6	6.3	0	20.
30	Left carbody anchor rod	7	-54.4	-22.	17.
31	Right carbody anchor rod	7	54.4	22.	17.
32	Left secondary suspension	8	-44.5	0	40.4
33	Right secondary suspension	8	44.5	0	40.4
34	Left rear secondary suspension	8	-44.5	-570.	40.4
35	Right rear secondary suspension	8	44.5	-570.	40.4

TABLE 5-3: STIFFNESS AND DAMPING VALUES FOR STANDARD P-III TRUCK MODEL AND SOFT BUSHING TRUCK

SET NO.	DESCRIPTION	DIRECTION	STIFFNESS, K DAMPING, C		
1	Track	Lat	K	170,000	lb/in
			C	200	lb-sec/in
		Vert	K	200,000	lb/in
			C	800	lb-sec/in
2	Standard primary suspension (see set no. 2A below for soft bushing suspension values)	Lat	K	200,000	lb/in
			C	170	lb-sec/in
		Long	K	295,000	lb/in
			C	375	lb-sec/in
		Vert	K	160,000	lb/in
			C	215	lb-sec/in
		Yaw	K	5,760,000	in-lb/rad
			C	73,000	in-lb-sec/rad
		Roll	K	7,400,000	in-lb/rad
			C	830,000	in-lb-sec/rad
3	Motor/gear box support	Lat	K	650	lb/in
			C	10	lb-sec/in
		Long	K	650	lb/in
			C	10	lb-sec/in
		Vert	K	7,050	lb/in
			C	27	lb-sec/in
4	Not used for this model				
5	Side bearer	Lat	C_1	1,000	lb-sec/in
	*v = 2. in/sec		*C_2	0	lb-sec/in
		Long	K_1	20,000	lb/in
	*d = .1 in		*K_2	0	lb/in
			C	50	lb-sec/in
		Vert	K	200,000	lb/in
			C	200	lb-sec/in
6	Side frame spider	Lat	K_1	0	lb/in
	*d = .05 in		*K_2	200,000	lb/in
			C	57	lb-sec/in
		Long	K_1	0	lb-sec/in
	*d = .05 in		*K_2	50,000	lb/in
			C	57	lb-sec/in
		Vert	K_1	0	lb/in
	*d = .1 in		K_2	100,000	lb/in
			C	57	lb-sec

TABLE 5-3: CONTINUED

SET NO.	DESCRIPTION	DIRECTION	STIFFNESS, K DAMPING, C		
7	Carbody anchor rod	Long	K	25,000	lb/in
			C	100	lb-sec/in
8	Secondary suspension	Lat	K_1	1,000	lb/in
	*d = 1. in		*K_2	10,000	lb/in
			C_1	94	lb-sec/in
	*v = 9. in/sec		*C_2	194	lb-sec/in
		Vert	K_1	2,500	lb/in
	*d = 1. in		*K_2	50,000	lb/in
			C_1	100	lb-sec/in
	*v = 9. in/sec		C_2	300	lb-sec/in
2A	Soft primary suspension bushing	Lat	K	1000,000	lb/in
			C	205	lb-sec/in
		Long	K	36,000	lb/in
			C	125	lb-sec/in
		Vert	K	48,000	lb/in
			C	205	lb-sec/in
		Yaw	K	350,000	in-lb/rad
			C	1,220	in-lb-sec/rad
		Roll	K	470,000	in-lb/rad
			C	2,000	in-lb-sec/rad

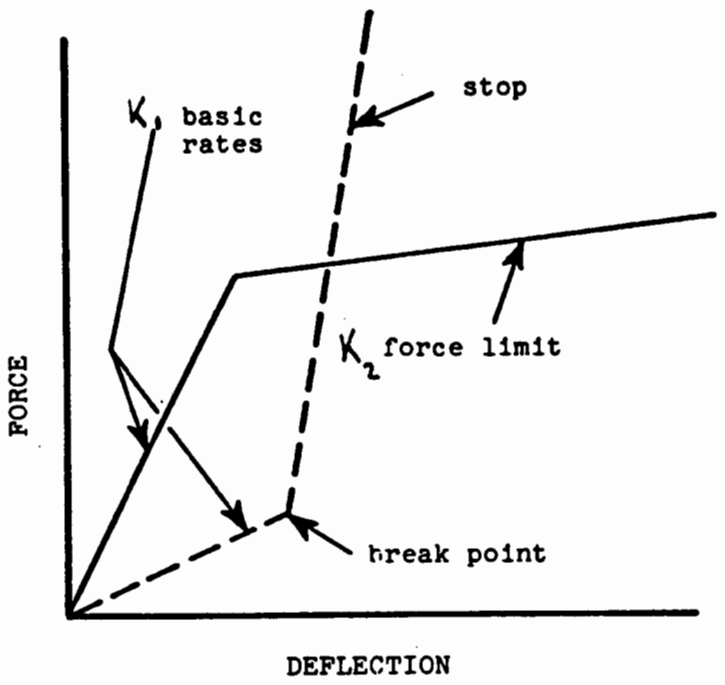

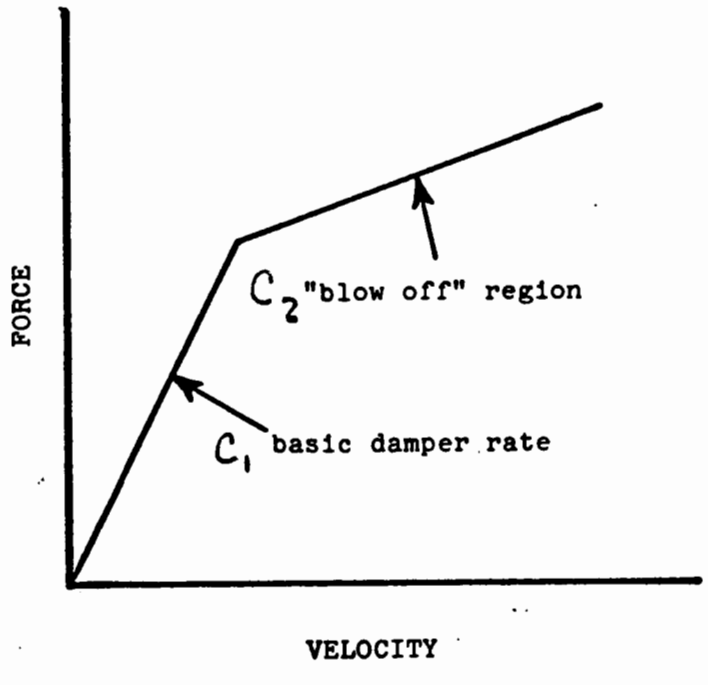

Figure 5-4: NON-LINEAR SPRING AND DAMPER REPRESENTATION

5.3 Steerable Truck Model Description

The steerable truck model is quite similar to the standard P-III truck model in many respects. The characteristics of the parts modeled, including mass, moments-of-inertia, and center-of-gravity locations are given in Table 5-4. The steerable truck is somewhat heavier than the standard P-III truck and this is reflected in the table. Also, note that a more detailed breakdown of truck weights was given previously in Section 3.3.

The interfaces that were modeled for the steerable truck are listed in Table 5-5 along with their locations. Interfaces 17 thru 25 are different for the steerable truck model, all others remain the same.

Table 5-6 gives the actual stiffness (K) and damping (C) values that were modeled and are cross-referenced with the intefaces listed in Table 5-5 by the Spring/Damper Set Number as before.

PART NO	DESCRIPTION	MASS (LB-SEC^2) IN	MOMENTS-OF-INERTIA (IN-SEC-LB^2) YAW	ROLL	PITCH	C.G. LOCATION (IN) LAT	LONG	VERT
1	Master Coordinate System	--	--	--	--	0	0	0
2	Leading Track Part	--	--	--	--	0	+45.	0
3	Trailing Track Part	--	--	--	--	0	-45.	0
4	End of Car Track Part	--	--	--	--	0	-570.	0
5	Leading Steering Arm, Motor/Axle Assy	13.48	7100	5750	2650	-3.1	34.5	14.1
6	Trailing Steering Arm, Motor/Axle Assy	13.48	7100	5750	2650	3.1	-34.5	14.1
7	Left Side Frame Assy	4.44	3020	1440	3070	-23.	0	16.
8	Right Side Frame Assy	4.44	3020	1440	3070	23.	0	16.
9	Bolster Assy	4.40	4570	5290	120	0	0	28.
10	Carbody	140.5	7.9×10^6	2.9×10^5	7.85×10^6	0	-285.	+70.

TABLE 5-4: PARTS MODELED FOR STEERABLE TRUCK

TABLE 5-5: INTERFACES MODELED FOR STEERABLE TRUCK

INTER-FACE NO.	DESCRIPTION	SPRING/ DAMPER SET NO.	LOCATION FROM ORIGIN (IN) LAT	LONG	VERT
1-6	Gravity force on real parts 5-10	--	--	--	--
7-12	Centrifugal force on real parts 5-10	--	--	--	--
13	Left-lead wheel/rail contact patch	1	-29.5	45.	0
14	Right-lead wheel/rail contact patch	1	29.5	45.	0
15	Left-trail wheel/rail contact patch	1	-29.5	-45.	0
16	Right-trail wheel/rail contact patch	1	29.5	-45.	0
17	Left-lead primary suspension (shear pad/slider)	2	-23.	46.5	14.
18	Right-lead primary suspension	2	23.	46.5	22.3
19	Left-trail primary suspension	2	-23.	-46.5	22.3
20	Right-trail primary suspension	2	23.	-46.5	22.3
21	Steering arm interconnection	3	0	0	6.7
22	Forced steering link	4	0	6.8	11.7
23	Traction link	5	0	0	11.7
24	Vert. support lead steering arm assy	3	- 7.1	7.	16.
25	Vert. support trail steering arm assy	6	7.1	- 7.	16.
26	Left side bearer	7	-23.	0	23.5
27	Right side bearer	7	23.	0	23.5
28	Left spider liner	8	- 6.3	0	20.
29	Right spider liner	8	6.3	0	20.
30	Left carbody anchor rod	9	-54.4	-22.	17.
31	Right carbody anchor rod	9	54.4	22.	17.
32	Left secondary suspension	10	-44.5	0	40.4
33	Right secondary suspension	10	44.5	0	40.4
34	Left rear secondary suspension	10	-44.5	-570.	40.4
35	Right rear secondary suspension	10	44.5	-570.	40.4

TABLE 5-6: STIFFNESS AND DAMPING VALUES FOR THE STEERABLE TRUCK MODEL

SET NO.	DESCRIPTION	DIRECTION	STIFFNESS, K DAMPING, C		
1	Track	Lat	K	170,000	lb/in
			C	200	lb-sec/in
		Vert	K	200,000	lb/in
			C	800	lb-sec/in
2	Standard primary suspension (Shear pad/slider assy)	Lat	K_1	0	lb/in
	*d = .06 in		*K_2	70,000	lb/in
			C_1	500	lb-sec/in
	*v = 2. in/sec		*C_2	0	lb-sec/in
		Long	K_1	40,000	lb/in
	*d = .025 in		*K_2	0	lb/in
			C	300	lb-sec/in
		Vert	K	150,000	lb/in
			C	600	lb-sec/in
3	Steering arm interconnection	Lat	K	30,000	lb/in
			C	60	lb-sec/in
		Long	K	50,000	lb/in
			C	60	lb-sec/in
		Vert	K	50,000	lb/in
			C	60	lb-sec/in
4	Forced steering link	Lat	K	7,500	lb/in
			C	60	lb-sec/in
5	Traction link	Long	K	100,000	lb/in
			C	100	lb-sec/in
6	Steering arm vert support	Vert	K	7,500	lb/in
			C	200	lb-sec/in
7	Side bearer	Lat	C_1	1,000	lb-sec/in
	*v = 2 in/sec		*C_2	0	lb-sec/in
		Long	K_1	20,000	lb/in
	*d = .1 in		*K_2	0	lb/in
			C	50	lb-sec/in
		Vert	K	200,000	lb/in
			C	100	lb-sec/in

TABLE 5-6: CONTINUED

SET NO.	DESCRIPTION	DIRECTION	STIFFNESS, K DAMPING, C		
8	Side frame spider	Lat	K_1	0	lb/in
	*d = .05 in		*K_2	200,000	lb/in
			C	57	lb-sec/in
		Long	K_1	0	lb-sec/in
	*d = .05 in		*K_2	50,000	lb/in
			C	57	lb-sec/in
		Vert	K_1	0	lb/in
	*d = .1 in		*K_2	100,000	lb/in
			C	57	lb-sec
9	Carbody anchor rod	Long	K	25,000	lb/in
			C	100	lb-sec/in
10	Secondary suspension	Lat	K_1	1,000	lb/in
	*d = 1. in		*K_2	10,000	lb/in
			C_1	94	lb-sec/in
	*v = 9. in/sec		*C_2	194	lb-sec/in
		Vert	K_1	2,500	lb/in
	*d = 1. in		*K_2	50,000	lb/in
			C_1	100	lb-sec/in
	*v = 9. in/sec		*C_2	300	lb-sec/in

5.4 Wheel/Rail Interface

Researchers in the United States and abroad have been developing a better understanding of the mechanics involved at the wheel/rail contact patch for a number of years. The subject can be generally broken down into two basic areas; wheel/rail contact geometry and the friction-creepage phenomena.

Contact geometry is concerned with rail and wheel profiles and how they conform to one another as a function of wheelset lateral displacement. The geometry can be readily defined by contact angle and rolling radius differences. Figure 5-5 shows the geometry data that was used in the computer model to make the wheel force predictions. The wheel profile that was modeled and also used on the instrumented wheelset is known as the BR 1:20 and is shown in Figure 5-6. This profile is similar to the AAR 1:20, which is also shown in Figure 5-6, except in the area of the flange fillet. The BR 1:20 has a fuller radius which tends to eliminate the two point contact phenomenon that is associated with new AAR 1:20 wheels. New AAR 1:20 wheels tend to wear to single point contact profiles within a few thousand miles. The computer program can model any combination of wheel and rail profiles. Figure 5-7 shows an enlarged view of the flange fillet area.

The second area involving the wheel/rail interface, and by far the most controversial, is the friction-creep phenomena. There are numerous references on the subject, such as, Kalker (2) (3), Rudd (4), Kumar (5), etc. Creep is defined as the ratio of the velocity of the wheel at the wheel/rail interface divided by the rolling velocity and can be expressed as a percentage. The creep term accounts for the relative micro-slip that occurs between the wheel and rail. Creep can be a combination of elastic deformation, plastic flow and ultimately gross sliding. The second part of this phenomena involves the coefficient of friction between the wheel and the rail as a function of creep. Figure 5-8 shows the two friction versus creep curves that were used to predict the wheel/rail forces. Both curves show the friction coefficient rising according to Kalker theory and saturating at maximum values of 0.3 and 0.5 at 0.6 percent and 1.0 percent creep, respectively. Modeling the friction-creep characteristics in this way will always produce steady state force estimates during curving.

Recent studies in this area suggest that the longitudinal friction-creep characteristic may follow trends as suggested by Figure 5-8; however, the lateral friction-creep characteristic may actually drop off for values of creep above one percent. A number of computer runs were made using the four curves shown in Figure 5-9.

The predicted force levels are presented in Section 5.5 and are also referenced in Section 6.3, which presents the actual force measurements.

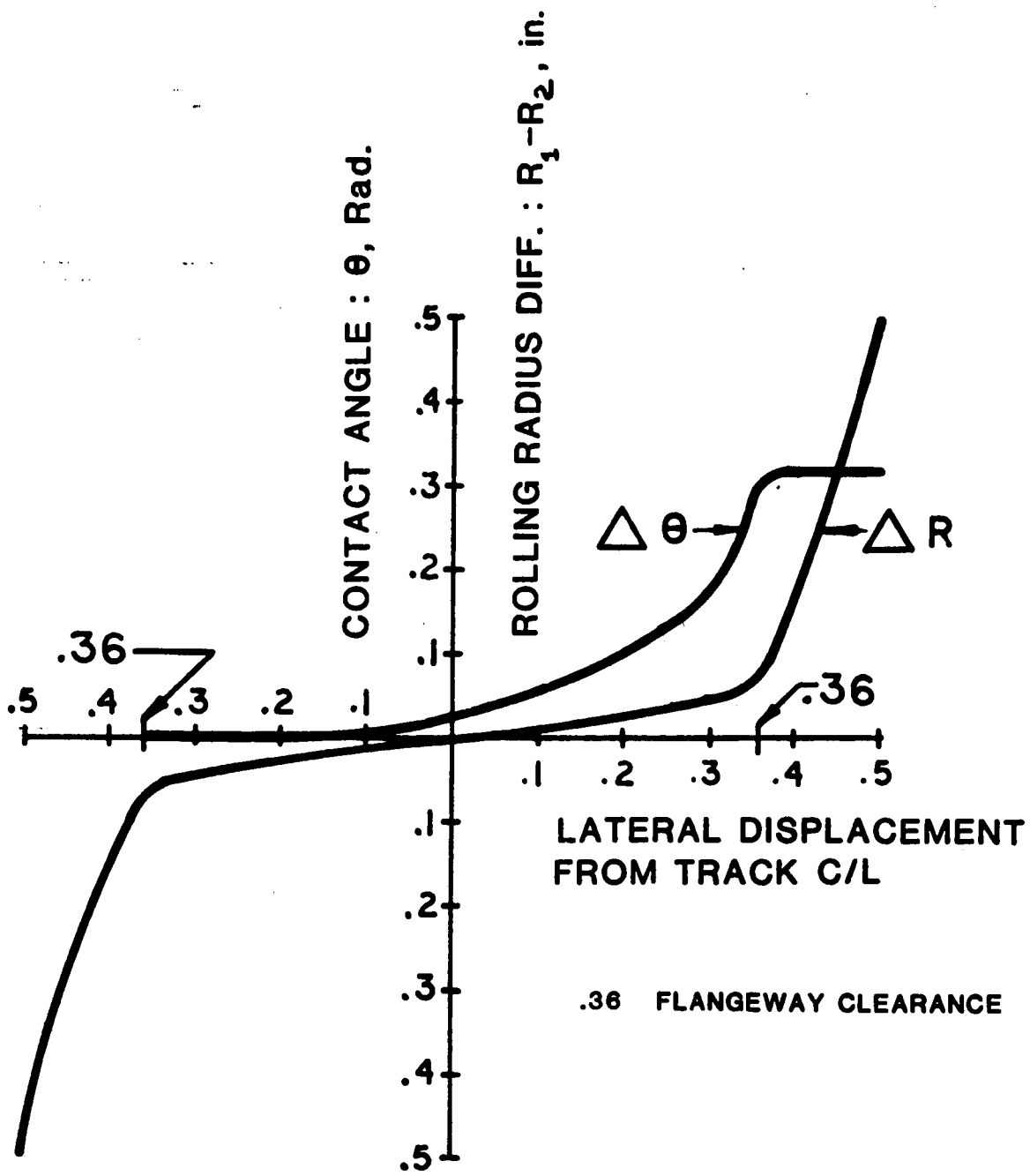

WORN WHEEL PROFILE GEOMETRY DATA

Figure 5-5: WORN WHEEL PROFILE GEOMETRY DATA

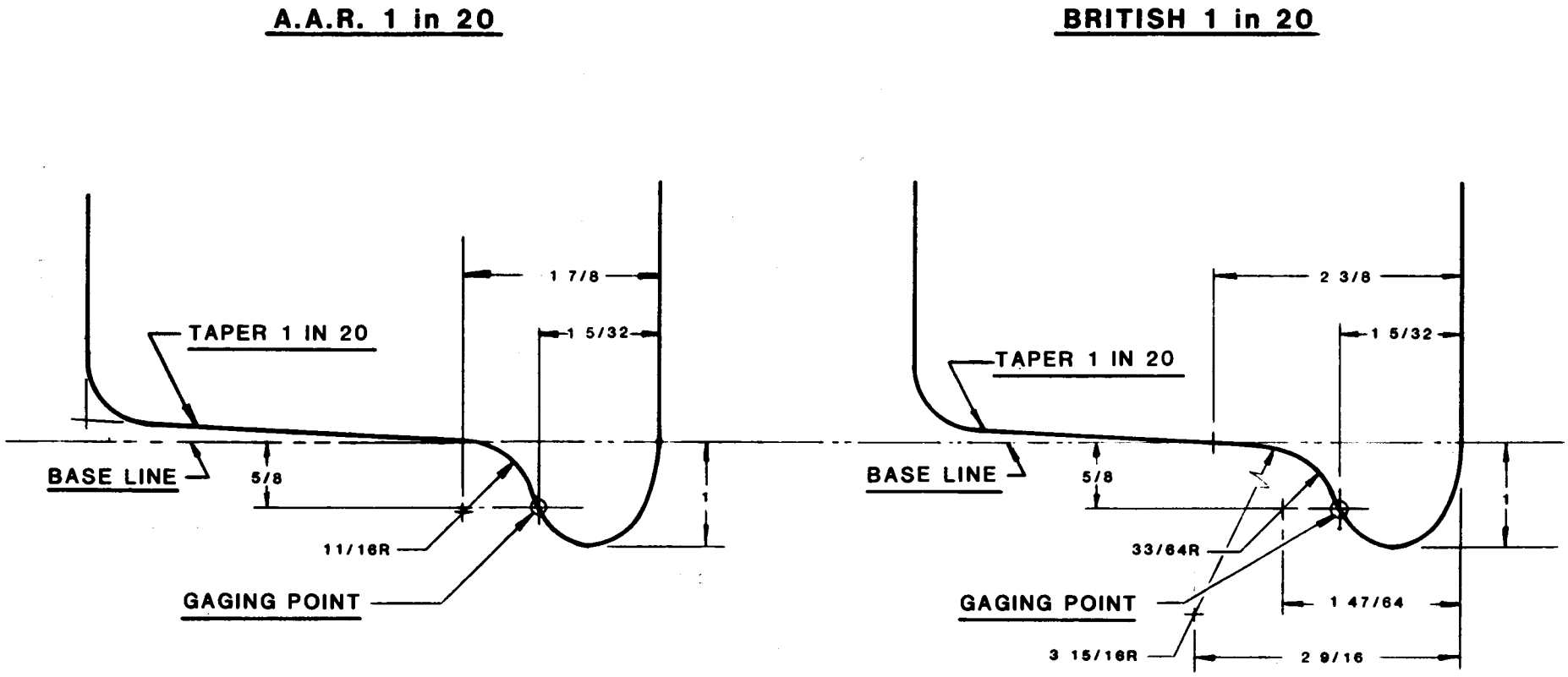

Figure 5-6: A.A.R. AND BRITISH 1 IN 20 PROFILES

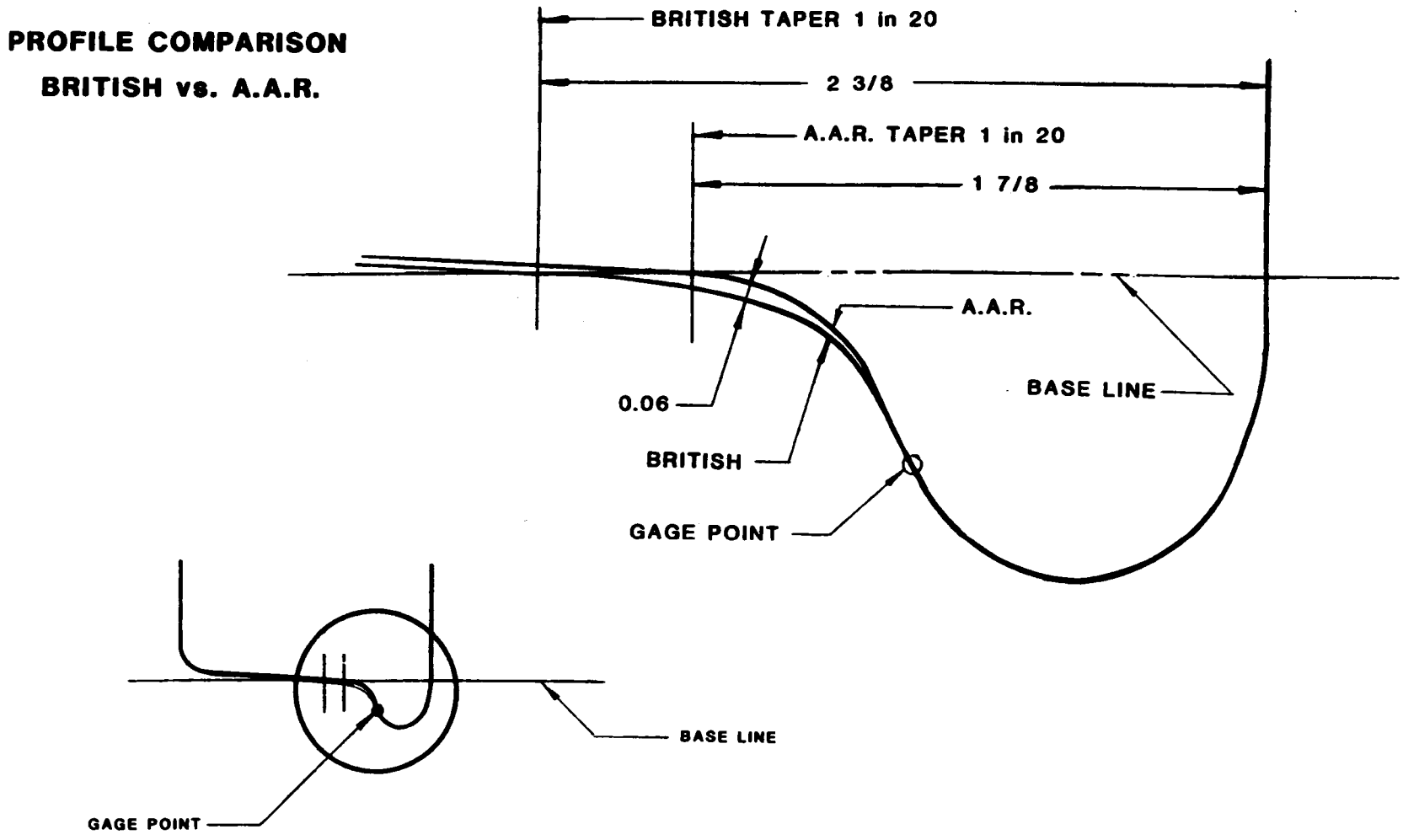

Figure 6-7: FLANGE-FILLET PROFILE COMPARISON

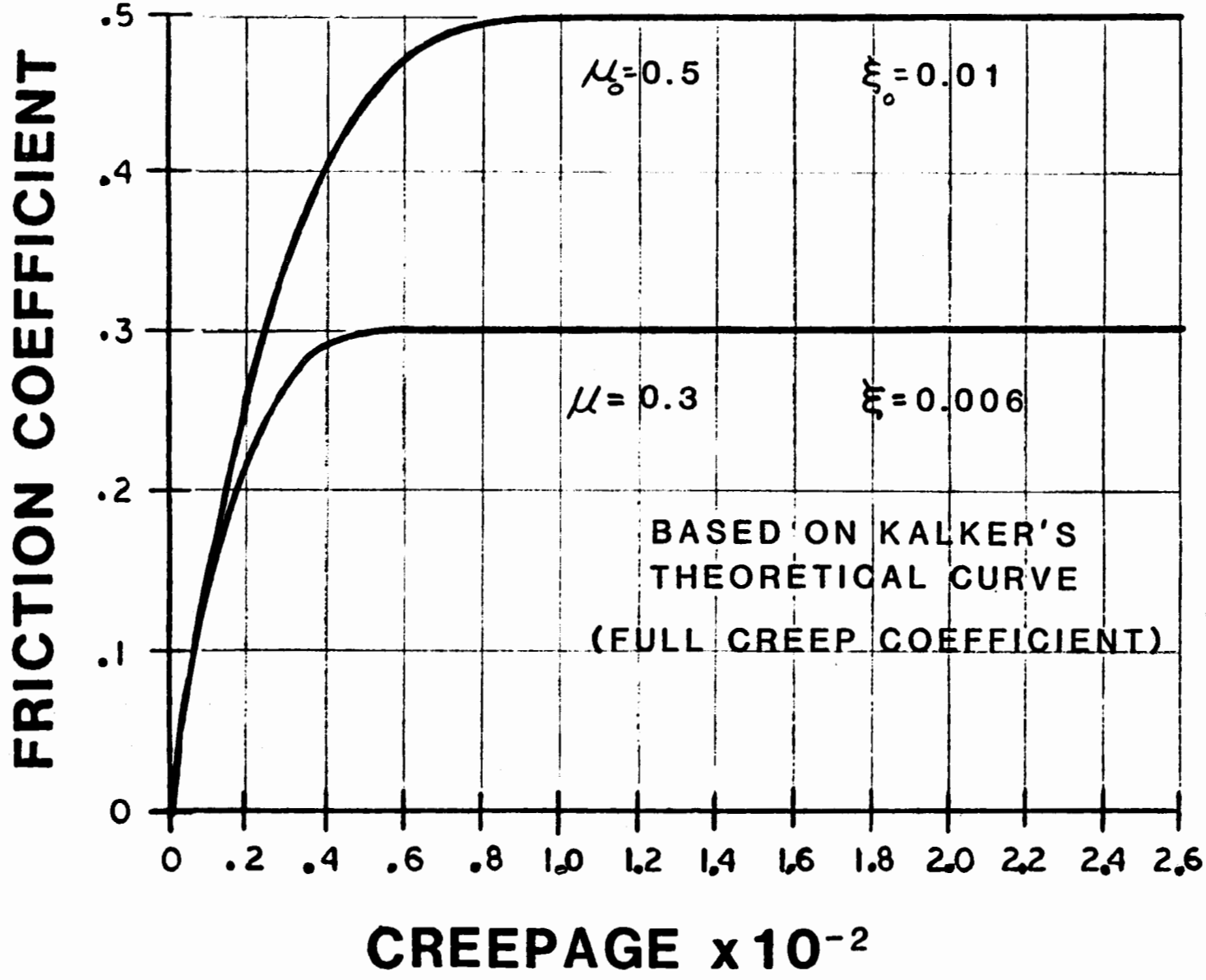

Figure 5-8: FRICTION VS. CREEPAGE-SATURATION

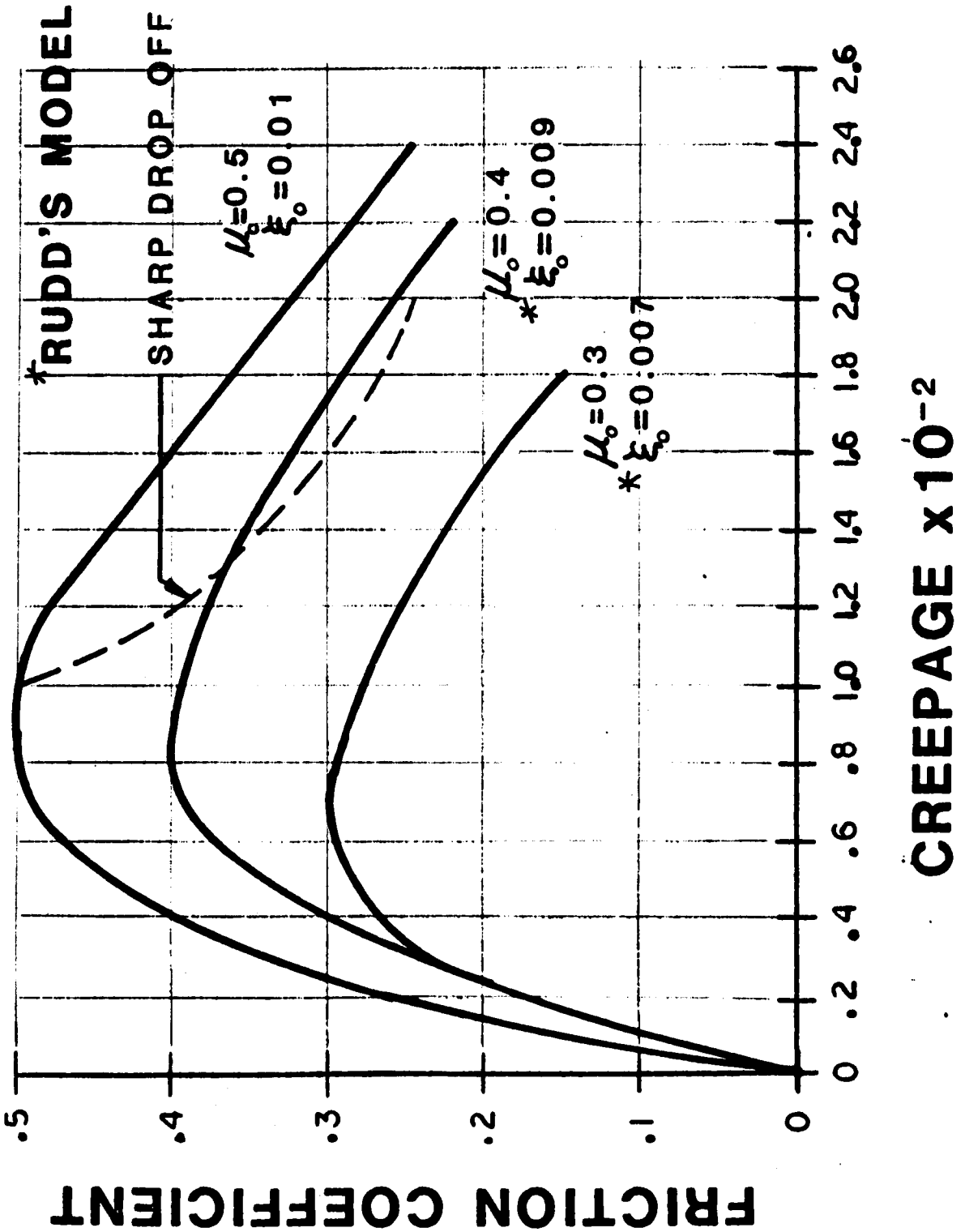

Figure 5-9: FRICTION VS. CREEPAGE-DROP OFF

5.5 Wheel/Rail Force Predictions

The wheel/rail force predictions for the three different truck configurations are presented in Table 5-7. This table gives the lateral, longitudinal, and vertical force levels of the inner and outer wheels of both the leading and trailing axles for two different friction coefficients. One of the most useful characteristics when comparing curving performance is the lateral force on the lead-outer wheel. At the 0.5 maximum friction level, we see that these predicted force levels are 4,050 lbs., 2,670 lbs. and 1,490 lbs. for the standard, soft bushing, and steerable truck configurations, respectively. These force levels represent a 34% reduction for the soft bushing truck and a 63% reduction for the steerable axle truck when compared to the standard baseline truck.

The angle-of-attack that the lead-outer wheel makes with the outer rail is also an important curving performance characteristic and is included in Table 5-7 for reference. Note that significant differences between the three truck configurations are predicted, i.e., at the 0.5 maximum friction level, 0.0093 radians for the standard, 0.0047 radians for the soft bushing, and 0.0001 radians for the steerable truck. The steerable truck is essentially radial, while the standard truck is at the lower level of the screech boundary. The screech boundary has been informally defined as the angle-of-attack at which the wheel/rail curving noise (screech or squeal) begins, usually on the order of 1/2 degree or about 0.01 radians. Keep in mind that these predicted values are for the 7°10' PATCO curve (800 ft. radius) and are based on the friction-creep characteristics shown in Figure 5-7.

As mentioned previously, computer runs were also made for each friction-creep curve shown in Figure 5-8. Some of the results were quite surprising. For instance, the curve which rises to 0.5 maximum friction coefficient and then drops off gradually produced essentially steady state operation while the 0.5 curve with the sharp drop off produced a lateral force oscillation on the lead axle when modeling the standard P-III truck. The oscillation was sinusoidal in nature with the force levels on the outer wheel rising to about 10,000 lbs. directed toward the track centerline and dropping past zero to about 2,000 lbs. in the opposite direction. The frequency was about 3.8 Hertz or about 15 ft. in length. The steerable truck model did not show any sign of oscillation for the same friction-creep curve.

The standard truck model was also run with the remaining two curves described by Rudd (4). The 0.4 maximum friction curve produced steady state operation, while the 0.3 maximum friction curve produced an oscillatory behavior. This oscillation was also sinusoidal with force levels on the outer wheel rising to about 9,000 lbs. directed toward the track centerline and dropping to zero. The frequency was about 7.4 Hertz or about 8 ft. in length. These results are preliminary and require further investigation.

TRUCK TYPE	FRICTION COEFFICIENT	LEADING AXLE FORCES (LBS.) INNER WHEEL LAT	LONG	VERT	OUTER WHEEL LAT	LONG	VERT	ANGLE OF ATTACK (RAD.)
Standard P-III	.3	2750	-1350	10200	-3190	930	9190	.0100
	.5	4230	-3020	10400	-4050	2300	9010	.0093
Soft Bushing	.3	2580	-1120	10300	-2570	750	9150	.0037
	.5	3560	-3660	10600	-2670	2710	8820	.0047
Steerable	.3	280	280	10300	-1490	-330	10400	.0002
	.5	220	310	10300	-1490	-360	10400	.0001

		TRAILING AXLE FORCES (LBS.) INNER WHEEL LAT	LONG	VERT	OUTER WHEEL LAT	LONG	VERT	ANGLE OF ATTACK (RAD.)
Standard P-III	.3	1140	750	9630	-290	-310	9780	.0009
	.5	690	1270	9430	-420	-580	9960	.0006
Soft Bushing	.3	1230	~0	9530	-870	370	9870	.0003
	.5	570	800	9240	-1030	120	10200	.0005
Steerable	.3	1640	480	10700	-60	-430	9990	.0013
	.5	1650	520	10700	80	-480	9990	.0012

TABLE 5-7: WHEEL/RAIL FORCE PREDICTIONS

6.0 Mainline Vehicle Testing

The purpose of the mainline vehicle test program was to measure the performance characteristics of the three different truck configurations (i.e., standard, soft bushing, and steerable) while operating on the PATCO system in simulated revenue service. A single carbody (Car #114) was used for testing the three different truck configurations sequentially. The primary sensor was an instrumented wheelset that could continuously measure the lateral and vertical forces between the wheels and rails during mainline operation. The instrumented wheelset, which was designed and built by ENSCO, is briefly described in the following section and in greater detail in Appendix C. The Technical Center provided sensors to measure primary suspension displacements, axle and side frame accelerations, truck yaw displacements, truck yaw resistance, carbody accelerations, and vehicle speed. In addition, a dual camera video-sound system with remote control pan, tilt, zoom, and focus was provided to monitor the instrumented wheelset in real time.

6.1 Instrumentation

Instrumented Wheelset

The instrumented wheelset consisted of an axle and gear box provided by PATCO and two wheels obtained from WMATA. The reason for using WMATA wheels versus PATCO wheels was that ENSCO had gained considerable experience with this wheel design on an earlier test program. Making use of prior calibration experience reduced cost and improved schedule requirements. The WMATA wheel design is very similar to the PATCO design. The major difference being wheel width (WMATA is 5-1/4", PATCO is 5-1/2") which was considered insignificant for measuring wheel rail forces. The wheel plate was machined to minimum allowable thickness to improve sensitivity.

A total of 32 strain gages were installed on each wheel. The gages on each wheel were grouped into four bridge circuits, two lateral and two vertical. The strain gauge bridge circuit signals were transmitted to carbody mounted processing equipment by means of 20-channel rotating slip ring assemblies mounted at each end of the axle. The individual strain gauge bridge circuit signals are initially sent to their respective gage amplifier. The strain gage amplifiers supply AC carrier excitation to the bridge and demodulate the bridge response to produce highly amplified DC signals proportional to the bridge strain summation.

As the wheels rotate, the output of the individual bridges (two bridges are required for each force channel) under a constant wheel/rail force vary as sine waves or triangular waves. High pass filtering is applied to the rotating wheel bridge output to eliminate all source of signal drift. Wheel rotation causes the bridge response to wheel/rail force to

become an AC signal at the wheel rotation frequency with drift resembling a change in DC level. High pass filtering eliminates the drift while preserving the AC waveform.

The strain signal processor combines the individual amplified DC bridge signals to form continuous wheel/rail force measurements. The processor also performs crosstalk correction and scaling to a ±10 VDC range proportional to ±25,000 lbs. wheel/rail force. A thorough discussion of instrumented wheelset theory and calibration is presented in Appendix C.

The four wheel/rail force signals (two lateral and two vertical) were continously monitored in real time on an 8-channel Brush Chart Recorder and recorded on a 14-channel Honeywell Analog tape recorder for post processing and permanent record.

Truck Mounted Instrumentation

Lateral and vertical axle accelerations were measured by two accelerometers mounted on the journal bearing housing centerline opposite the gear box on the instrumented wheelset. Similarly, lateral and vertical side frame accelerations were measured by two accelerometers mounted on the side frame directly across the primary suspension element, i.e., unbonded shock ring and soft bushing for P-III truck configurations #1 and #2, or the shear-pad-slider assembly for the steerable truck, configuration #3.

The yaw displacement of the instrumented wheelset across the primary suspension elements was measured by two linear variable displacement transducers - LVDT's. Each LVDT was mounted perpendicular to the axle and parallel to the rail. This measurement gave some indication of axle steering, although the ideal measurement would have been angle-of-attack. Measuring directly the angle-of-attack between the wheel and rail requires instrumentation that was comparable in cost to the instrumented wheelset and therefore, was not considered because of budget restraints.

Truck yaw displacement relative to the bolster was measured with string type displacement transducers, sometimes called yo-yo's. This measurement was made primarily for identifying the curved track sections when analyzing the wheel/rail force measurements.

Truck yaw resistance was measured by two carbody radius rods equipped with strain gage bridge circuits. The main purpose of this measurement was to compare the frictional characteristics of the two side bearings currently used by PATCO. A list of the instrumentation used is given in Table 6-1.

Carbody Mounted Instrumentation

A total of five accelerometers were floor mounted inside the carbody. Lateral and vertical accelerometers were mounted in

the center of the carbody and also over the center of the truck. The fifth accelerometer was mounted vertically over the truck but near the wall of the carbody. These five accelerometers were used to evaluate carbody ride quality in the lateral, vertical, pitch, yaw, and roll directions.

TABLE 6-1: INSTRUMENTATION LIST

ITEM	DESCRIPTION	LOCATION	RANGE
1	Long. primary suspension displacement	right front journal	±1.0 in.
2	Long. primary suspension displacement	left front journal	±1.0 in.
3	Truck yaw displacement	right side frame to bolster	±6 deg.
4	Lat. journal accel.	right front journal	±50 g's
5	Vert. journal accel.	right front journal	±50 g's
6	Lat. side frame accel.	right front journal	±50 g's
7	Vert. side frame accel.	right front journal	±50 g's
8	Lat. carbody accel.	center of carbody	±1 g
9	Vert. carbody accel.	center of carbody	±1 g
10	Lat. carbody accel.	over center of truck	±1 g
11	Vert. carbody accel.	over center of truck	±1 g
12	Vert. carbody accel.	over truck near carbody wall	±1 g
13	Truck yaw resistance	right radius rod	±3,000#
14	Truck yaw resistance	left radius rod	±3,000#

6.2 Vehicle Test Description and Log

The primary test objective was to collect wheel/rail force data on the entire PATCO systems including both westbound and eastbound tracks with the instrumented wheelset in a leading and trailing position for all three truck configurations. This task represents a minimum of six test runs. In addition, special attention was given to the curve that was used for the wheel/rail force predictions. This curve was located on the westbound track just east of Camden, and several more runs were dedicated for this purpose. Plus a few runs had to be repeated because of the various instrumentation problems which are usually present on any large scale field test program.

A total of 18 test runs were made from Lindenwold to Philadelphia, stopping at 13th or 16th Street. The following log (Table 6-2) gives the run number, date, instrumented wheelset position (leading or trailing), track used (westbound or eastbound), and the stations identifying beginning and end of test run.

Each test run was conducted during PATCO's off peak hours during the day or evening. Daytime hours were from 10:00 a.m. to 3:00 p.m., and evening hours were after 7:00 p.m. The test vehicle, Car #114, was normally operated automatically by the ATO system (automatic train operation) because this was considered most representative of normal revenue service.

The test results are presented in the following sections in the order of wheel/rail force measurements, truck accelerations, truck yaw resistance, and carbody accelerations.

TABLE 6-2: TEST LOG

STANDARD P-III TRUCK TESTING

RUN NO.	DATE	WHEELSET POSITION	TRACK	STATIONS
1A	7-30-84	Lead	W.B.	Lindenwold - 16th Street
B		Trail	E.B.	16th Street - Lindenwold
2A	7-30-84	Trail	W.B.	Lindenwold - 16th Street
B		Lead	E.B.	16th Street - Lindenwold
3A	7-31-84	Lead	W.B.	Lindenwold - 16th Street
B		Trail	E.B.	16th Street - Ferry Avenue
4A	8-1-84	Lead	W.B.	Lindenwold - 16th Street
B		Trail	E.B.	16th Street - Ferry Avenue
5A	8-1-84	Trail	W.B.	Lindenwold - 16th Street
B		Lead	E.B.	16th Street - Lindenwold
6A	8-2-84	Trail	W.B.	Lindenwold - 16th Street
B		Lead	E.B.	16th Street - Lindenwold
7A	8-2-84	Lead	W.B.	Lindenwold - 13th Street
B		Trail	E.B.	13th Street - Lindenwold

SOFT BUSHING TRUCK TESTING

RUN NO.	DATE	INSTR. WHEELSET POSITION	TRACK	STATION
8A	8-22-84	Lead	W.B.	Lindenwold - 16th Street
B		Trail	E.B.	16th Street - Ferry Avenue
C		Lead	W.B.	Ferry Avenue - 16th Street
D		Trail	E.B.	16th Street - Lindenwold
9A	8-22-84	Trail	W.B.	Lindenwold - 16th Street
B		Lead	E.B.	16th - Lindenwold
10A	8-23-84	Lead	W.B.	Lindenwold - 16th Street
B		Trail	E.B.	16th Street - Lindenwold
11A	8-24-84	Lead	W.B.	Lindenwold - 16th Street
		Trail	E.B.	16th Street - Lindenwold

STEERABLE TRUCK TESTING

RUN NO.	DATE	INSTR. WHEELSET POSITION	TRACK	STATION
12A	10-10-84	Lead	W.B.	Lindenwold - 16th Street
B		Trail	E.B.	16th Street - Ferry Avenue
C		Lead	W.B.	Ferry Avenue - 13th Street
D		Trail	E.B.	13th Street - Lindenwold
13A	10-11-84	Lead	W.B.	Lindenwold - 16th Street
B		Trail	E.B.	16th Street - Lindenwold
14A	10-11-84	Trail	W.B.	Lindenwold - 13th Street
B		Lead	E.B.	13th Street - Ferry Avenue
C		Trail	W.B.	Ferry Avenue - 13th Street
D		Lead	E.B.	13th Street - Lindenwold
15A	10-16-84	Trail	W.B.	Lindenwold -
B		Lead	E.B.	
16A	10-24-84	Lead	W.B.	Lindenwold - 8th Street
B		Trail	E.B.	8th Street - Lindenwold
17A	10-24-84	Lead	W.B.	Lindenwold - 13th Street
B		Trail	E.B.	13th Street - Lindenwold
18A	10-25-84	Lead	W.B.	Lindenwold - 13th Street
B		Trail	E.B.	13th Street - Lindenwold
19A	10-30-84	Lead	W.B.	Lindenwold - Camden
B		Trail	E.B.	Camden - Ferry Avenue
C		Lead	W.B.	Ferry Avenue - Camden
D		Trail	E.B.	Camden - Ferry Avenue
E		Lead	W.B.	Ferry Avenue - Camden
F		Trail	E.B.	Camden - Lindenwold

6.3 Wheel/Rail Curving Force Measurements

Lead Axle Wheel Force - 800 ft. Radius Curve

The wheel/rail force measurements that were especially made for comparison with the computer predictions are presented below. This data was taken while negotiating the 7°10' curve (800 ft. radius) just east of Broadway Station in Camden. The operating speed was 40 mph which is also the balance speed. The wheel/rail curving forces measured by the instrumented wheelset when in the leading axle position and installed in the standard P-III truck, the soft bushing truck and the steerable axle truck are given in Figures 6-1, 6-2, and 6-3. Each Figure shows four analog traces; two lateral L1, L2 and two vertical V1, V2. Since this curve is left-hand, wheel 1 is on the inner or low rail and wheel 2 is on the outer or high rail.

Both lateral and vertical traces show an oscillating behavior consisting of several different frequencies. Two fundamental frequencies associated with the vertical force trace are wheel rotation (about 8.1 Hz) and secondary suspension vertical bounce frequency (about 1.1 Hz). The wheel rotation is based on a 27.75 inch diameter wheel translating at 40 mph. There is also a track geometry input or signature that is unique for each curve and includes both lateal and vertical track features.

The lateral force traces are the most important when evaluating curving performance. These traces show that the curving performance of full size vehicles negotiating realworld rail conditions is a very dynamic environment. In fact, the term steady state curving performance may well be a term that is only suitable for describing computer simulations.

The lateral force traces consist of several different frequencies resulting from the combination of all horizontal parameters effecting the wheel/rail interface. These parameters include the longitudinal and lateral truck primary suspension spring rates, the truck wheelbase, the lateral spring rate of the track support system, the longitudinal and lateral friction coefficient versus creepage characteristics of the wheel/rail material combination, the wheel/rail profile geometry, and others.

Comparing the lead-outer wheel lateral force traces for the three truck configurations, repeated on Figure 6-4 for ease of comparison, one can easily see significant reductions for the soft bushing and steerable truck configurations. Average force values were initially estimated by visual inspection and later verified by digitizing the data and finding RMS values. The average values and the peak values from the measured data are presented in Table 6-3. The computer predicted steady state values are also included for comparison.

STANDARD P-III TRUCK

RUN 7 8/2/84

LEADING AXLE WHEEL FORCES - WESTBOUND TRACK, 40 mph

LEFT HAND $7^{\circ}10'$ CURVE, 8" S.E.

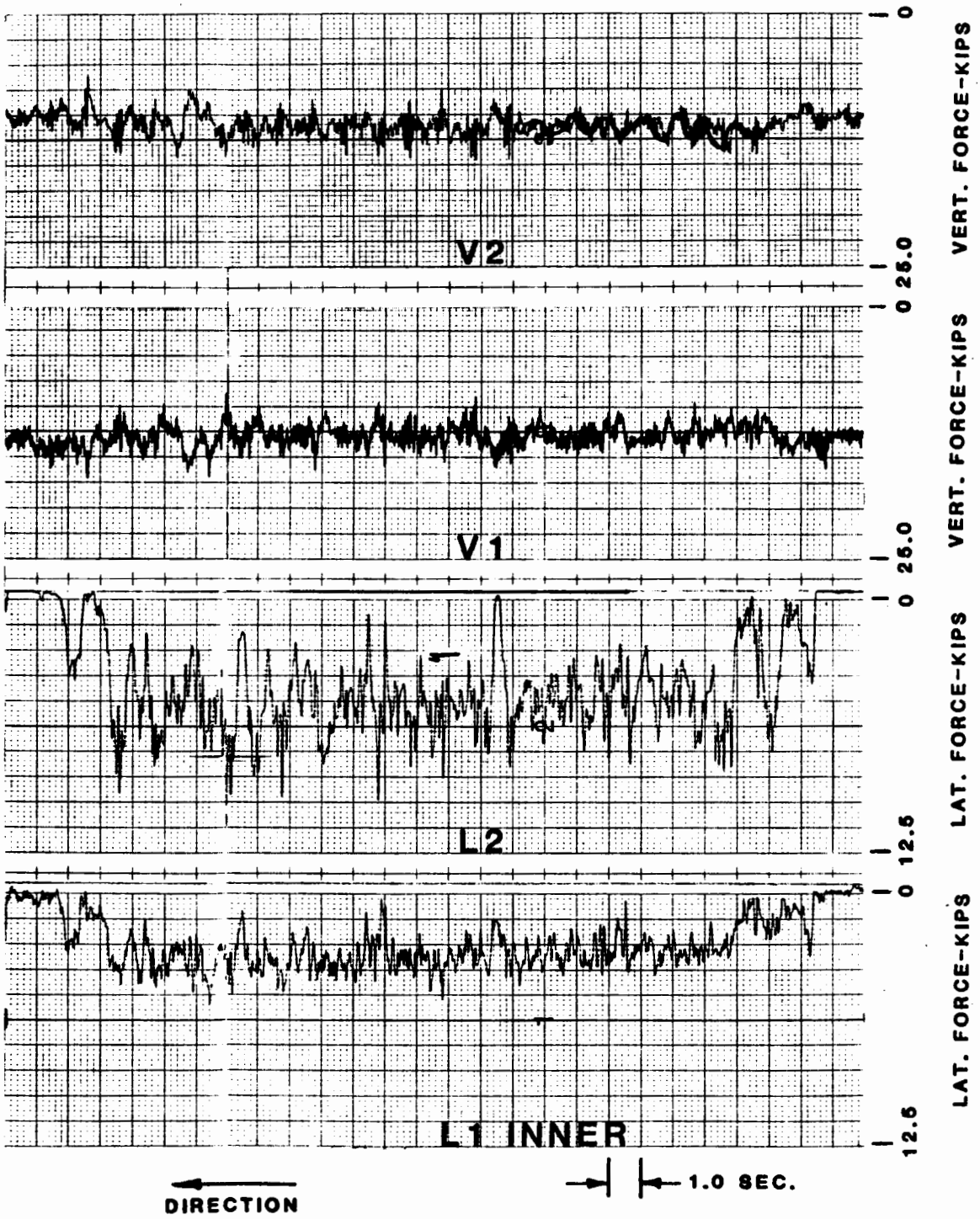

Figure 6-1

STANDARD TRUCK (SOFT BUSHING)

RUN 8 8/22/84

LEADING AXLE WHEEL FORCES - WESTBOUND TRACK, 40 mph

LEFT HAND 7°10' CURVE, 8" S.E.

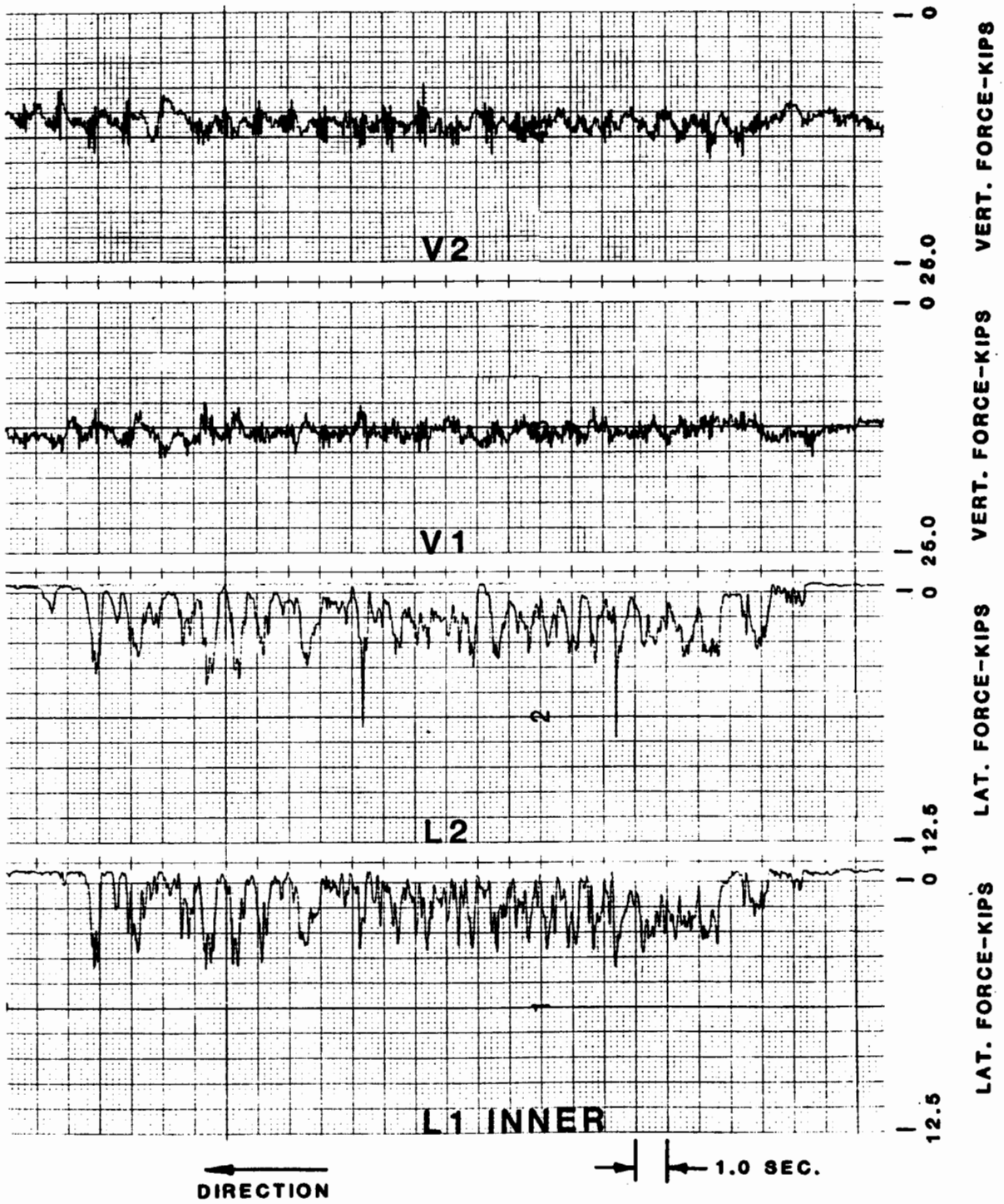

Figure 6-2

STEERABLE TRUCK

RUN 18 10/25/84

LEADING AXLE WHEEL FORCES - WESTBOUND TRACK, 40 mph

LEFT HAND 7°10' CURVE, 8" S.E.

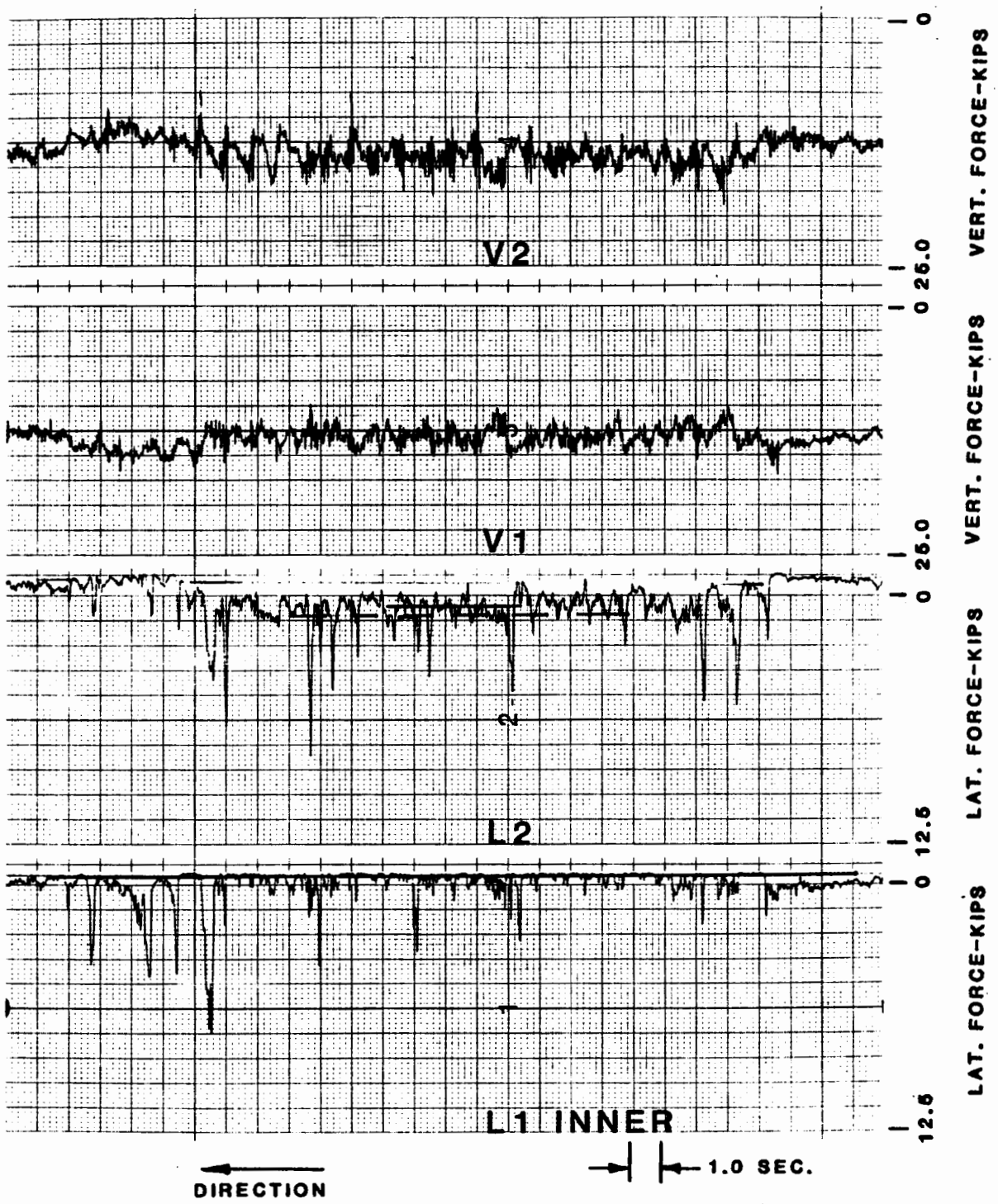

Figure 6-3

LEAD-OUTER WHEEL FORCE COMPARISON

STANDARD P-III TRUCK

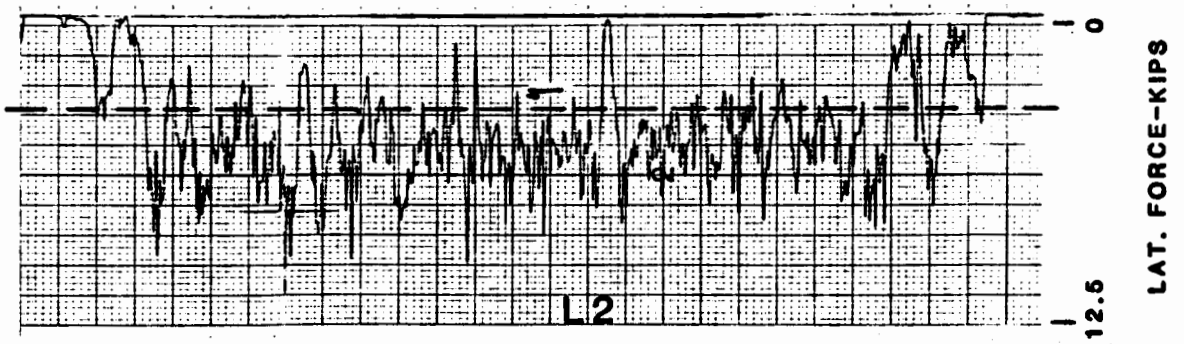

STANDARD TRUCK (SOFT BUSHING)

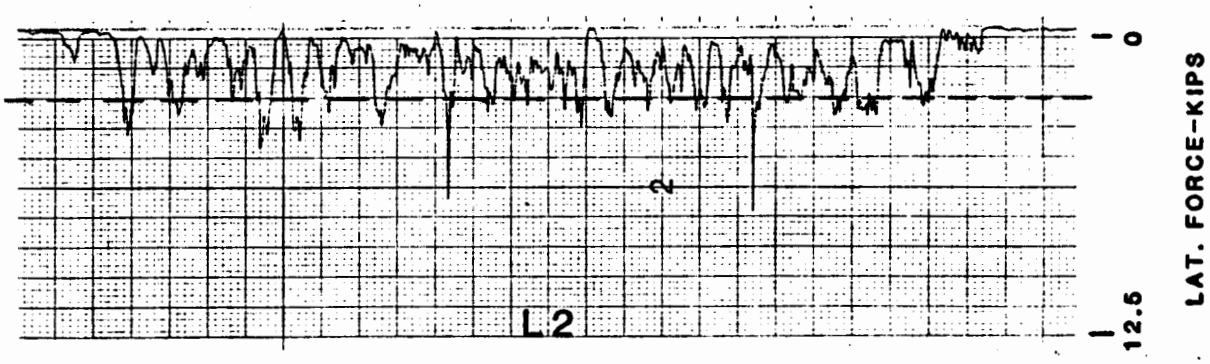

STEERABLE TRUCK

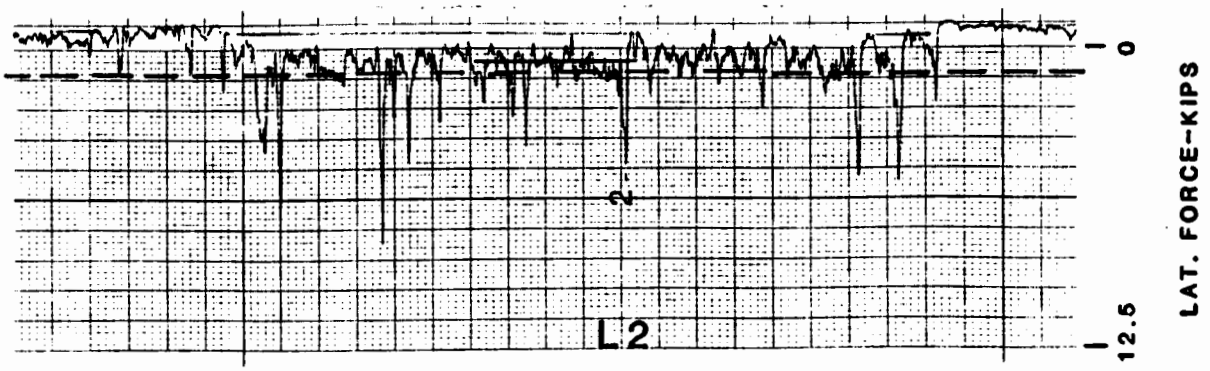

Figure 6-4

TABLE 6-3: OUTER WHEEL FORCE COMPARISON

TRUCK TYPE	OUTER WHEEL LATERAL FORCE, KIPS MEASURED AVERAGE	MEASURED PEAK	PREDICTED STEADY STATE
Standard P-III	5.3	8.3	4.1
Soft Bushing	2.6	4.2	2.7
Steerable	1.5	3.8	1.6

The average measured data shows that when compared to the baseline standard P-III truck, the soft bushing truck had a 63% lower force level and the steerable truck had a 75% lower force level. The average measured values are in reasonable agreement with the computer predicted steady state values; however, the peak force values associated with the oscillations can only be predicted with a revised description of the friction versus creepage theory as discussed in Section 5.3. More detailed track geometry input data is also required to improve the predictions.

Trailing Axle Wheel Force - 800 ft. Radius Curve

The wheel/rail curving forces measured by the instrumented wheelset when in the trailing axle position of the trailing truck for the three configurations are given in Figures 6-5, 6-6, and 6-7. This data was taken on the same 800 ft. radius curve. Since the wheelset is trailing, wheel 1 is now the outer wheel and wheel 2 the inner. The trailing axle forces are much lower than the leading axle forces as expected. Note that the trailing axle of the steerable truck, Figure 6-7, experiences a higher force level than the standard truck and soft bushing truck. This is expected and results from the radial positioning which forces the trailing axle to ride toward the outer rail, making flange contact much like the lead axle. The opposite holds true for conventional trucks, including the standard P-III and soft bushing. In their case, the trailing axle rides more toward the inner rail.

Lead Axle Wheel Force Summary

Table 6-4 presents a summary of the lateral lead axle wheel forces measured on PATCO curves having curvatures greater than three degrees. These curves are numbered one thru nine as they appear on the westbound track just west of Ferry Avenue Station starting near mile post five. Table 6-5 gives the curvature in degrees-minutes and the curve radius in feet for reference along with the curve service speed, balance speed, and superelevation. See Appendix A for more information concerning curve location

STANDARD P-III TRUCK

RUN 6 8/2/84

TRAILING AXLE WHEEL FORCES - WESTBOUND TRACK, 40 mph

LEFT HAND 7°10' CURVE, 8" S.E.

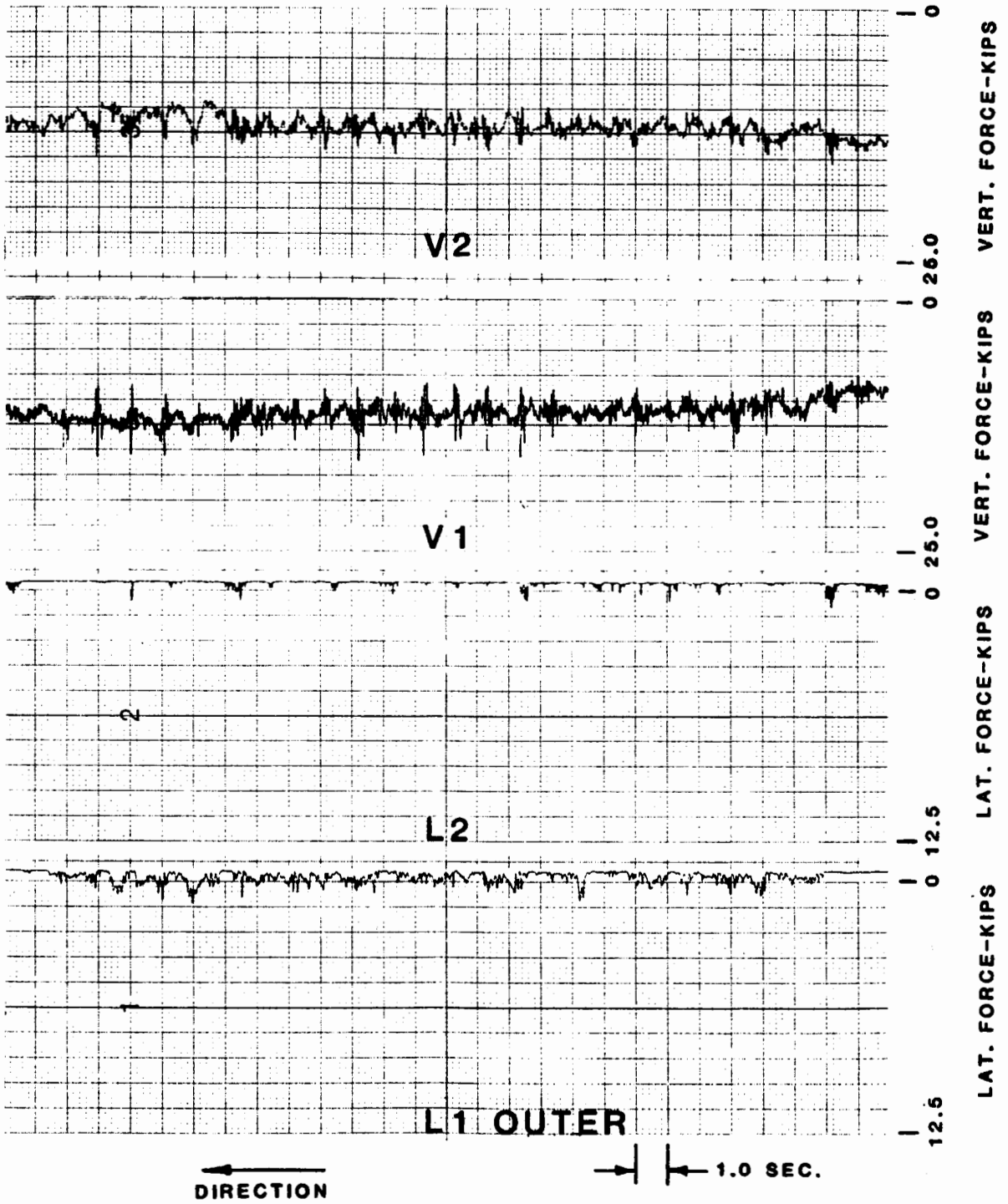

Figure 6-5

STANDARD TRUCK (SOFT BUSHING)

RUN 9 8/22/84

TRAILING AXLE WHEEL FORCES - WESTBOUND TRACK, 40 mph

LEFT HAND 7°10' CURVE, 8" S.E.

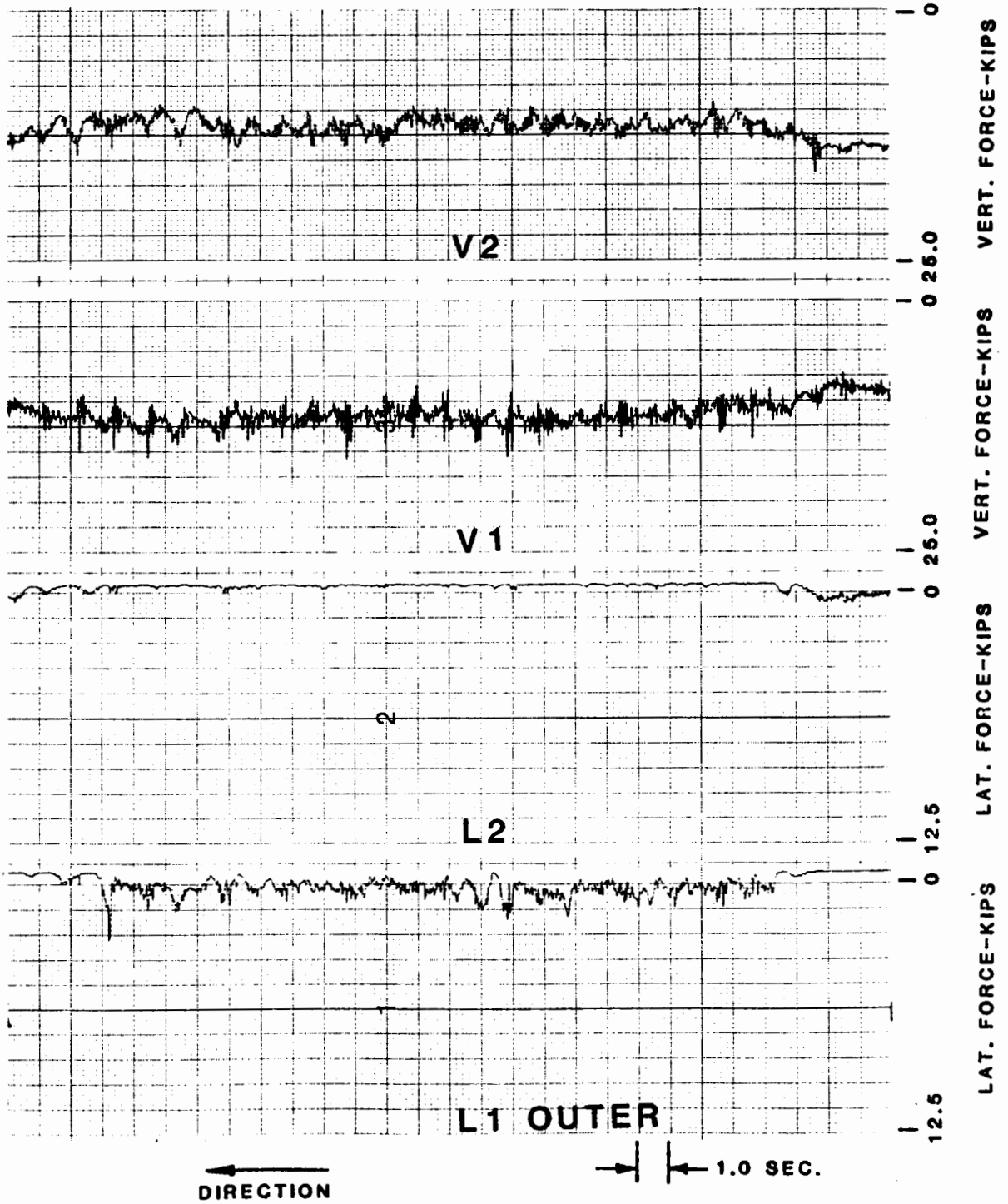

Figure 6-6

STEERABLE TRUCK

RUN 14 10/11/84

TRAILING AXLE WHEEL FORCES - WESTBOUND TRACK, 40 mph

LEFT HAND 7°10' CURVE, 8" S.E.

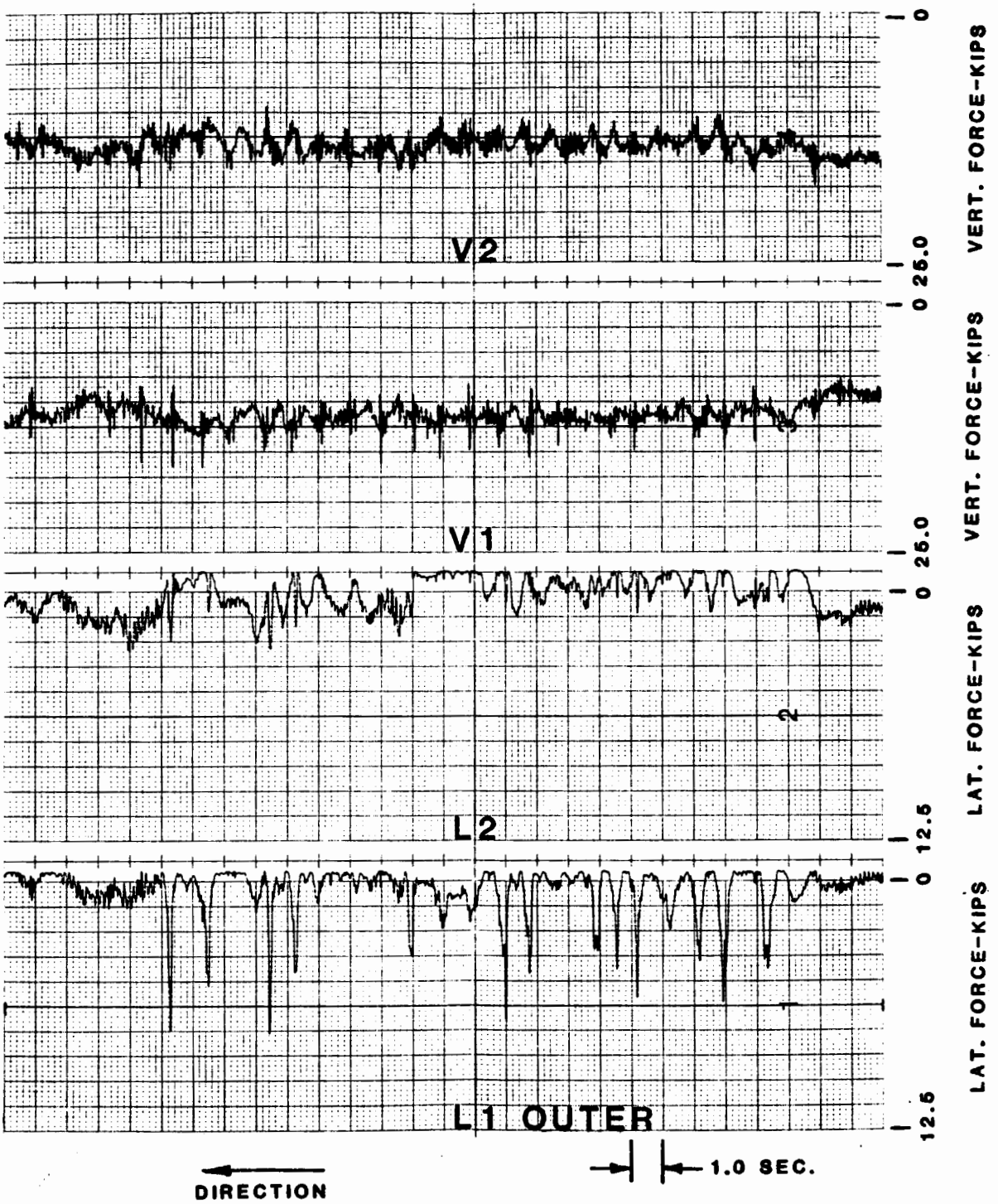

Figure 6-7

and sequence. The lead axle forces for both the low or inner rail and the high or outer rail are given. Average and peak force levels are given for comparison with the peak levels enclosed in parenthesis.

CURVE NO.	LATERAL WHEEL/RAIL FORCE, (KIPS)					
	STANDARD P-III		SOFT BUSHING		STEERABLE	
	LOW RAIL	HIGH RAIL	LOW RAIL	HIGH RAIL	LOW RAIL	HIGH RAIL
1	2.0 (3.5)	2.9 (6.2)	.9 (1.2)	1.2 (4.1)	.7 (1.0)	1.1 (2.4)
2	3.3 (4.6)	5.3 (8.3)	1.7 (4.0)	2.6 (4.2)	.5 (3.7)	1.5 (3.8)
3	*5.8 (6.9)	2.4 (11.3)	*3.6 (4.3)	1.7 (10.7)	*4.9 (7.9)	1.6 (10.4)
4	*6.8 (11.)	1.5 (4.8)	*3.8 (5.3)	1.6 (3.5)	*6.2 (9.9)	2.5 (5.4)
5	*4.6 (5.7)	1.4 (2.7)	*4.3 (6.2)	.7 (1.5)	*3.9 (5.7)	1.6 (2.5)
6	*6.4 (7.8)	.6 (2.3)	*4.2 (5.0)	1.0 (1.8)	*6.5 (8.3)	.5 (1.1)
7	*2.9 (3.6)	.2 (.8)	*3.3 (3.0)	.1 (.3)	*3.5 (4.5)	.5 (1.0)
8	*3.7 (5.1)	1.4 (3.3)	*3.5 (4.8)	.6 (1.5)	*4.3 (5.8)	2.4 (4.9)
9	*4.9 (8.2)	.5 (2.0)	*4.2 (5.7)	.6 (1.8)	*3.9 (5.3)	.6 (2.6)

*Low rail equipped with restraining rail

TABLE 6-4: LEAD AXLE WHEEL FORCE SUMMARY

CURVE NO.	CURVATURE (DEG-MIN)	CURVE RADIUS (FT)	SERVICE SPEED (MPH)	BALANCE SPEED (MPH)	SUPERELEVATION (IN)
1	3°	1910	65	53.5	6.0
2	7° 10'	800	40	40	8.0
3	12° 45'	450	30	9.2	.75
4	21°	275	20	13.1	2.5
5	11° 15'	510	30	21.2	3.5
6	9°	637	20	21.9	3.0
7	18° 45'	307	20	19.6	5.0
8	27° 30'	210	20	11.5	2.5
9	28° 07'	206	20	16.	5.0

TABLE 6-5: PATCO TEST CURVE DESCRIPTION

Curves one and two are the only PATCO curves with curvatures greater than three degrees not equipped with restraining rail. The lead outer wheel average force values are plotted on Figure 6-8 against degree of curvature for the three truck configurations. This plot clearly shows the relative improvement of the soft bushing and steerable truck configurations. This data, as well as theory, suggest that the trend for improvement will continue for greater curvatures.

Curves numbered three thru nine are equipped with restraining rail on the inner rail as noted on Table 6-4. The purpose of restraining rail is to react a portion of the lateral wheelset force by contacting the inside surface of the wheel flange on the inner wheel. This results in a much lower force between the outer wheel and high rail which reduces flange wear and derailment risk on very sharp curves. The restraining rail was spaced 1 7/8" from the inner rail when installed.

The average lead axle lateral wheel forces measured on curves equipped with restraining rail are plotted in Figures 6-9, 6-10, and 6-11 for the standard, soft bushing, and steerable truck configurations. The plotted restraining rail force data shows considerable scatter. However, in all cases, the outer wheel forces are considerably lower than the inner wheel forces, as expected. The data scatter seems to be related more towards specific curve conditions rather than truck configuration. A number of factors can account for the data scatter, such as, lubrication, wear, and curving speed. Some of the curves with especially low wheel/rail force levels were heavily lubricated. Lubrication is normally applied to the rail gauge face to reduce rail gauge face wear and wheel flange wear. If not adjusted properly, the lubricators can apply excessive amounts of lubricant which can work its way onto the rail head surface. This condition can significantly reduce the lateral creep force and also degrade braking performance.

Excessive gauge face wear can also reduce the lateral wheel/rail force in sharp curves. This is equivalent to widening the gauge.

Curving speed also has an effect on lateral wheel/rail force. Negotiating curves at speeds greater than balance speed increase the lateral forces while the opposite is true for under balance speed operation. Table 6-5 gives the calculated balance speed based on curve radii and superelevations taken from PATCO track charts. An attempt was made to adjust the data to balance speed conditions. However, this had minimal effect on reducing the scatter. Therefore, it was decided to only present the actual data.

Comparing the restraining rail force data (Figures 6-9, 6-10, and 6-11) from the standpoint of truck configuration, a few additional observations can be made. First, the soft bushing truck experienced a much lower force level on the inner wheel than the standard or steerable truck. Also, the soft bushing

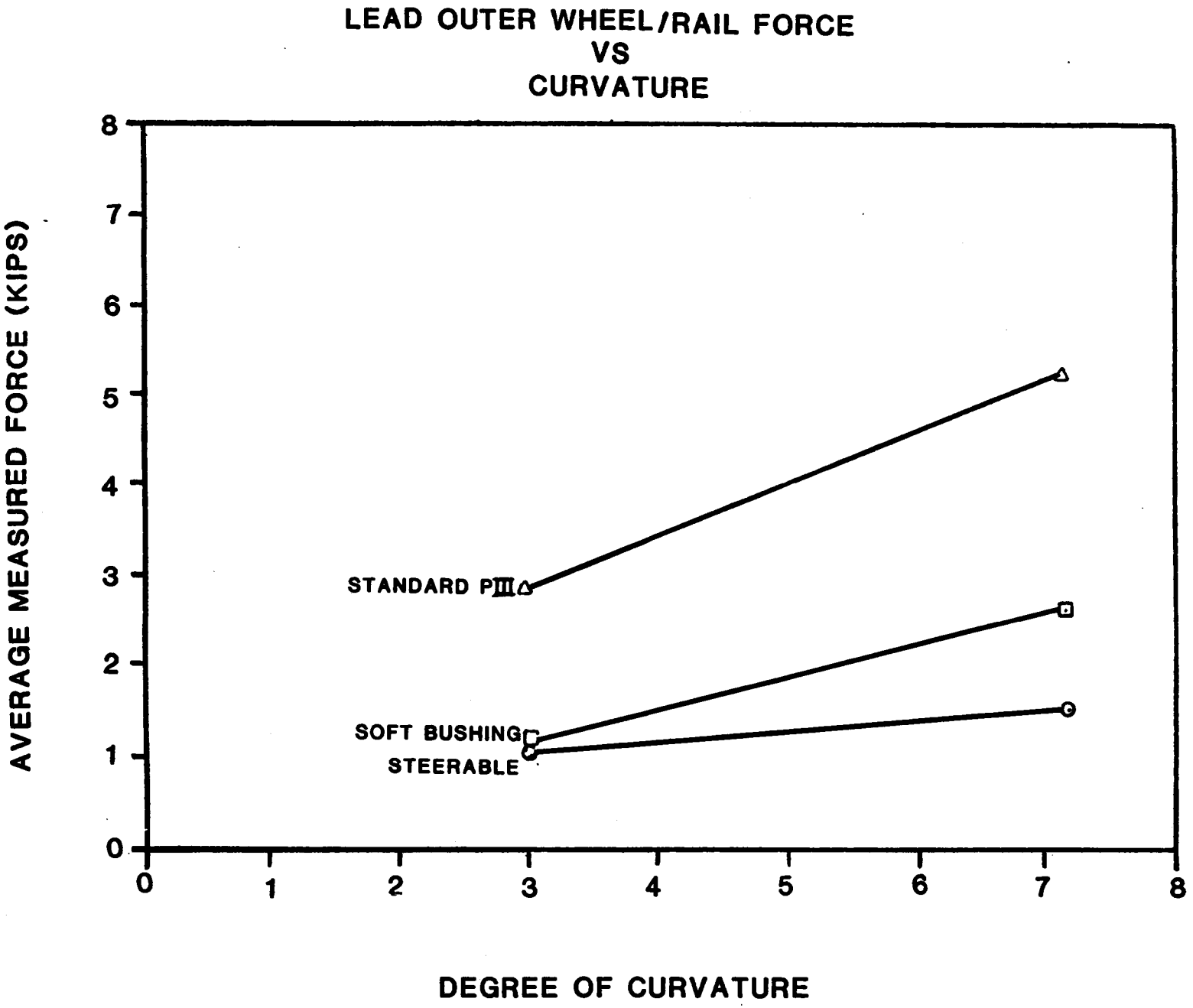

Figure 6-8: LEAD OUTER WHEEL FORCE VS CURVATURE

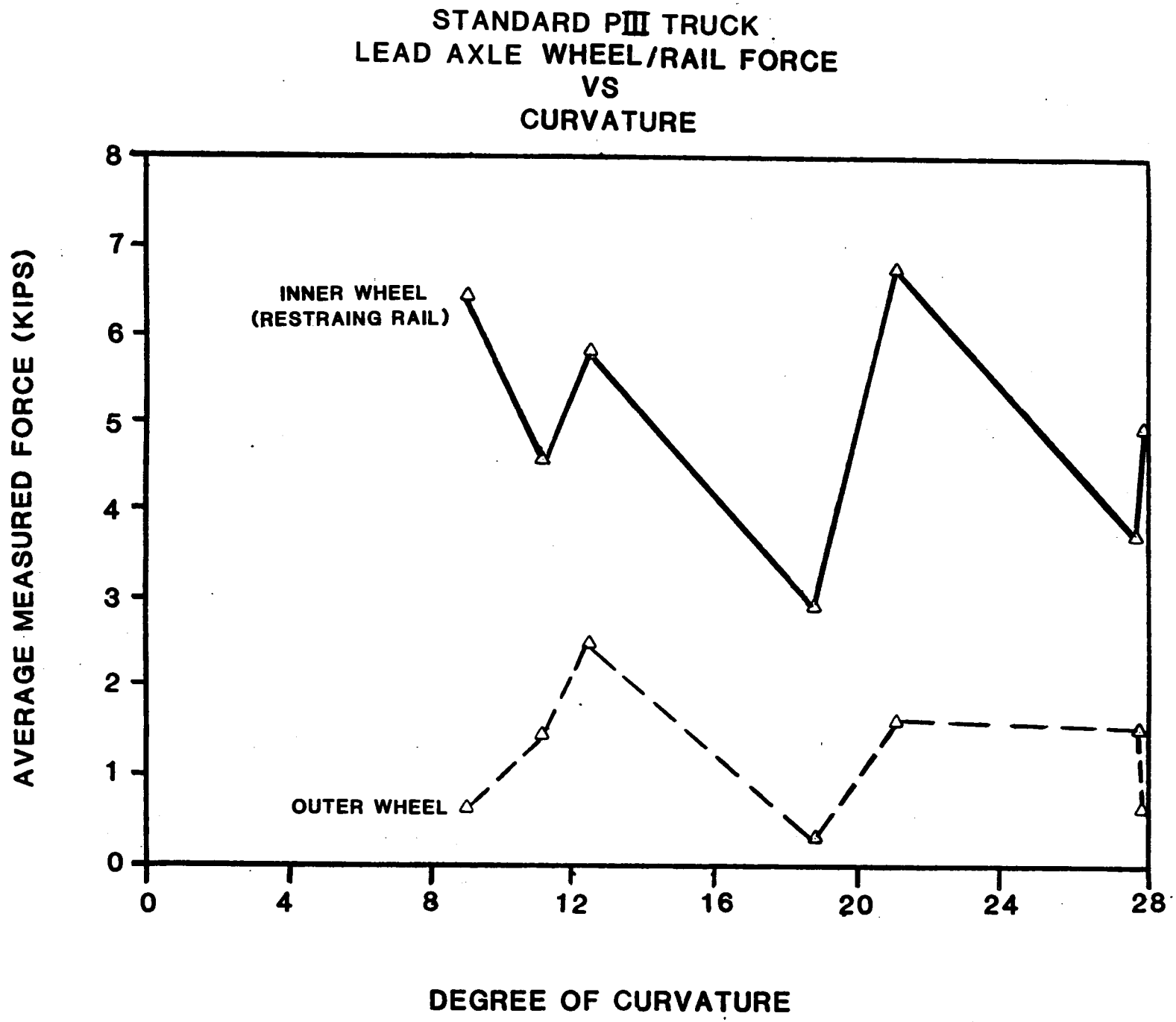

Figure 6-9: STANDARD PIII TRUCK, WHEEL FORCE VS CURVATURE

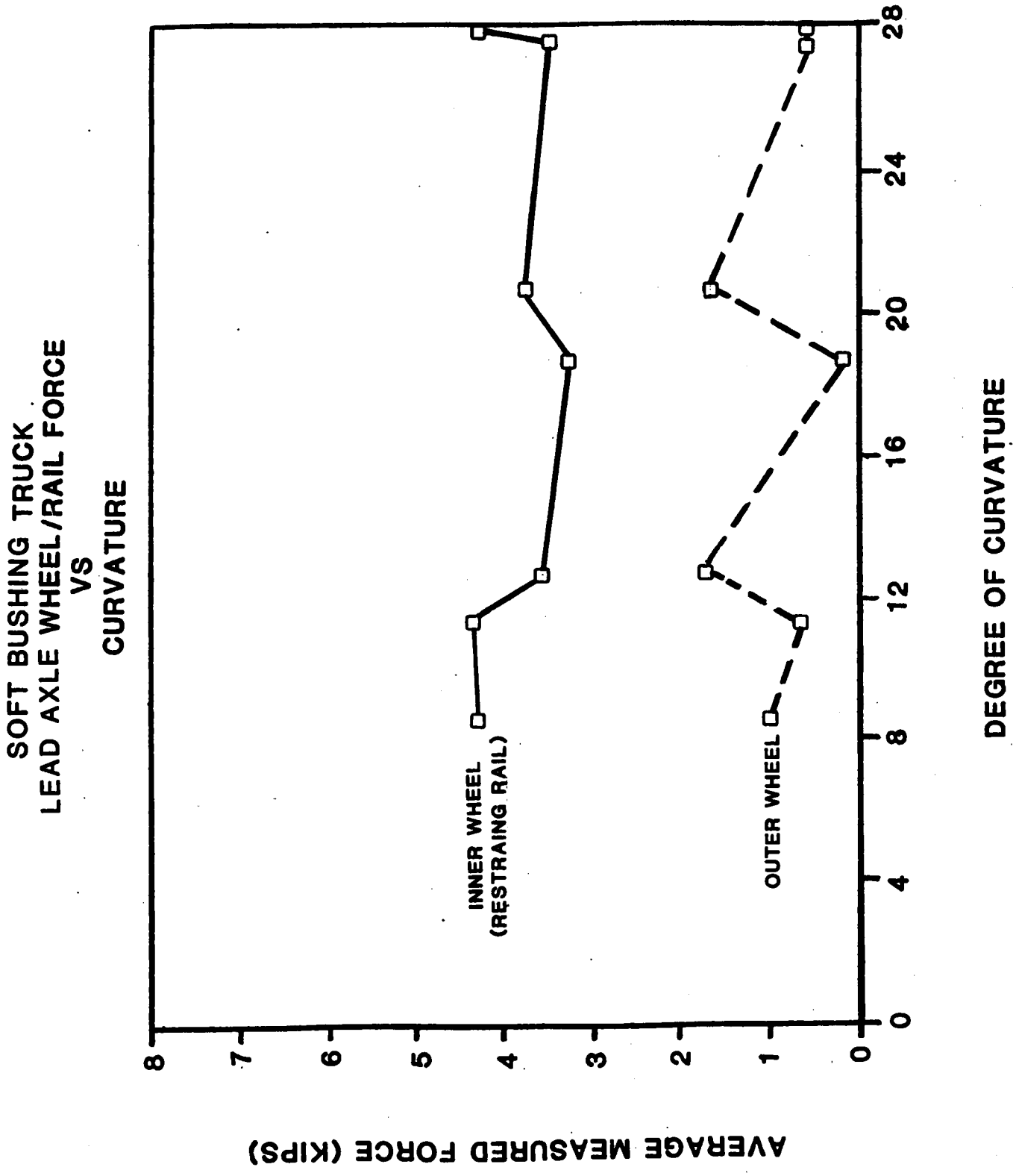

Figure 6-10: SOFT BUSHING TRUCK, WHEEL FORCE VS CURVATURE

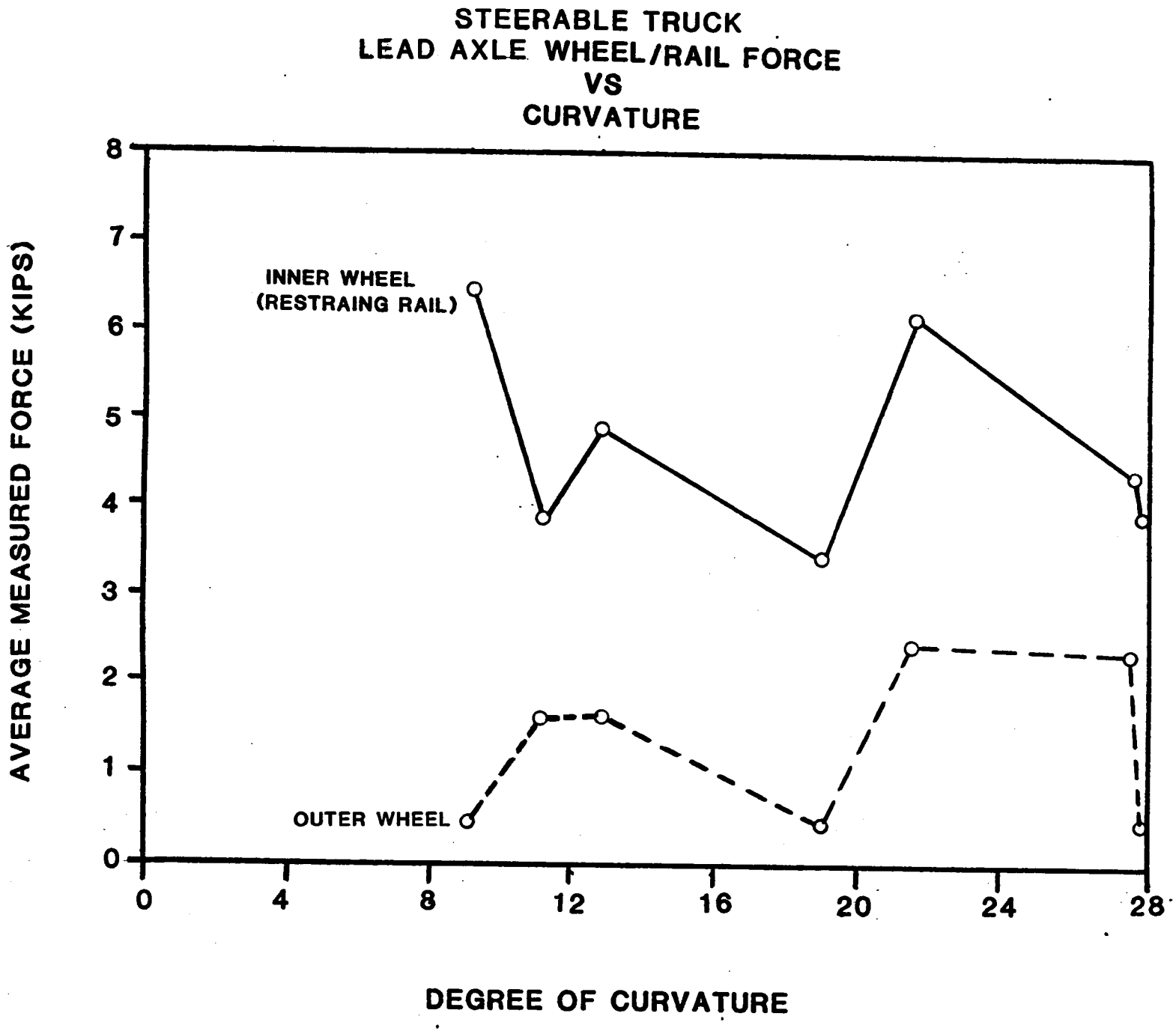

Figure 6-11: STEERABLE TRUCK, WHEEL FORCE VS CURVATION

truck showed a more uniform inner wheel force versus curvature than the standard or steerable truck. The most probable explanation for these results is that the soft bushing primary lateral suspension stiffness is considerably lower than that of the standard P-III or steerable truck. Keep in mind that the steerable truck uses the same unbonded rubber shock ring that is used on the standard P-III truck.

The steerable truck showed minimal improvement when compared to the standard truck negotiating curves with restraining rail. It should be mentioned that restraining rail and rail lubricators would be unnecessary if the entire fleet had steerable trucks.

6.4 Truck Vibration Measurements

Lateral and vertical acceleration measurements were made on both the journal bearing and side frame for one complete roundtrip and for each truck configuration. The data was thoroughly reviewed and shows that the PATCO track system is well maintained and is generally void of irregularities that can cause significant truck disturbances. As one of the few areas that did produce a disturbance, the crossover near Collingswood Station was selected for comparitive shock analysis. This involved comparing the peak to peak acceleration level due to impact for each truck configuration at the crossover. The data shows that the soft bushing design can significantly reduce the truck frame vibration due to impact in both the lateral and vertical directions on the order of 50 percent.

A frequency spectrum analysis was also performed by feeding the raw acceleration signals that were recorded on magnetic tape to a frequency spectrum analyzer. The analyzed data represented 65 seconds of real time operation from Collingswood to Ferry Avenue. The output was root mean square acceleration level (rms) as a function of frequency.

The vertical journal acceleration data shows little difference between truck configurations up to a frequency of about 10 Hz with the maximum value of about 0.11 g'rms occuring at 1.2 Hz. However, above 10 Hz the soft bushing truck shows significant reductions, while the steerable truck shows only slight reductions when compared to the baseline truck. The vertical response of the journal for the soft bushing truck was essentially flat above 30 Hz.

The vertical side frame acceleration data also shows very little difference between truck configurations up to about 10 Hz. Above 10 Hz, the soft bushing truck shows a sizeable reduction, while the steerable truck shows an increase when compared to the baseline truck. The vertical response of the side frame for the soft bushing truck was essentially flat above 50 Hz.

The lateral journal acceleration data shows a relatively flat

response for all configurations above their peaks, which all occur around 1.5 Hz.

The lateral side frame acceleration data shows that the soft bushing response is essentially flat above 25 Hz when compared to the standard and steerable truck configurations.

In summary, the acceleration data shows very little difference between the standard truck and the steerable truck because both configurations use the same rubber shock ring for their primary suspension elements. However, the soft bushing data shows significant reductions in the truck frame vibration environment which can prolong the service life of frame mounted equipment.

6.5 Truck Rotational Resistance

The rotational resistance of the Budd P-III truck is primarily a function of the frictional characteristics of the side bearings used. Since PATCO is currently using side bearings manufactured by two different sources, it was decided to determine their frictional differences. The first bearing is known as Gatke and consists of a teflon fabric surface that is impregnated with phenolic resin. The second bearing is known as Dayco and consists of a homogeneous ultra high molecular weight polyethylene. The rotational resistance torque developed by these side bearings between the truck frame and carbody bolster was measured using a pair of instrumented carbody radius rods. The radius rods were equipped with full strain gauge bridge circuits calibrated for tension and compression force measurements which were then converted to torques and equivalent side bearing friction coefficients.

The results of these measurements are shown below for tests using new and worn Gatke pads and worn Dayco pads.

Side Bearing	Secondary Yaw Breakaway Torque (ft-lbs)	Friction Coefficients
Gatke - new	6,800	.123
Gatke - worn	3,600	.065
Dayco - worn	3,800	.069

These tests clearly show that the Gatke and Dayco pads have similar frictional characteristics after being service worn. The data also shows that the Gatke pad goes thru a break-in period starting from a new "resin rich surface" to a service worn surface with a lower friction coefficient. These breakaway torque levels are consistent with good design practice that ensures both high speed truck yaw stability margins and good low speed curving performance.

6.6 Carbody Ride Quality

Carbody ride quality was evaluated using five floor mounted accelerometers. The raw data signals were fed to a frequency spectrum analyzer which produced an output of acceleration in g's rms versus frequency in Hertz. The analyzed data represented 65 seconds of realtime operation between Collingswood and Ferry Avenue. The results show that there was very little difference in ride quality between the three different truck configurations. This was expected since ride quality is primarily a function of the secondary suspension system performance in trucks with this range of primary suspension stiffnesses.

7.0 Wayside Vibration Measurements

7.1 Test Objective and Description

The purpose of this test series was to determine the affect that the three different truck configuraitons would have on induced wayside vibrations. During this test series, the steerable trucks were mounted under Car #114 which was coupled to Car #102, which was equipped with standard trucks. The soft bushing trucks were mounted under Car #284, which was coupled to Car #283, which was equiped with standard trucks. Additional married pairs equipped with standard trucks included Cars #263 and #264; Cars #273 and #274, and Cars #291 and #292. Wayside vibrations measurements were made at six different sites as the above mentioned married pairs traveled by in approximately ten minute intervals during scheduled revenue service.

7.2 Instrumentation

Two accelerometers were mounted at each consecutive site in the lateral and vertical plane. The accelerometers were made by Setra Systems, Inc. type 114 with a 0 - 2g range. The raw signal was conditioned by Gould DC amplifiers and recorded on a Gould 4-channel Brush recorder for immediate viewing and also recorded on a 16-channel, Sabre VI, magnetic tape recorder for post processing and permanent record. The data was recorded at 7 1/2 inches per sec in the FM mode on magnetic tape, which permitted maximum frequency response of the accelerometers (140 Hertz).

7.3 Wayside Site Description

The six wayside measurement sites are described below and are also referenced on the PATCO track chart given in Appendix A.

Site 1 Accelerometers were mounted on the west end of the concrete viaduct near Westmont Station alongside the westbound track.

Site 2 Accelerometers were mounted on a concrete equipment support pillar in the roadbed beside the westbound track about 35 feet west of the concrete viaduct described in Site 1.

Site 3 Accelerometers were mounted on a concrete equipment pillar in the roadbed beside the eastbound track directly across from the switch at Wood Interlock.

Site 4 Accelerometers were mounted directly to the concrete roof of an unused pedestrian underpass located between Ferry Avenue Station and Whitman Avenue underpass. The concrete test section was alongside the eastbound track and under approximately 18 inches

of ballasted roadbed.

Site 5 Accelerometers were mounted directly to the concrete floor alongside the westbound track at the western most end of the Mickel Street tunnel. This is the 800 feet radius curve that was used for computer modelling and extensive vehicle testing.

Site 6 Accelerometers were mounted on a concrete ground strap support block about 50 feet west of site 5 alongside the westbound track.

7.4 Test Results

The data gathered indicates that individual site characteristics have a much greater influence on wayside vibration characteristics than do the different truck configurations. Each site had its own vertical and lateral natural frequencies and damping factors. The viaduct site 1, for example, with a natural frequency of approximately 150 Hz was very much underdamped. Site 4, however, had a natural frequency of about 10 Hz with considerable damping. The remaining sites were generally somewhere within this range. Sites 1 and 5 did not produce data that was useful. Structural vibration levels completely overpowered any relative differences between the various truck configurations.

The remaining 4 sites did produce data where some comparison was possible. At each of these sites, it was possible to determine when each truck and or axle of each car passed over the measurement site. For each car that passed by, either the peak g's per axle or the peak to peak g's per truck were tabulated and averaged on a per car basis. This data is summarized in Table 7-1.

Analysis of the data in Table 7-1 indicates that the different truck configurations do influence wayside vibration. The soft bushing truck configuration shows a slightly lower vibration level than the standard and steerable truck. To get a better quantitative measure of the affects of the different truck configurations will require additional refinement of the test conditions. These refinements include using accelerometers similar to those used for seismic measurements. Also, test only when all cars in the consist have the same truck configuration. It is recommended that this test series be repeated in the future when PATCO has equipped ten additional cars with soft bushings. Ideally, the test should be conducted using six car trains.

	TRUCK CONFIGURATION		
SITE	STANDARD P-III	SOFT BUSHING	STEERABLE
Site 2 Vertical	.037 g	.035 g	.047 g
Lateral	.149 g	.100 g	.146 g
Site 3 Vertical	.162 g	.124 g	.144 g
Lateral	.243 g	.210 g	.215 g
Site 4 Vertical	.042 g	.036 g	.048 g
Lateral	N/A	N/A	N/A
Site 6 Vertical	.058 g	.038 g	.047 g
Lateral	.098 g	.132 g	.079 g

TABLE 7-1: AVERAGE WAYSIDE VIBRATION LEVEL COMPARISON

8.0 Conclusions

- The soft bushing equipped trucks and the steerable axle trucks have demonstrated significant reductions in lateral wheel/rail forces while negotiating PATCO curves without restraining rail.

- The soft bushing equipped trucks also demonstrated significant reductions in lateral wheel/rail forces while negotiating PATCO curves equipped with restraining rail.

- The steerable axle trucks demonstrated slight reductions in lateral wheel/rail forces while negotiating PATCO curves equipped with restraining rail. Note that a fleet of steerable axle trucks would eliminate the need for restraining rail and rail gauge lubricators.

- Restraining rail significantly reduces the lateral force between the lead outer wheel and rail on sharp curves.

- The soft bushing suspension reduced the truck frame vibration environment.

- Carbody ride quality was essentially the same for the three different truck configurations.

- The soft bushing equipped trucks and the steerable axle trucks produced less curving noise than the standard truck. However, on curves that were heavily lubricated, the noise level difference was minimal.

- Analytical studies using the Budd computer model and classical wheel/rail friction versus creepage theory can accurately predict steady state curving conditions which are in agreement with the average measured values.

- Measured wheel/rail force data indicates that the forces oscillate with significant differences between the peaks and valleys and at various frequencies.

- Using modified wheel/rail friction versus creepage characteristics, the Budd computer model was able to predict force oscillations with varying amplitudes and frequencies.

- The groundborne vibration data showed that the soft bushing truck reduced vertical vibrations transmitted to the wayside.

9.0 Recommendations

- Continue monitoring the steerable and soft bushing trucks at PATCO to accurately determine the service mileage between required wheel turnings.

- Determine if soft suspension bushings installed in the prototype steerable axle truck can further improve its performance.

- Continue analytical studies with modified wheel/rail friction versus creepage characteristics to more accurately predict measured wheel/rail force oscillations.

- Continue analytical studies to refine methods for inputing rail geometry measured in six to ten inch increments.

- Perform groundborne wayside vibration measurements at PATCO using six car trains; one train equipped with standard trucks and the other with trucks equipped with soft bushings when installed.

APPENDIX "A"

PORT AUTHORITY TRANSIT CORPORATION

CONDENSED PROFILE

16th AND LOCUST ST.

PHILADELHIA, PENNA.

TO

LINDENWOLD, NEW JERSEY

SYMBOL CODES:-


= MILE POST MARKERS


= CURVE NUMBERS
REFERENCE SECTION 6.3


= WAYSIDE VIBRATION SITES

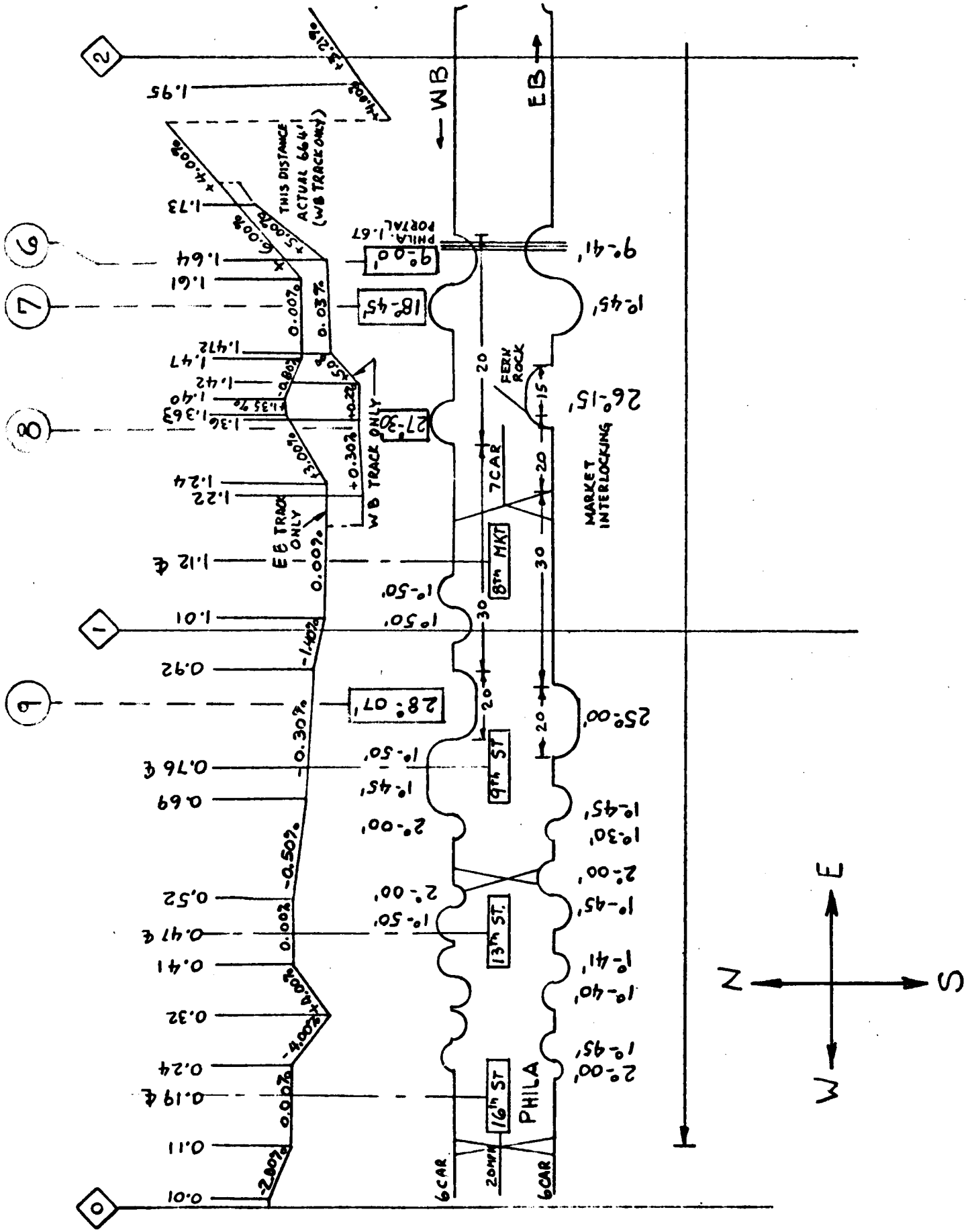
WB
EB
THIS DISTANCE ACTUAL 664'
(WB TRACK ONLY)
PHILA. PORTAL
WB TRACK ONLY
EB TRACK ONLY
FERN ROCK
MARKET INTERLOCKING
7CAR
8th MKT
9th ST
13th ST.
16th ST
PHILA
6CAR
20MH
6CAR
N
S
E
W

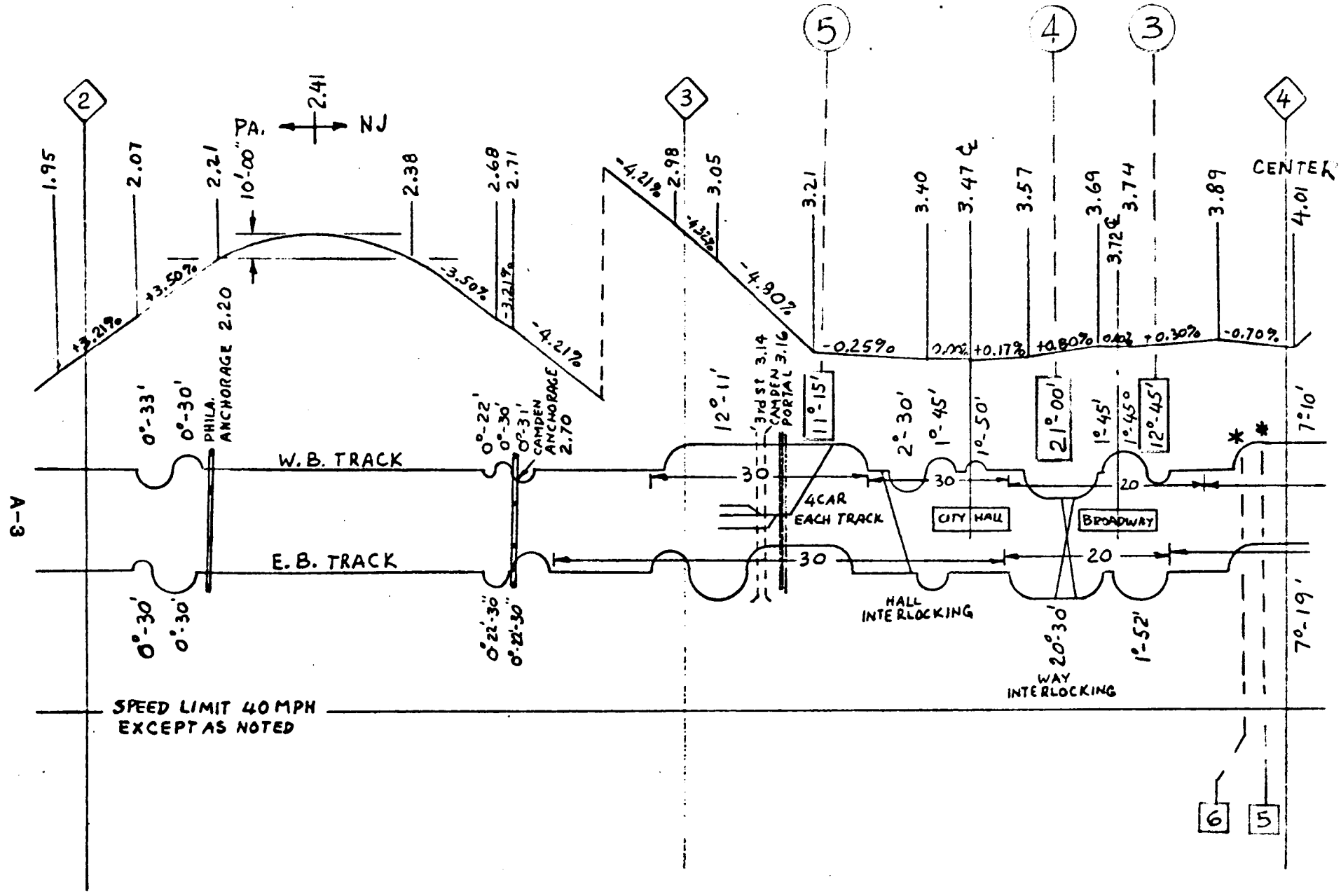
2
3
5
4
3
4
PA.
NJ
2.41
10'-00"
1.95
2.07
2.21
2.38
2.68
2.71
2.98
3.05
3.21
3.40
3.47 ℄
3.57
3.69
3.72 ℄
3.74
3.89
4.01
CENTER
+3.21%
+3.50%
-3.50%
-3.21%
-4.21%
-4.21%
-4.30%
-4.90%
-0.25%
0.0%
+0.17%
+0.80%
0.0%
+0.30%
-0.70%
PHILA. ANCHORAGE 2.20
CAMDEN ANCHORAGE 2.70
3rd St 3.14
CAMDEN PORTAL 3.16
0°-33'
0°-30'
0°-22'
0°-30'
0°-31'
12°-11'
11°-15'
2°-30'
1°-45'
1°-50'
21°-00'
1°-45'
1°-45°
12°-45'
7°-10'
W.B. TRACK
E.B. TRACK
30
30
20
20
4 CAR EACH TRACK
CITY HALL
BROADWAY
HALL INTERLOCKING
20°-30'
WAY INTERLOCKING
1°-52'
7°-19'
0°-30'
0°-30'
0°22'-30"
0°22'-30"
SPEED LIMIT 40 MPH EXCEPT AS NOTED
A-3
6
5

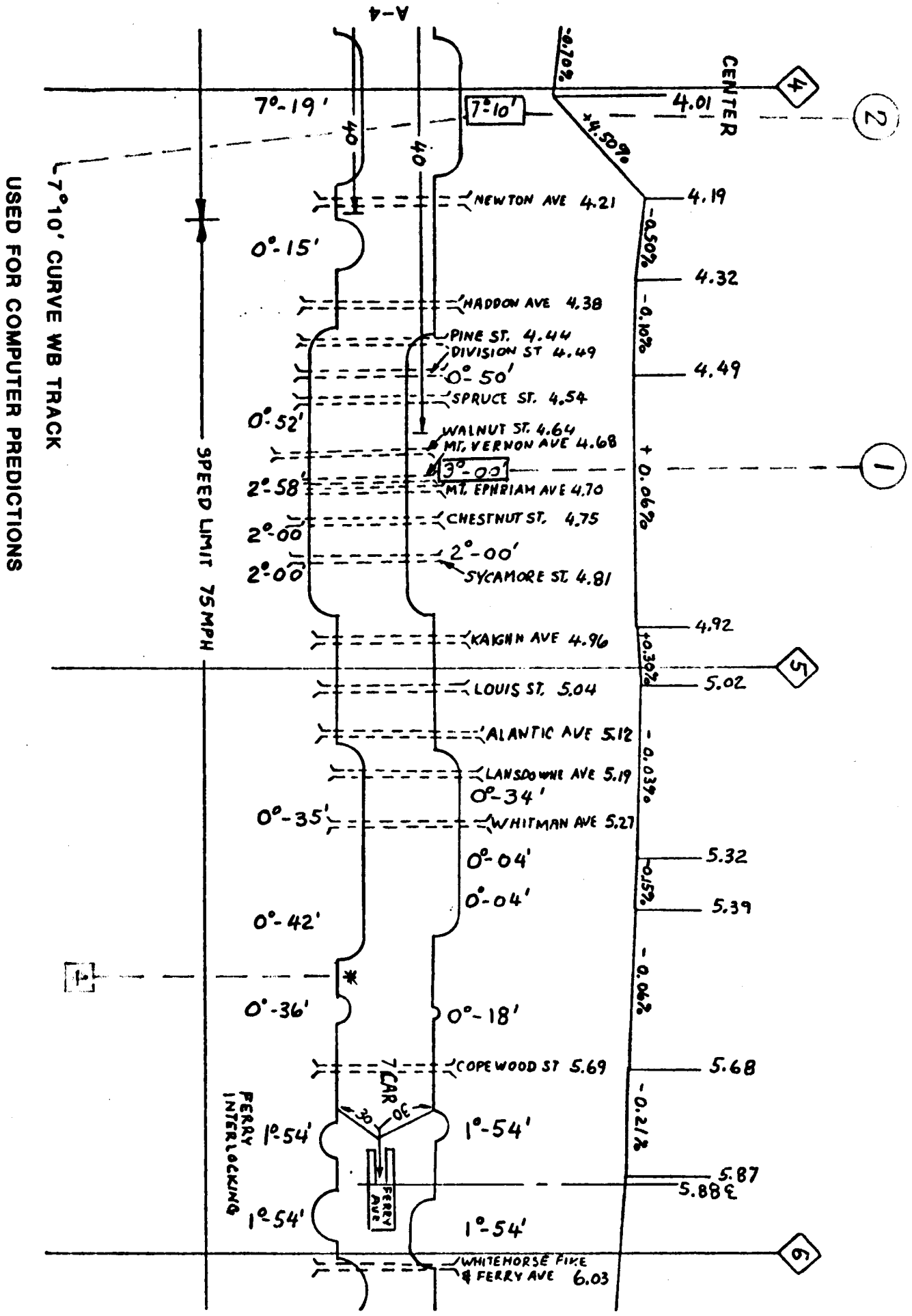

USED FOR COMPUTER PREDICTIONS

5.88℄
1°-54'
FERRY AVE
1°-54'
6
WHITEHORSE FIKE & FERRY AVE 6.03
1°-05'
-0.30%
CRESCENT BLVD 6.18
1°-07'
0°-33'
6.25
0°-04'
+1.50%
0°-02'
6.42
BROWNING ROAD 6.49
ZANE AVE 6.75
+0.10%
7
COLLINS AVE 7.11
7.17
+0.12%
7.29
0°47'
LEES AVE 7.37
+0.25%
1°-15'
COLLINGWOOD
7.49℄
HOMESTEAD AVE 7.59
0°-47'
CONRAD AVE 7.65
END OF VIADUCT
7.44-7.54
CUTHBERT ROAD 7.87
7.88
-1.00%
8
8.06
SPEED LIMIT-75 MPH

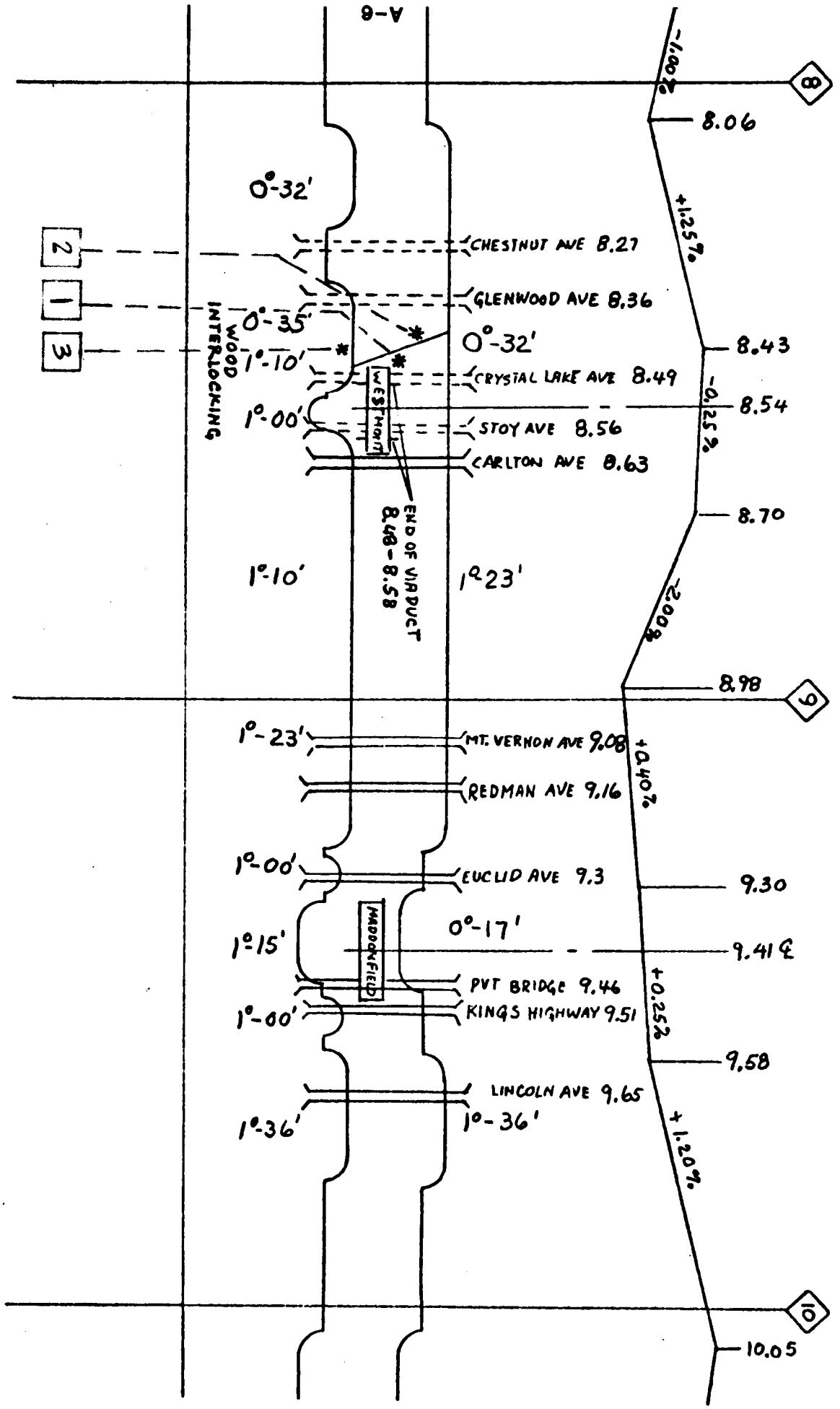
A-6
8
9
10
8.06
-1.00%
+1.25%
8.43
-0.25%
8.54
8.70
-2.00%
8.98
+0.40%
9.30
9.41 ℄
+0.25%
9.58
+1.20%
10.05
CHESTNUT AVE 8.27
GLENWOOD AVE 8.36
CRYSTAL LAKE AVE 8.49
STOY AVE 8.56
CARLTON AVE 8.63
MT. VERNON AVE 9.08
REDMAN AVE 9.16
EUCLID AVE 9.3
PVT BRIDGE 9.46
KINGS HIGHWAY 9.51
LINCOLN AVE 9.65
0°-32'
0°-35'
1°-10'
1°-00'
1°-10'
1°23'
0°-32'
1°-23'
1°-00'
1°15'
0°-17'
1°-00'
1°-36'
1°-36'
2
1
3
WOOD INTERLOCKING
WESTHOFF
END OF VIADUCT 8.48-8.58
MADDOX FIELD

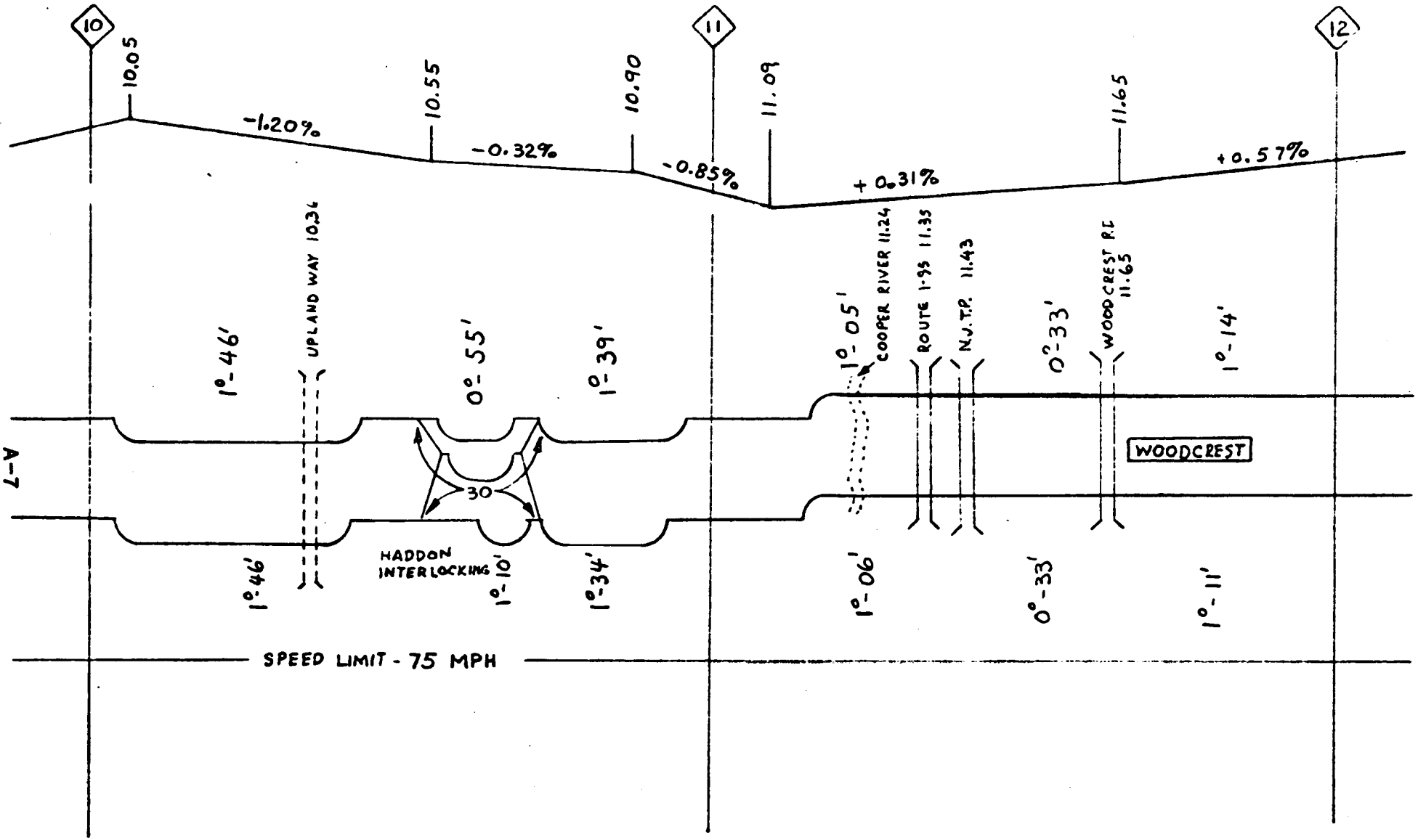
10
10.05
-1.20%
10.55
-0.32%
10.90
-0.85%
11
11.09
+0.31%
11.65
+0.57%
12
1°-46'
UPLAND WAY 10.34
0°-55'
1°-39'
1°-05'
COOPER RIVER 11.24
ROUTE 1-95 11.35
N.J.T.P. 11.43
0°-33'
WOODCREST R.E. 11.65
1°-14'
WOODCREST
A-7
30
HADDON INTERLOCKING
1°-46'
1°-10'
1°-34'
1°-06'
0°-33'
1°-11'
SPEED LIMIT - 75 MPH

14
13
12
14.02
13.83
13.51
13.22
12.96
12.76
12.60 ℄
12.53
12.31
0.00%
-0.35%
-1.00%
0.45%
0.00%
0.55%
+1.00%
SOMERDALE ROAD 13.2
EVESHAM AVE 13.54
ASHLAND
SPEED LIMIT-75MPH
0°-19'
0°-19'
10°-05'
9°-06'
0°-43'
10°-09'
0°-19'
0°-51'
0°-19'
0°-43'
0°-59'
10°-00'

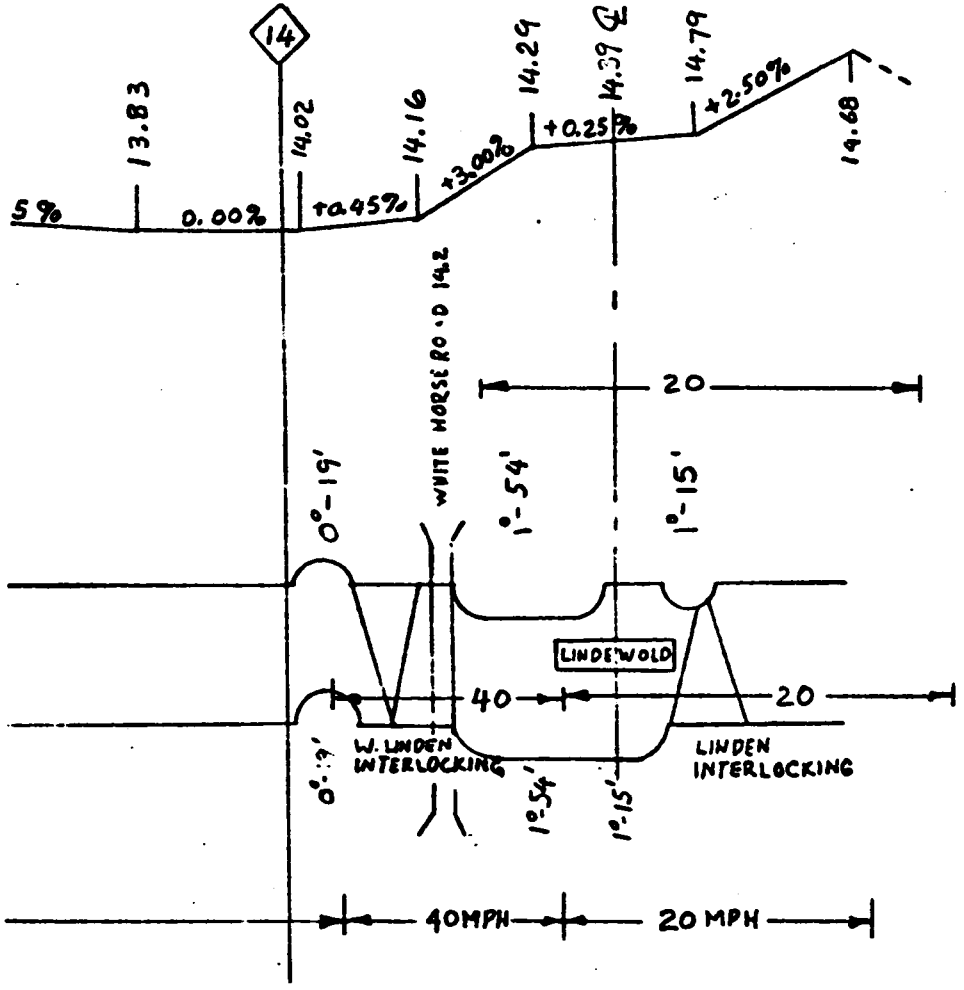
14
13.83
14.02
14.16
14.29
14.39 ℄
14.79
14.68
5%
0.00%
+4.45%
+3.00%
+0.25%
+2.50%
WHITE HORSE RD. 0.142
20
0°-19'
1°-54'
1°-15'
LINDENWOLD
40
20
W. LINDEN INTERLOCKING
LINDEN INTERLOCKING
40MPH
20 MPH

APPENDIX B

COMPUTER MODEL INPUT DATA

FOR STANDARD P-III TRUCK

TITLE CARDS
JANUARY 3,1985 RUN 7
STANDARD P-III TRUCK- PATCO
CURVING PERFORMANCE THRU 4 SEC SPIRAL AND 7 DEG 10 MIN CURVE
40 MPH
INITIALLY CENTERED ON TANGENT TRACK
WORN WHEEL PROFILE
.5 MAX FRICTION COEF. - SATURATION
FULL KALKER COEF.

SPIRAL OR OTHER DYNAMIC TRACK INPUT.
SEE DYNECHO FILE FOR LISTING OF DATA READ FROM DYNFILE.

ACCELERATION OF GRAVITY, CURVE CONSTANT
386.4 6.880E 04

VEHICLE SPEED, DEGREE OF CURVE, HALF WHEEL TREAD, WHEEL RADIUS
704.0 7.166 29.50 14.00

MAXIMUM NUMBER OF INTERFACES, DERIVATIVES,
DIMENSIONS, DEGREES OF FREEDOM, FIRST TRUE PART,
MAXIMUM NUMBER OF PARTS
35 2 35 6 5 10

INITIAL, MINIMUM, MAXIMUM STEP SIZES, MAXIMUM TIME , PRINT STEP SIZE, PLOT STEP SIZE
2.000E-04 2.000E-04 1.000E-02 12.00 1.000 5.000E-02

MAX ALLOWABLE DIFFERENCES PER STEP, EACH PART, DEGREE OF FREEDOM, AND DERIVATIVE

8.000E-03	8.000E-03	8.000E-03	2.000E-03	2.000E-03	2.000E-03
500.0	500.0	500.0	2.000E-02	2.000E-02	2.000E-02
8.000E-03	8.000E-03	8.000E-03	2.000E-03	2.000E-03	2.000E-03
500.0	500.0	500.0	2.000E-02	2.000E-02	2.000E-02
8.000E-03	8.000E-03	8.000E-03	2.000E-03	2.000E-03	2.000E-03
500.0	500.0	500.0	2.000E-02	2.000E-02	2.000E-02
8.000E-03	8.000E-03	8.000E-03	2.000E-03	2.000E-03	2.000E-03
500.0	500.0	500.0	2.000E-02	2.000E-02	2.000E-02
1.000E-03	1.000E-03	1.000E-03	2.000E-04	2.000E-04	2.000E-04
1.000E-02	1.000E-02	1.000E-02	1.000E-03	1.000E-03	1.000E-03
1.000E-03	1.000E-03	1.000E-03	2.000E-04	2.000E-04	2.000E-04
1.000E-02	1.000E-02	1.000E-02	1.000E-03	1.000E-03	1.000E-03
1.000E-03	1.000E-03	1.000E-03	2.000E-04	2.000E-04	2.000E-04
1.000E-02	1.000E-02	1.000E-02	1.000E-03	1.000E-03	1.000E-03
1.000E-03	1.000E-03	1.000E-03	2.000E-04	2.000E-04	2.000E-04
1.000E-02	1.000E-02	1.000E-02	1.000E-03	1.000E-03	1.000E-03
1.000E-03	1.000E-03	1.000E-03	2.000E-04	2.000E-04	2.000E-04
1.000E-02	1.000E-02	1.000E-02	1.000E-03	1.000E-03	1.000E-03
1.000E-03	1.000E-03	1.000E-03	2.000E-04	2.000E-04	2.000E-04
1.000E-02	1.000E-02	1.000E-02	1.000E-03	1.000E-03	1.000E-03

NUMBER OF POINTS TO PLOT, PLOT CONTROL
10 1

PLOT ARRAY DATA
TYPE, INDICES(3), INCREMENT PER DIVISION, REFERENCE VALUE, PLOT CHARACTER

3.000	14.000	1.000	1.000	.100	.000	A	WHEEL/RAIL POSITION,RIGHT FRONT WHEEL
3.000	16.000	1.000	1.000	.100	.000	B	WHEEL/RAIL POSITION,RIGHT REAR WHEEL
3.000	14.000	4.000	1.000	.005	.000	X	ANGLE OF ATTACK,FRONT AXLE
3.000	16.000	4.000	1.000	.005	.000	Y	ANGLE OF ATTACK,REAR AXLE
4.000	5.000	13.000	1.000	2000.000	.000	F	LATERAL FORCE, LEFT FRONT WHEEL
4.000	5.000	14.000	1.000	2000.000	.000	E	LATERAL FORCE, RIGHT FRONT WHEEL
4.000	5.000	14.000	2.000	1000.000	.000	C	CREEP FORCE, RIGHT FRONT WHEEL
4.000	5.000	13.000	2.000	1000.000	.000	D	CREEP FORCE, LEFT FRONT WHEEL
4.000	5.000	14.000	3.000	5000.000	.000	G	VERTICAL FORCE, RIGHT FRONT WHEEL
4.000	8.000	27.000	2.000	1000.000	.000	V	LONG. FORCE, RIGHT SIDE BEARER

PRINT CONTROL DATA
7 6 5 4 3 0 0 0 0 0

```
 INTERFACE NUMBER      1
 INTERFACE TYPE      1 BETWEEN PARTS      1 AND      5
 THE SPRING AND DASHPOT GROUP IS      1.  THE INTERFACE IS IN COORDINATE SYSTEM      1

 INTERFACE NUMBER      2
 INTERFACE TYPE      1 BETWEEN PARTS      1 AND      6
 THE SPRING AND DASHPOT GROUP IS      1.  THE INTERFACE IS IN COORDINATE SYSTEM      1

 INTERFACE NUMBER      3
 INTERFACE TYPE      1 BETWEEN PARTS      1 AND      7
 THE SPRING AND DASHPOT GROUP IS      1.  THE INTERFACE IS IN COORDINATE SYSTEM      1

 INTERFACE NUMBER      4
 INTERFACE TYPE      1 BETWEEN PARTS      1 AND      8
 THE SPRING AND DASHPOT GROUP IS      1.  THE INTERFACE IS IN COORDINATE SYSTEM      1

 INTERFACE NUMBER      5
 INTERFACE TYPE      1 BETWEEN PARTS      1 AND      9
 THE SPRING AND DASHPOT GROUP IS      1.  THE INTERFACE IS IN COORDINATE SYSTEM      1

 INTERFACE NUMBER      6
 INTERFACE TYPE      1 BETWEEN PARTS      1 AND     10
 THE SPRING AND DASHPOT GROUP IS      1.  THE INTERFACE IS IN COORDINATE SYSTEM      1

 INTERFACE NUMBER      7
 INTERFACE TYPE      2 BETWEEN PARTS      1 AND      5
 THE SPRING AND DASHPOT GROUP IS      1.  THE INTERFACE IS IN COORDINATE SYSTEM      1

 INTERFACE NUMBER      8
 INTERFACE TYPE      2 BETWEEN PARTS      1 AND      6
 THE SPRING AND DASHPOT GROUP IS      1.  THE INTERFACE IS IN COORDINATE SYSTEM      1

 INTERFACE NUMBER      9
 INTERFACE TYPE      2 BETWEEN PARTS      1 AND      7
 THE SPRING AND DASHPOT GROUP IS      1.  THE INTERFACE IS IN COORDINATE SYSTEM      1

 INTERFACE NUMBER     10
 INTERFACE TYPE      2 BETWEEN PARTS      1 AND      8
 THE SPRING AND DASHPOT GROUP IS      1.  THE INTERFACE IS IN COORDINATE SYSTEM      1

 INTERFACE NUMBER     11
 INTERFACE TYPE      2 BETWEEN PARTS      1 AND      9
 THE SPRING AND DASHPOT GROUP IS      1.  THE INTERFACE IS IN COORDINATE SYSTEM      1

 INTERFACE NUMBER     12
 INTERFACE TYPE      2 BETWEEN PARTS      1 AND     10
 THE SPRING AND DASHPOT GROUP IS      1.  THE INTERFACE IS IN COORDINATE SYSTEM      1

 INTERFACE NUMBER     13
 INTERFACE TYPE      6 BETWEEN PARTS      2 AND      5
 THE SPRING AND DASHPOT GROUP IS      1.  THE INTERFACE IS IN COORDINATE SYSTEM      1
 THE DISTANCES (X,Y,Z) FROM THE FIRST AND SECOND PARTS TO THE INTERFACE ARE:
  -1       0       2      -3       5      -6
 INTERFACE CLEARANCES X,XDOT,Y,YDOT,Z,ZDOT
9.000       9.000       9.000       9.000       9.000       9.000

 INTERFACE NUMBER     14
 INTERFACE TYPE      6 BETWEEN PARTS      2 AND      5
 THE SPRING AND DASHPOT GROUP IS      1.  THE INTERFACE IS IN COORDINATE SYSTEM      1
 THE DISTANCES (X,Y,Z) FROM THE FIRST AND SECOND PARTS TO THE INTERFACE ARE:
   1       0       2       4       5      -6
 INTERFACE CLEARANCES X,XDOT,Y,YDOT,Z,ZDOT
9.000       9.000       9.000       9.000       9.000       9.000

 INTERFACE NUMBER     15
 INTERFACE TYPE      6 BETWEEN PARTS      3 AND      6
 THE SPRING AND DASHPOT GROUP IS      1.  THE INTERFACE IS IN COORDINATE SYSTEM      1
 THE DISTANCES (X,Y,Z) FROM THE FIRST AND SECOND PARTS TO THE INTERFACE ARE:
  -1       0       2      -4      -5      -6
 INTERFACE CLEARANCES X,XDOT,Y,YDOT,Z,ZDOT
9.000       9.000       9.000       9.000       9.000       9.000

 INTERFACE NUMBER     16
 INTERFACE TYPE      6 BETWEEN PARTS      3 AND      6
 THE SPRING AND DASHPOT GROUP IS      1.  THE INTERFACE IS IN COORDINATE SYSTEM      1
 THE DISTANCES (X,Y,Z) FROM THE FIRST AND SECOND PARTS TO THE INTERFACE ARE:
   1       0       2       3      -5      -6
 INTERFACE CLEARANCES X,XDOT,Y,YDOT,Z,ZDOT
9.000       9.000       9.000       9.000       9.000       9.000
```

```
  INTERFACE NUMBER     17
  INTERFACE TYPE       3 BETWEEN PARTS     5 AND      7
  THE SPRING AND DASHPOT GROUP IS     2.  THE INTERFACE IS IN COORDINATE SYSTEM     1
  THE DISTANCES (X,Y,Z) FROM THE FIRST AND SECOND PARTS TO THE INTERFACE ARE:
    -7        5      -10        0       11      -12
  INTERFACE CLEARANCES X,XDOT,Y,YDOT,Z,ZDOT
9.000        9.000        9.000        9.000        9.000        9.000

  INTERFACE NUMBER     18
  INTERFACE TYPE       3 BETWEEN PARTS     5 AND      8
  THE SPRING AND DASHPOT GROUP IS     2.  THE INTERFACE IS IN COORDINATE SYSTEM     1
  THE DISTANCES (X,Y,Z) FROM THE FIRST AND SECOND PARTS TO THE INTERFACE ARE:
     8        5      -10        0       11      -12
  INTERFACE CLEARANCES X,XDOT,Y,YDOT,Z,ZDOT
9.000        9.000        9.000        9.000        9.000        9.000

  INTERFACE NUMBER     19
  INTERFACE TYPE       3 BETWEEN PARTS     6 AND      7
  THE SPRING AND DASHPOT GROUP IS     2.  THE INTERFACE IS IN COORDINATE SYSTEM     1
  THE DISTANCES (X,Y,Z) FROM THE FIRST AND SECOND PARTS TO THE INTERFACE ARE:
    -8       -5      -10        0      -11      -12
  INTERFACE CLEARANCES X,XDOT,Y,YDOT,Z,ZDOT
9.000        9.000        9.000        9.000        9.000        9.000

  INTERFACE NUMBER     20
  INTERFACE TYPE       3 BETWEEN PARTS     6 AND      8
  THE SPRING AND DASHPOT GROUP IS     2.  THE INTERFACE IS IN COORDINATE SYSTEM     1
  THE DISTANCES (X,Y,Z) FROM THE FIRST AND SECOND PARTS TO THE INTERFACE ARE:
     7       -5      -10        0      -11      -12
  INTERFACE CLEARANCES X,XDOT,Y,YDOT,Z,ZDOT
9.000        9.000        9.000        9.000        9.000        9.000

  INTERFACE NUMBER     21
  INTERFACE TYPE       3 BETWEEN PARTS     5 AND      7
  THE SPRING AND DASHPOT GROUP IS     3.  THE INTERFACE IS IN COORDINATE SYSTEM     1
  THE DISTANCES (X,Y,Z) FROM THE FIRST AND SECOND PARTS TO THE INTERFACE ARE:
   -13      -15       16       17       18       19
  INTERFACE CLEARANCES X,XDOT,Y,YDOT,Z,ZDOT
9.000        9.000        9.000        9.000        9.000        9.000

  INTERFACE NUMBER     22
  INTERFACE TYPE       3 BETWEEN PARTS     5 AND      8
  THE SPRING AND DASHPOT GROUP IS     3.  THE INTERFACE IS IN COORDINATE SYSTEM     1
  THE DISTANCES (X,Y,Z) FROM THE FIRST AND SECOND PARTS TO THE INTERFACE ARE:
    14      -15       16      -17       18       19
  INTERFACE CLEARANCES X,XDOT,Y,YDOT,Z,ZDOT
9.000        9.000        9.000        9.000        9.000        9.000

  INTERFACE NUMBER     23
  INTERFACE TYPE       3 BETWEEN PARTS     6 AND      7
  THE SPRING AND DASHPOT GROUP IS     3.  THE INTERFACE IS IN COORDINATE SYSTEM     1
  THE DISTANCES (X,Y,Z) FROM THE FIRST AND SECOND PARTS TO THE INTERFACE ARE:
   -14       15       16       17      -18       19
  INTERFACE CLEARANCES X,XDOT,Y,YDOT,Z,ZDOT
9.000        9.000        9.000        9.000        9.000        9.000

  INTERFACE NUMBER     24
  INTERFACE TYPE       3 BETWEEN PARTS     6 AND      8
  THE SPRING AND DASHPOT GROUP IS     3.  THE INTERFACE IS IN COORDINATE SYSTEM     1
  THE DISTANCES (X,Y,Z) FROM THE FIRST AND SECOND PARTS TO THE INTERFACE ARE:
    13       15       16      -17      -18       19
  INTERFACE CLEARANCES X,XDOT,Y,YDOT,Z,ZDOT
9.000        9.000        9.000        9.000        9.000        9.000

  INTERFACE NUMBER     25
  INTERFACE TYPE       3 BETWEEN PARTS     9 AND     10
  THE SPRING AND DASHPOT GROUP IS     4.  THE INTERFACE IS IN COORDINATE SYSTEM     1
  THE DISTANCES (X,Y,Z) FROM THE FIRST AND SECOND PARTS TO THE INTERFACE ARE:
     0        0        0        0       29      -35
  INTERFACE CLEARANCES X,XDOT,Y,YDOT,Z,ZDOT
9.000        9.000        9.000        9.000        9.000        9.000

  INTERFACE NUMBER     26
  INTERFACE TYPE       7 BETWEEN PARTS     7 AND      9
  THE SPRING AND DASHPOT GROUP IS     5.  THE INTERFACE IS IN COORDINATE SYSTEM     1
  THE SPECIAL AND/OR GOVERNING DIRECTION IS   2.
  THE DISTANCES (X,Y,Z) FROM THE FIRST AND SECOND PARTS TO THE INTERFACE ARE:
     0        0       21      -20        0      -22
  INTERFACE CLEARANCES X,XDOT,Y,YDOT,Z,ZDOT
9.000        2.000        .1000        9.000        9.000        9.000
```

```
  INTERFACE NUMBER     27
  INTERFACE TYPE      7 BETWEEN PARTS     8 AND      9
  THE SPRING AND DASHPOT GROUP IS     5.  THE INTERFACE IS IN COORDINATE SYSTEM     1
  THE SPECIAL AND/OR GOVERNING DIRECTION IS   2.
  THE DISTANCES (X,Y,Z) FROM THE FIRST AND SECOND PARTS TO THE INTERFACE ARE:
    0        0       21       20        0       -22
  INTERFACE CLEARANCES X,XDOT,Y,YDOT,Z,ZDOT
9.000       2.000       .1000       9.000       9.000       9.000

  INTERFACE NUMBER     28
  INTERFACE TYPE      5 BETWEEN PARTS     7 AND      9
  THE SPRING AND DASHPOT GROUP IS     6.  THE INTERFACE IS IN COORDINATE SYSTEM     1
  THE SPECIAL AND/OR GOVERNING DIRECTION IS   1.
  THE DISTANCES (X,Y,Z) FROM THE FIRST AND SECOND PARTS TO THE INTERFACE ARE:
   23        0       25       -24        0       -26
  INTERFACE CLEARANCES X,XDOT,Y,YDOT,Z,ZDOT
5.000E-02   9.000       5.000E-02   9.000       .1000       9.000

  INTERFACE NUMBER     29
  INTERFACE TYPE      5 BETWEEN PARTS     8 AND      9
  THE SPRING AND DASHPOT GROUP IS     6.  THE INTERFACE IS IN COORDINATE SYSTEM     1
  THE SPECIAL AND/OR GOVERNING DIRECTION IS   1.
  THE DISTANCES (X,Y,Z) FROM THE FIRST AND SECOND PARTS TO THE INTERFACE ARE:
  -23       0       25       24        0       -26
  INTERFACE CLEARANCES X,XDOT,Y,YDOT,Z,ZDOT
5.000E-02   9.000       5.000E-02   9.000       .1000       9.000

  INTERFACE NUMBER     30
  INTERFACE TYPE      3 BETWEEN PARTS     9 AND     10
  THE SPRING AND DASHPOT GROUP IS     7.  THE INTERFACE IS IN COORDINATE SYSTEM     1
  THE DISTANCES (X,Y,Z) FROM THE FIRST AND SECOND PARTS TO THE INTERFACE ARE:
  -27       0      -28      -27       29       -30
  INTERFACE CLEARANCES X,XDOT,Y,YDOT,Z,ZDOT
9.000       9.000       9.000       9.000       9.000       9.000

  INTERFACE NUMBER     31
  INTERFACE TYPE      3 BETWEEN PARTS     9 AND     10
  THE SPRING AND DASHPOT GROUP IS     7.  THE INTERFACE IS IN COORDINATE SYSTEM     1
  THE DISTANCES (X,Y,Z) FROM THE FIRST AND SECOND PARTS TO THE INTERFACE ARE:
   27       0      -28       27       29       -30
  INTERFACE CLEARANCES X,XDOT,Y,YDOT,Z,ZDOT
9.000       9.000       9.000       9.000       9.000       9.000

  INTERFACE NUMBER     32
  INTERFACE TYPE      3 BETWEEN PARTS     9 AND     10
  THE SPRING AND DASHPOT GROUP IS     8.  THE INTERFACE IS IN COORDINATE SYSTEM     1
  THE DISTANCES (X,Y,Z) FROM THE FIRST AND SECOND PARTS TO THE INTERFACE ARE:
  -31       0       32      -31       29       -33
  INTERFACE CLEARANCES X,XDOT,Y,YDOT,Z,ZDOT
1.000       9.000       9.000       9.000       6.478       9.000

  INTERFACE NUMBER     33
  INTERFACE TYPE      3 BETWEEN PARTS     9 AND     10
  THE SPRING AND DASHPOT GROUP IS     8.  THE INTERFACE IS IN COORDINATE SYSTEM     1
  THE DISTANCES (X,Y,Z) FROM THE FIRST AND SECOND PARTS TO THE INTERFACE ARE:
   31       0       32       31       29       -33
  INTERFACE CLEARANCES X,XDOT,Y,YDOT,Z,ZDOT
1.000       9.000       9.000       9.000       6.478       9.000

  INTERFACE NUMBER     34
  INTERFACE TYPE      3 BETWEEN PARTS     4 AND     10
  THE SPRING AND DASHPOT GROUP IS     8.  THE INTERFACE IS IN COORDINATE SYSTEM     1
  THE DISTANCES (X,Y,Z) FROM THE FIRST AND SECOND PARTS TO THE INTERFACE ARE:
  -31       0       34      -31      -29       -33
  INTERFACE CLEARANCES X,XDOT,Y,YDOT,Z,ZDOT
1.000       9.000       9.000       9.000       6.478       9.000

  INTERFACE NUMBER     35
  INTERFACE TYPE      3 BETWEEN PARTS     4 AND     10
  THE SPRING AND DASHPOT GROUP IS     8.  THE INTERFACE IS IN COORDINATE SYSTEM     1
  THE DISTANCES (X,Y,Z) FROM THE FIRST AND SECOND PARTS TO THE INTERFACE ARE:
   31       0       34       31      -29       -33
  INTERFACE CLEARANCES X,XDOT,Y,YDOT,Z,ZDOT
1.000       9.000       9.000       9.000       6.478       9.000
```

```
 MAXIMUM NUMBER OF SPRING/DASHPOT SETS
   8

  RATES FOR SPRING/DASHPOT SET NUMBER     1
5.000E 04   .0000       2.000E 05   .0000       .0000       .0000
5.000E 04   .0000       2.000E 05   .0000       .0000       .0000
200.0       .0000       800.0       .0000       .0000       .0000
200.0       .0000       800.0       .0000       .0000       .0000

  RATES FOR SPRING/DASHPOT SET NUMBER     2
2.000E 05   2.950E 05   1.600E 05   5.760E 06   7.400E 06   .0000
2.000E 05   2.950E 05   1.600E 05   5.760E 06   7.400E 06   .0000
170.0       375.0       815.0       7.300E 04   8.300E 05   .0000
170.0       375.0       215.0       7.300E 04   8.300E 05   .0000

  RATES FOR SPRING/DASHPOT SET NUMBER     3
650.0       650.0       7050.       .0000       .0000       .0000
650.0       650.0       7050.       .0000       .0000       .0000
10.00       10.00       27.00       .0000       .0000       .0000
10.00       10.00       27.00       .0000       .0000       .0000

  RATES FOR SPRING/DASHPOT SET NUMBER     4
.0000       .0000       .0000       .0000       .0000       .0000
.0000       .0000       .0000       .0000       .0000       .0000
.0000       .0000       .0000       .0000       .0000       .0000
.0000       .0000       .0000       .0000       .0000       .0000

  RATES FOR SPRING/DASHPOT SET NUMBER     5
.0000       2.000E 04   2.000E 05   .0000       .0000       .0000
.0000       .0000       2.000E 05   .0000       .0000       .0000
1000.       50.00       100.0       .0000       100.0       100.0
.0000       50.00       100.0       .0000       100.0       100.0

  RATES FOR SPRING/DASHPOT SET NUMBER     6
.0000       .0000       .0000       .0000       .0000       .0000
2.000E 05   5.000E 04   1.000E 05   .0000       .0000       .0000
57.00       57.00       57.00       .0000       .0000       .0000
57.00       57.00       57.00       .0000       .0000       .0000

  RATES FOR SPRING/DASHPOT SET NUMBER     7
.0000       2.500E 04   .0000       .0000       .0000       .0000
.0000       2.500E 04   .0000       .0000       .0000       .0000
.0000       100.0       .0000       .0000       .0000       .0000
.0000       100.0       .0000       .0000       .0000       .0000

  RATES FOR SPRING/DASHPOT SET NUMBER     8
1000.       .0000       2500.       .0000       .0000       .0000
1.000E 04   .0000       5.000E 04   .0000       .0000       .0000
94.00       .0000       100.0       .0000       .0000       .0000
194.0       .0000       300.0       .0000       .0000       .0000

  INTERFACES FOR REAL PART NUMBER     5
    1       7       13      14      17      18      21      22

  INTERFACES FOR REAL PART NUMBER     6
    2       8       15      16      19      20      23      24

  INTERFACES FOR REAL PART NUMBER     7
    3       9       17      19      21      23      26      28

  INTERFACES FOR REAL PART NUMBER     8
    4       10      18      20      22      24      27      29

  INTERFACES FOR REAL PART NUMBER     9
    5       11      25      26      27      28      29      30      31      32
   33

  INTERFACES FOR REAL PART NUMBER    10
    6       12      25      30      31      32      33      34      35
```

```
  MASSES AND MOMENTS OF INERTIA, ALL REAL PARTS
 10.57        10.57        10.57        4755.        4543.        1572.
 10.57        10.57        10.57        4755.        4543.        1572.
 3.781        3.781        3.781        5406.        2192.        3408.
 3.781        3.781        3.781        5406.        2192.        3408.
 4.283        4.283        4.283        4305.        5008.        800.0
 140.5        140.5        140.5        7.900E 06    2.900E 05    7.850E 06

  FLANGEWAY CLEARANCE IS  .360

  WHEEL/RAIL GEOMETRY DATA, SETS OF THREE
-.5000       -.5000        .0000       -.4000       -.1500        .0000
-.3600       -7.000E-02    .0000       -.3400       -5.000E-02    .0000
-.2000       -3.000E-02    .0000        .0000        .0000        2.000E-02
 .2000        3.000E-02    .1000        .3400        5.000E-02    .2400
 .3600        7.000E-02    .3200        .4000        .1500        .3200
 .5000        .5000        .3200

  CREEP COEFFICIENT DATA, SETS OF TWO
 .0000        .0000        2.000E-03    .2480        3.000E-03    .3330
 4.000E-03    .3960        5.000E-03    .4410        6.000E-03    .4710
 7.000E-03    .4880        8.000E-03    .4970        9.000E-03    .4990
 1.000E-02    .5000        2.000E-02    .5000        50.00        .5000

  DIMENSIONS
 29.50        4.980E-02    25.60        33.40        7.700        14.50
 19.10        26.90        37.30        .4470        45.00        2.000
 12.10        19.90        17.30        2.565        7.000        20.00
 1.000        23.00        7.572        4.500        16.75        6.250
 4.000        8.000        54.40        11.00        285.0        53.00
 44.50        17.70        29.60        45.88        42.00

  INITIAL CONDITIONS, ALL PARTS IN ALL DEGREES OF
  FREEDOM, POSITIONS ON FIRST LINE, VELOCITIES ON SECOND
 .0000        .0000        .0000        .0000        .0000        .0000
 .0000        704.0        .0000        .0000        .0000        .0000
 .0000        45.00        .0000        .0000        .0000        .0000
 .0000        .0000        .0000        .0000        .0000        .0000
 .0000       -45.00        .0000        .0000        .0000        .0000
 .0000        .0000        .0000        .0000        .0000        .0000
 .0000       -570.0        .0000        .0000        .0000        .0000
 .0000        .0000        .0000        .0000        .0000        .0000
-3.900        37.30        14.50        .0000        .0000        .0000
 .0000        .0000        .0000        .0000        .0000        .0000
 3.900       -37.30        14.50        .0000        .0000        .0000
 .0000        .0000        .0000        .0000        .0000        .0000
-23.00        .0000        16.00        .0000        .0000        .0000
 .0000        .0000        .0000        .0000        .0000        .0000
 23.00        .0000        16.00        .0000        .0000        .0000
 .0000        .0000        .0000        .0000        .0000        .0000
 .0000        .0000        28.00        .0000        .0000        .0000
 .0000        .0000        .0000        .0000        .0000        .0000
 .0000       -285.0        70.00        .0000        .0000        .0000
 .0000        .0000        .0000        .0000        .0000        .0000

  INITIAL ACCELERATIONS FOR ALL PARTS, SOME MAY BE RECALCULATED INTERNALLY
 .0000        .0000        .0000        .0000        .0000        .0000
 .0000        .0000        .0000        .0000        .0000        .0000
 .0000        .0000        .0000        .0000        .0000        .0000
 .0000        .0000        .0000        .0000        .0000        .0000
 .0000        .0000        .0000        .0000        .0000        .0000
 .0000        .0000        .0000        .0000        .0000        .0000
 .0000        .0000        .0000        .0000        .0000        .0000
 .0000        .0000        .0000        .0000        .0000        .0000
 .0000        .0000        .0000        .0000        .0000        .0000
 .0000        .0000        .0000        .0000        .0000        .0000
OUTPUT AT T =   .000     WITH DT =  2.00E-04
  LOWEST DT=  2.00E-04, HIGHEST DT=  2.00E-04, AVERAGE DT=  2.00E-04, AND DT STD DEV=   .000
Q(P,O,J)
  P=  1
```

APPENDIX C

DETAILS ON THE DESIGN AND USE OF INSTRUMENTED WHEELSETS AND CALIBRATION CHARACTERISTICS OF FORCE SENSING PATCO CAR WHEELSET AFTER RETRUEING AT WMATA

PATRICK L. BOYD

ENSCO, INC.

DETAILS ON THE DESIGN AND USE OF INSTRUMENTED WHEELSETS

Figure 3 is a block diagram of the instrumented wheelset system from the strain gage bridges to the continuous analog voltage output. The following material is a detailed account of the design considerations involved in instrumenting wheelsets. It is an exerpt from ENSCO's report to the Federal Railroad Administration concerning several wheelsets produced for the FRA, but since a major design goal was to identify a technique that could be used on any wheelplate shape and size, the instrumented wheels used on the WMATA car are very similar to those developed previously for high cant deficiency curving tests conducted by the FRA.

5. Current FRA Instrumented Wheelset Approach

The FRA instrumented wheelsets typify many facets of the state-of-the-art and may be used to illustrate specific design considerations in using wheels as force transducers. The basic objective of the design of force measuring wheels is to obtain adequate primary sensitivity for low signal/noise ratio and high resolution while controlling crosstalk, load point sensitivity, ripple, and the effects of heat, centrifugal force and longitudinal forces. The design philosophy was to choose strain gage bridge configurations which inherently minimized as many extraneous influences as possible and which were responsive to the general strain patterns expected in any rail wheel subjected to vertical and lateral forces. Such bridge configurations could be adapted to the standard production wheels of the desired test vehicles, eliminating problems of supply, mechanical compatibility, and possible alterations of vehicle behavior due to special wheels. The radial locations of the strain gages were optimized for each wheel size and shape while their angular locations were fixed by the chosen bridge configurations. Locomotive, passenger coach and freight car wheels having a large variation in tread diameter and wheelplate shape have been instrumented successfully using the same general procedures.

WHEELSET DATA FLOW

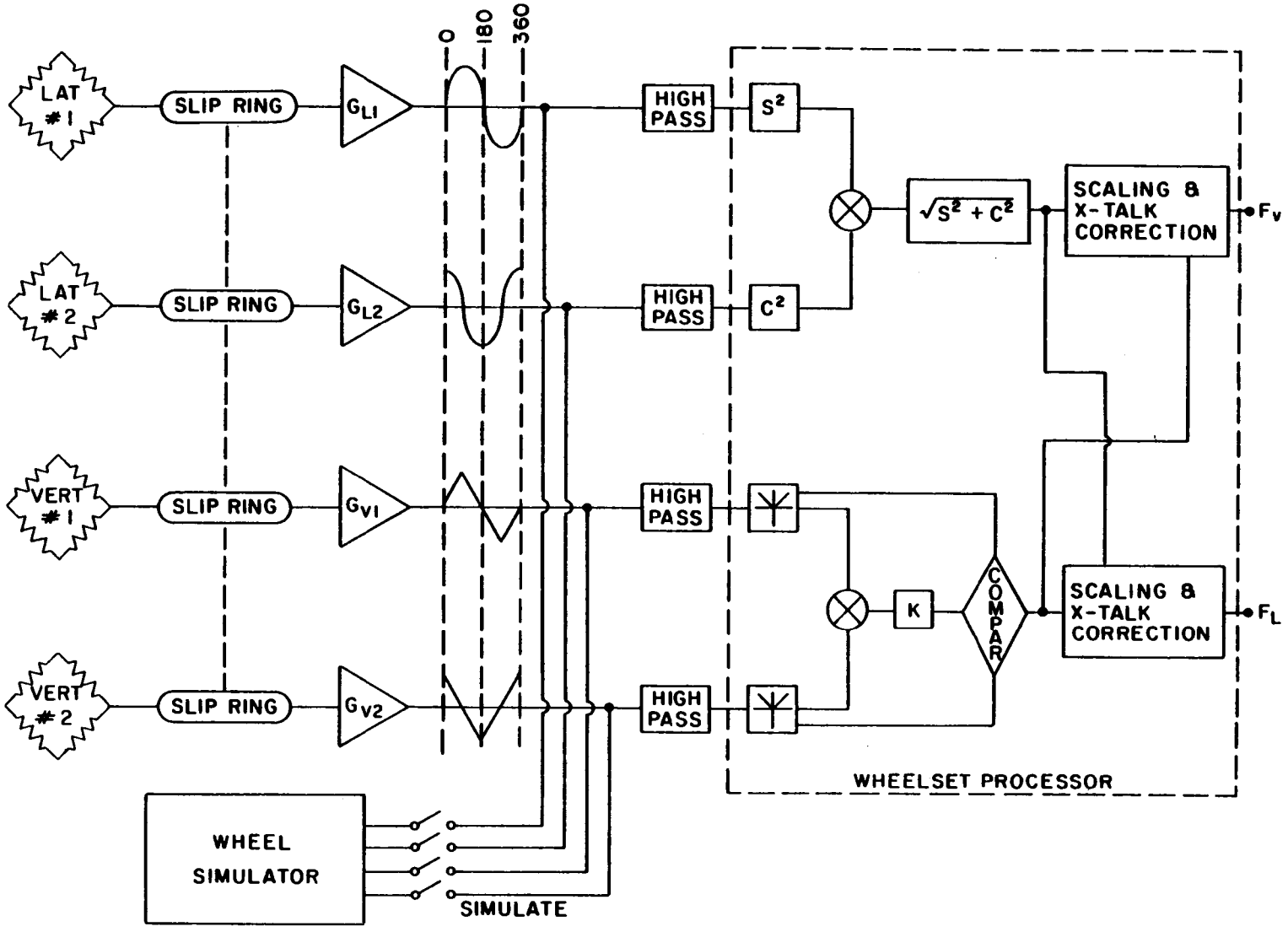

Figure 3

5.1 Description of Strain Gage Bridges

The vertical force measuring bridges follow a concept used by ASEA/SJ[1]. Each bridge consists of eight strain gages arranged in a wheatstone bridge having 2 gages per leg. Each leg of the bridge has one strain gage on the field side and one strain gage on the gage side of the wheel. The four legs are evenly spaced 90° apart on the wheel as shown in Figure 5.1.. The general strain distribution in a typical rail wheelplate due to a purely vertical load is characterized by maximum strains which are compressive and highly localized in the wheelplate above the point of rail contact. As the pair of gages in each leg of the bridge consecutively passes over the rail contact point, two negative and two positive peak bridge outputs occur per revolution. By correctly choosing the radial position of the gages, the bridge output as a function of rotational position of the wheel can be made to resemble a triangular waveform having two cycles per revolution. The purpose of having gages on both sides of the wheelplate in each leg is to cancel the effect of changes in the bending moments in the wheelplate due to lateral force and the change of axial tread/rail contact point.

When two triangular waveforms equal in amplitude and out of phase by one fourth the wavelength, are rectified and added, the sum is a constant equal to the peak amplitude of the individual waveforms. In order to generate a strain signal proportional to vertical force and independent of wheel rotational position, the outputs of two identical vertical bridges out of phase by 45° of wheel arc are rectified and summed as shown in Figure 5.2. Since the bridge outputs do not have the sharp peaks of true triangular waveforms, the sum of one bridge peak and one bridge null is lower than that of two concurrent intermediate bridge outputs. In order to reduce the ripple or variation in force channel output with wheel rotation, the bridge sum is scaled down between the dips coinciding with the rounded bridge peaks. By taking as the force channel output the greatest of either individual bridge output or the scaled down sum of both bridges, the scaling down is applied selectively to the part of the force channel output between the dips as shown in Figure 5.2.

VERTICAL FORCE MEASUREMENT BRIDGE

"A + B" TRIANGULAR OUTPUT (ASEA/SJ)

- TWO BRIDGES
- GAGES ON BOTH SIDES OF WHEELPLATE
- TRIANGULAR WAVEFORMS-2-CYCLES PER REVOLUTION
- OUTPUT = MAX $\{|A|, |B|, K(|A| + |B|)\}$

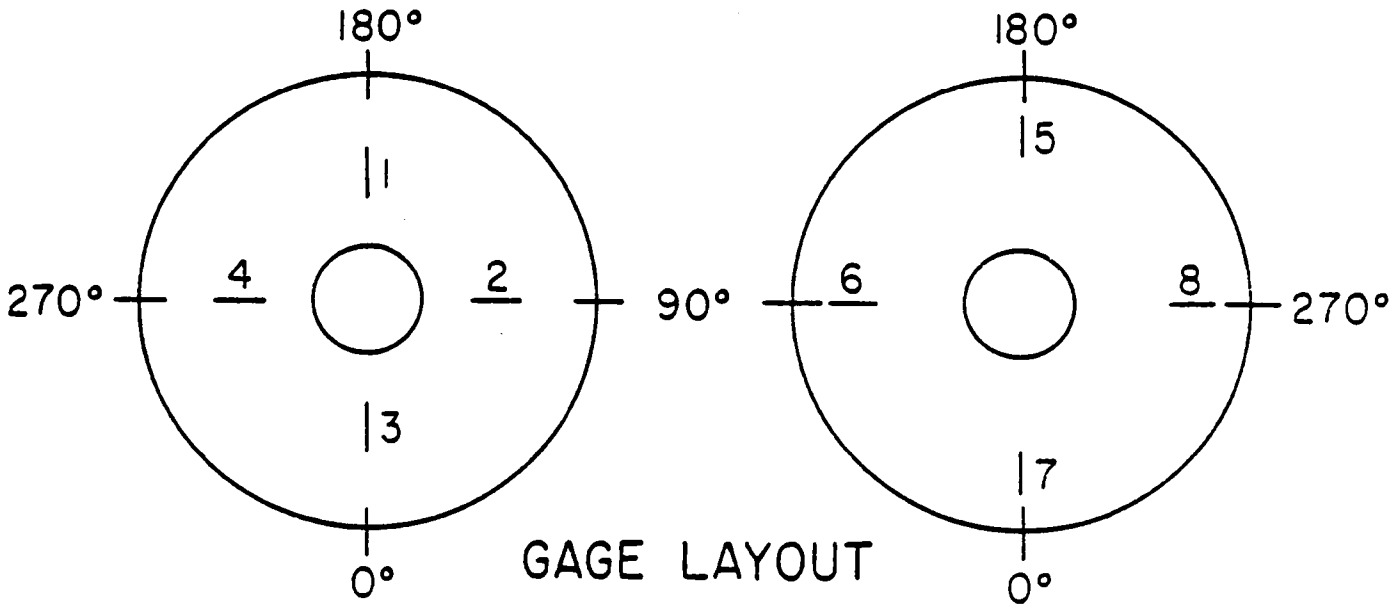

GAGE LAYOUT

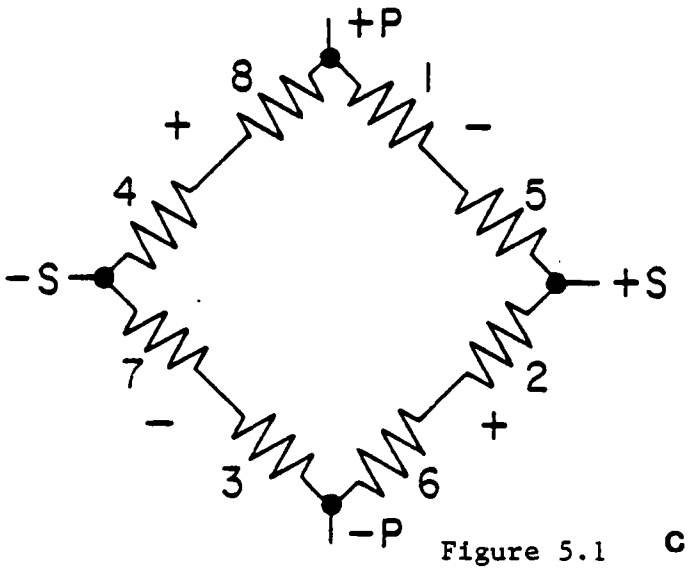

BRIDGE WIRING

Figure 5.1

TRIANGULAR OUTPUT AND "A + B" PROCESSING

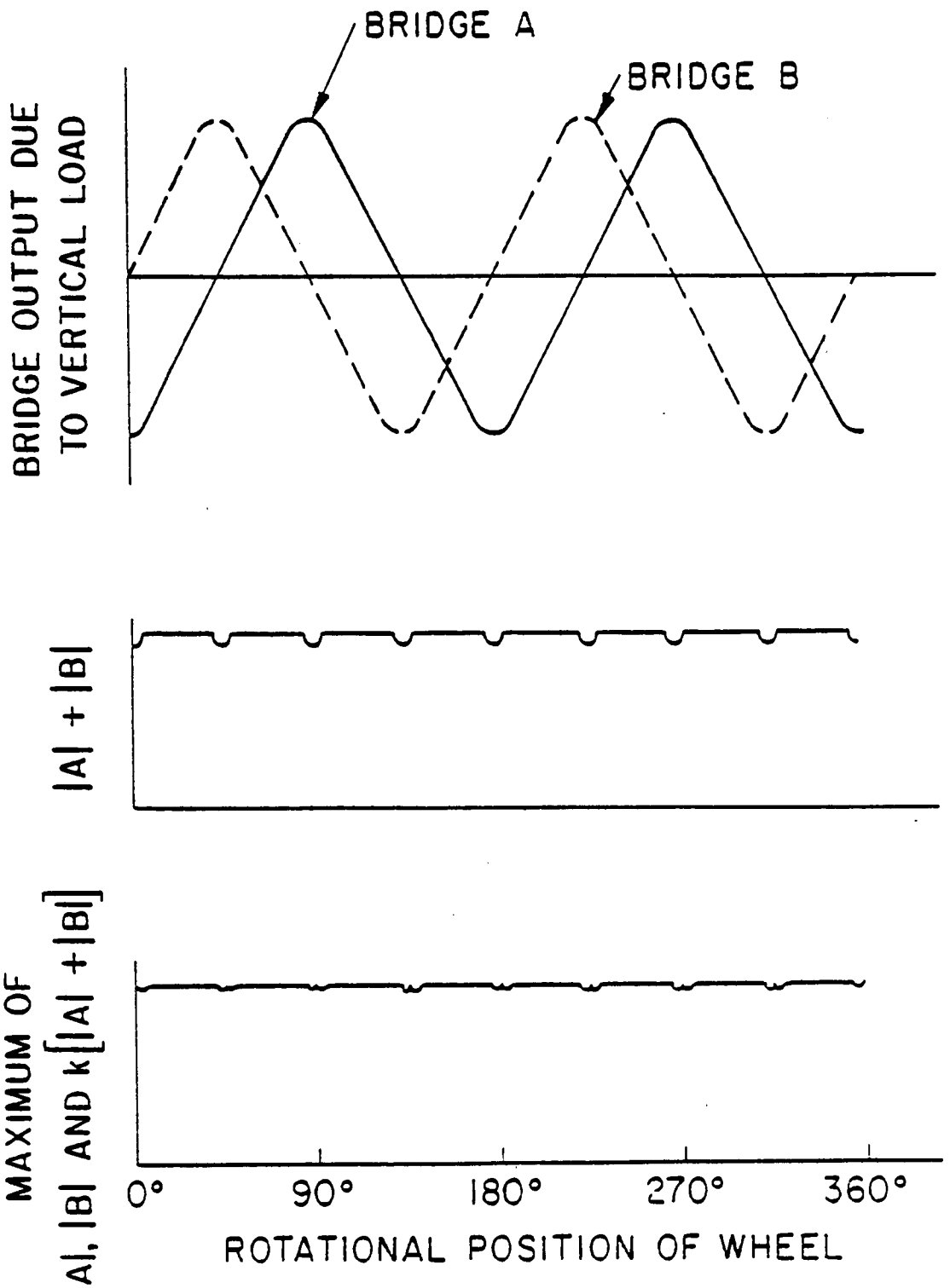

Figure 5.2 C-6

The general strain distribution of a typical rail wheelplate due to a purely lateral flange force is characterized by two components as shown in Figure 4.1. One component is a function of radius only because the wheelplate acts as a symmetric diaphram in opposing the lateral force at the axle. The second component results from the moment about the hub caused by the flange force and it tends to vary at a given radius with the cosine of the angular distance from the wheel/rail contact point. The strain distributions on the gage and field sides of the wheelplate are similar in magnitude but opposite in sign (compression or tension).

Lateral force measuring bridges which follow a concept advanced by EMD[2] take advantage of the general strain distribution in a standard rail wheelplate. As shown in Figure 5.3, each bridge is composed of eight gages evenly spaced around the field side of the wheelplate at the same radius. The first four adjacent gages are placed in legs of the bridge that cause a positive bridge output for tensile strain and the next four gages are placed in legs causing a negative bridge output for tensile strain. The resulting bridge cancels out the strain due to the axial load because all eight gages are at the same radius with four causing positive and four causing negative bridge outputs. However the bridge is very sensitive to the sinusoidal strain component associated with the hub moment due to the flange force because the tensile strains and the compressive strains above and below the axle are fully additive in bridge output twice each revolution (once as a positive peak and once as a negative peak). Radial gage locations may be chosen such that the bridge output varies sinusoidally with one cycle per wheel revolution. Two identical bridges 90° out of phase are used to obtain a force channel output independent of wheel rotational position as a consequence of the geometric identity: $\sqrt{(L\sin\theta)^2+(L\sin\{\theta+90^{\circ}\})^2} = |L|$ for any θ.

5.2 Primary Sensitivity and Crosstalk

The first step in the production of instrumented wheels is the machining of all wheels in a production group to an identical concour. The concour is dictated by the minimum allowable wheelplate thickness and by the production variation of the available sample of wheels. The machining contour is usually close to the original design shape but at the minimum

LATERAL FORCE STRAIN DISTRIBUTION

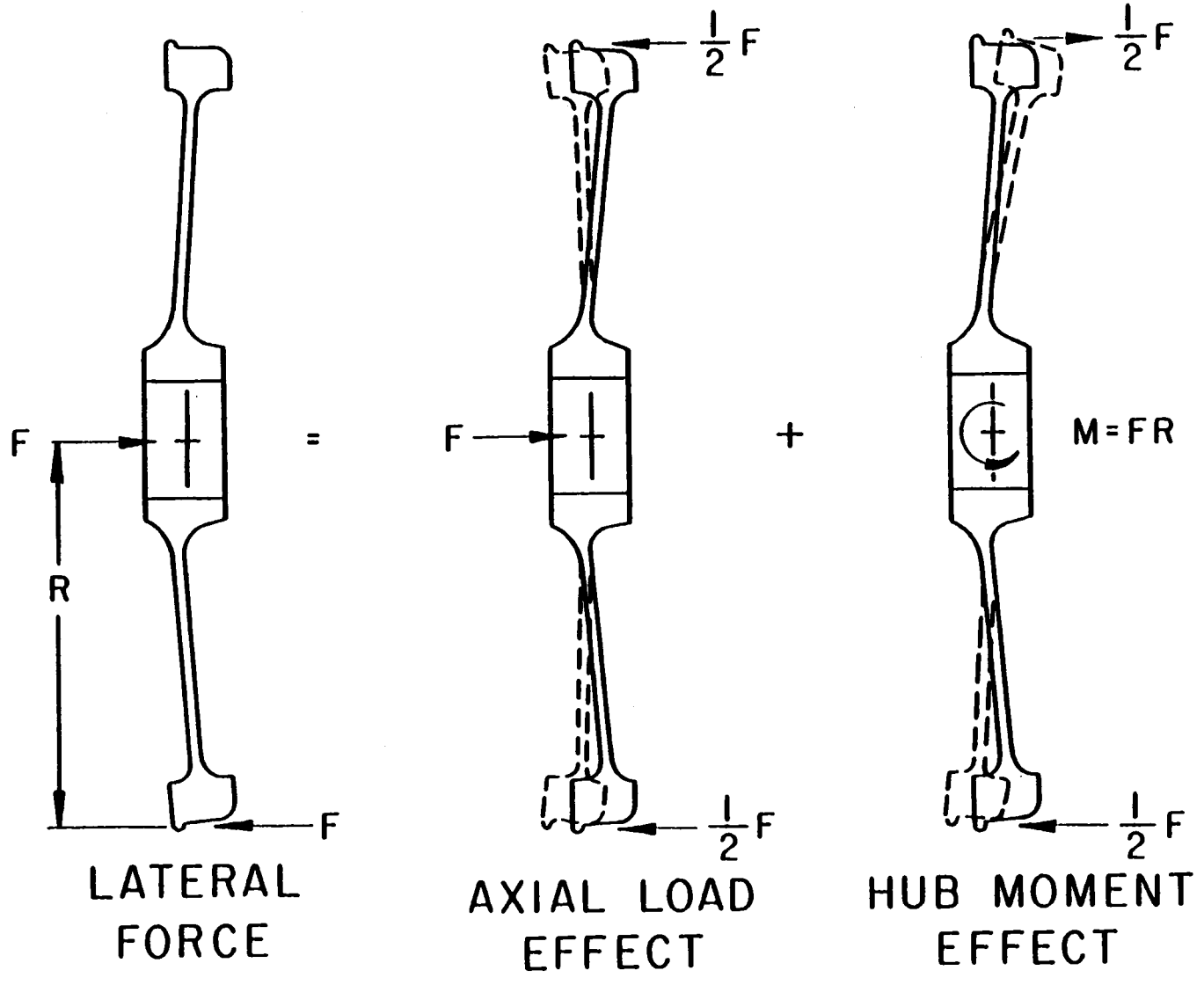

Figure 4.1

LATERAL FORCE MEASUREMENT BRIDGE

$\sqrt{\sin^2 + \cos^2}$ TECHNIQUE (EMD)

- TWO BRIDGES
- SINUSOIDAL OUTPUT
- 90° OUT OF-PHASE
- APPLIED AT SINGLE RADIUS TO ONE SIDE OF WHEELPLATE

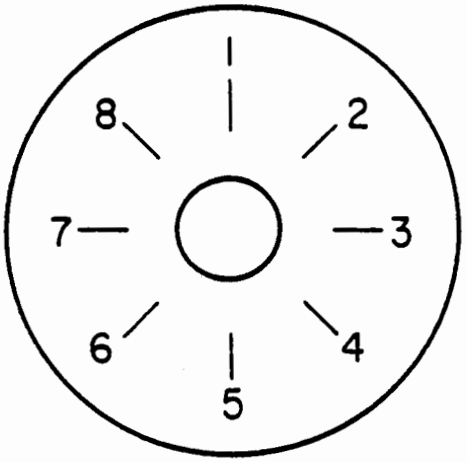

GAGE LAYOUT

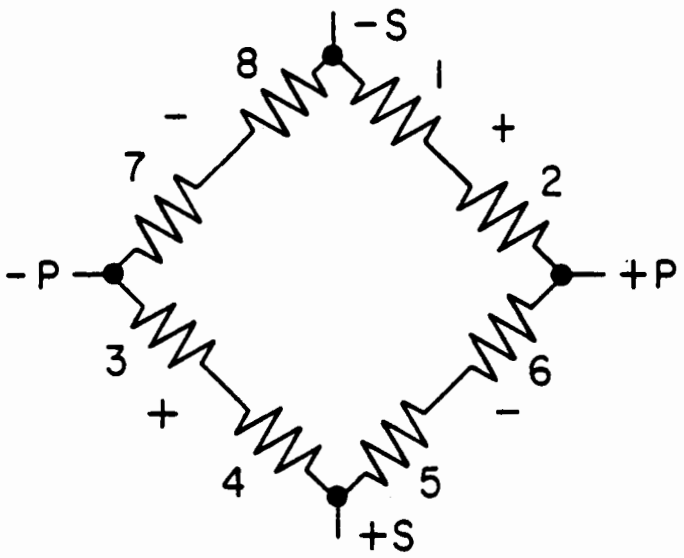

BRIDGE WIRING

Figure 5.3 C-9

thickness. The thinning of the wheelplate is the easiest step in maximizing sensitivity because it does not involve compromise with the other measurement properties of the wheel.

The most powerful tool in selecting the radial locations of the strain gages for the best compromise between primary sensitivity, crosstalk, ripple, and sensitivity to axial load point variation is a detailed empirical survey of the strains induced in the given wheelplate by the expected service loads. The use of wheels machined to an identical profile makes the empirical approach to wheelset instrumentation practical because the results of the strain survey may be applied to all wheels in the group. The calibration loads and the reference lateral position of the wheel on the rail should reflect the type of experiment in which the wheels will be used.

For example, wheels destined to measure high speed curving forces should be loaded to about 1 1/2 times the nominal vertical wheel load (to simulate load transfer) with the rail adjacent to the flange to determine the primary vertical sensitivity. Primary lateral sensitivity should be determined from a high lateral load (corresponding to expected L/V ratios) applied with a device which bears against the gage sides of two wheels on an axle at the tread radius and spreads them apart. Loads applied in this manner create strains of equal magnitude and opposite sign to those produced by the hub moment effect of a flange load but they eliminate the extraneous effect of the vertical load hub moment (treated as crosstalk) from the determination of primary lateral sensitivity. A combined vertical and lateral loading at the expected service L/V ratio level accomplished by forcing the wheelset laterally against a rail while maintaining a vertical load is necessary to select strain gage locations for minimal crosstalk. Vertical loadings at several points across the tread should be taken to evaluate the sensitivity to axial load point.

In the strain survey conducted on the FRA wheels strain gages were applied at intervals of one inch or less on both field and gages sides of the wheelplate along two radial lines separated by 180° of wheel arc. The calibration loads were repeated at every 15° of wheel arc until the strain along

twenty-four equally spaced radial lines on both gage and field side was mapped for each load. This data was used in a computer program to predict the output of a force channel as a function of the radial locations of the gages in the companion bridges.

The vertical force measuring bridges of the FRA wheels have strain gages on both sides of the wheelplate. The simulation program allows the rapid trail of many combinations of gage and field side radii as potential strain gage locations. The maximum sensitivity possible for a purely vertical load on a given wheel of a bridge actually producing the triangular waveform is rapidly revealed. The "triangularity" of the waveform of a candidate bridge can be tested by adding its output at each angular load position to that at a load position advanced by 45^{o} of wheel arc. This test determines the ripple expected of a force channel composed of two out of phase candidate bridges.

A lateral force effects the vertical bridge both by directly changing the strain pattern in the wheelplate and by moving the point of vertical load contact with the rail toward the flange. By using as a measure of crosstalk the difference in bridge output caused by adding a lateral load to an existing vertical load, correction factors may be chosen which compensate for net lateral force crosstalk which includes direct lateral force crosstalk and the effect of vertical load point movement. It is desirable to identify vertical bridges in which the direct lateral force crosstalk and the effect of load point change are opposed and yield a minimum net crosstalk for flange forces in service. The accuracy of the highly loaded flanged wheel is enhanced using a correction factor in processing based on the net lateral force crosstalk. Compromises in bridge selection are usually biased in favor of the flanged wheel because it generates the most vital data for vehicle dynamics or rail wear studies.

The primary sensitivities and crosstalk factors achieved for several types of wheels are shown in Figure 5.4. The vertical bridges were chosen from a detailed simulation with radial position increments of 0.1 inch on a basis of maximum primary sensitivity while holding the simulated crosstalk and

TYPICAL WHEELSET CALIBRATION CONSTANTS

WHEEL DESCRIPTION	VERTICAL FORCE MEASUREMENT			LATERAL FORCE MEASUREMENT	
	SENSITIVITY	K	NET LATERAL FORCE CROSSTALK	SENSITIVITY	VERTICAL FORCE CROSSTALK
30" TREAD DIA., CONCAVE CONICAL WHEEL PLATE, 3/4" MIN. THICKNESS	$6 \frac{\mu\epsilon}{kip}$	.94	2%	$18 \frac{\mu\epsilon}{kip}$	1 1/2%
33" TREAD DIA., CONCAVE CURVED WHEEL PLATE, 3/4" MIN. THICKNESS	$5\ 1/2 \frac{\mu\epsilon}{kip}$	.94	4%	$16\ 1/2 \frac{\mu\epsilon}{kip}$	3%
36" TREAD DIA., CONVEX CONICAL WHEEL PLATE, 3/4" MIN. THICKNESS	$4\ 1/4 \frac{\mu\epsilon}{kip}$	.94	5%	$17 \frac{\mu\epsilon}{kip}$	4%
40" TREAD DIA., CONCAVE CONICAL WHEEL PLATE, 1" MIN. THICKNESS	$3\ 1/2 \frac{\mu\epsilon}{kip}$	.92	1 1/2%	$33 \frac{\mu\epsilon}{kip}$	1/2 %

Figure 5.4

ripple below 5% and minimizing sensitivity to axial load point. The primary sensitivity was observed to be linear within about 1% because the strains at each gage are low and the wheelplate behaves elastically. Primary vertical force sensitivity appears to be inversely proportional to tread diameter and wheelplate thickness across several wheelplate shapes.

The lateral force measuring bridges of the FRA wheels have gages on only one side of the wheelplate and the trial simulation of bridges is used to determine the most advantagous side of the wheel and radial gage position. The primary sensitivity was determined from pure lateral loads applied with a spreader bar. The absolute value difference in lateral force indication between a combined vertical and lateral load on a rail and the pure lateral load with the spreader bar at the same lateral load is attributed to vertical force crosstalk. This method of crosstalk determination takes into account the vertical load point at the L/V ratios of interest. While a correction factor based on the vertical force crosstalk perfectly compensates a lateral force at the optimized L/V ratio, it is usually still accurate to about 2% of the lower lateral force at one-half the optimized L/V ratio.

The measurement of low lateral forces requires special considerations. Since the lateral force is computed from the sum of the squares of two bridge outputs all measurements have a positive sign. The convenient determination of the direction of a lateral creep force requires a wheel rotational position sensor. (It can also be accomplished by careful examination of the sinusoidal output of a single bridge.) It is possible that a purely vertical load can cause a lateral bridge output having a sign opposite to that caused by lateral force, but the crosstalk would appear positive because of squaring. The first increment of lateral load would cause a reduction rather than an increase in the output of such a bridge and bridge strains at low lateral forces would not be unique to a particular force. Although this would be of little concern in an experiment to measure high L/V ratios, low force measurements are vital in rail wear experiments. The sign of the vertical crosstalk as well as its magnitude must be considered in the design of wheels to measure low lateral forces.

Figure 5.4 gives the primary sensitivity and vertical force crosstalk actually achieved for several types of wheels. Lateral force measuring bridges of maximum sensitivity having less than 2% crosstalk and 5% ripple were sought in a simulation of possible bridges. Vertical load point sensitivity is not a great factor because the range of load points is narrow while lateral flange forces are being measured. The sensitivity of the sinusoidal lateral bridge is much greater than that of the triangular vertical bridges. Wheels of larger tread diameter in general produce greater sensitivity.

5.3 Ripple

Ripple is caused by the failure of the bridges to produce the desired waveform and by deviation from the correct phase relationship between the companion bridges which are processed together as a force channel.

The wheelplates are machined for uniformity to reduce ripple and a grid of radial and circumferential lines is scribed on the wheelplate to aid accurate gage placement. The massive computer aided simulation of trial bridges was used to determine gage locations of minimum inherent ripple. The ripple of the vertical force channel is reduced by attenuating the high bridge sums occuring between the rounded bridge peaks as shown in Figure 5.2. This method achieves a substantial reduction in ripple at a small cost in average sensitivity.

The lateral bridge output is inherently very sinusoidal. The requirement for two bridges at the same radius out of phase by 90° is in conflict with the 45° spacing between the gages in each bridge because both bridges should occupy the same space. Placing the gages side by side causes a deviation from the proper phase relationship which manifests itself as ripple. Figure 5.5 gives the maximum ripple for each set of four wheels of four types. Larger wheels which have less phase deviation between lateral bridges also have less ripple. Combined loads caused greater ripple for both vertical and lateral channels because crosstalk produced distortions of the waveforms.

TYPICAL UNCORRECTED VARIABILITY

WHEEL DESCRIPTION	VERTICAL FORCE MEASUREMENT			LATERAL FORCE MEASUREMENT		
	SENSITIVITY TO AXIAL LOAD POINT	MAX. RIPPLE VERTICAL LOAD	MAX. RIPPLE COMBINED LOAD	SENSITIVITY TO AXIAL LOAD POINT	MAX. RIPPLE	MAX. RIPPLE COMBINED LOAD
30" TREAD DIA., CONCAVE CONICAL WHEEL PLATE, 3/4" MIN. THICKNESS	$+5.7\frac{\%}{inch}$	±5 %	±8 %	$-2.4\frac{\%}{inch}$	±7 %	±7 %
33" TREAD DIA., CONCAVE CURVED WHEEL PLATE, 3/4" MIN. THICKNESS	$+9.5\frac{\%}{inch}$	±6 %	±6 %	$-1\frac{\%}{inch}$	±6 %	±7.5 %
36" TREAD DIA., CONVEX CONICAL WHEEL PLATE, 3/4" MIN. THICKNESS	$-4.8\frac{\%}{inch}$	±7 %	±10 %	$-3.2\frac{\%}{inch}$	±4 %	±6 %
40" TREAD DIA., CONCAVE CONICAL WHEEL PLATE, 1" MIN. THICKNESS	$+4.7\frac{\%}{inch}$	±5 %	±5 %	$-3\frac{\%}{inch}$	±4 %	±4 %

Figure 5.5

Ripple does not create as much error as might be supposed. Even the peak wheel forces measured during vehicle dynamics testing are averaged for 50 to 100 milliseconds. A 36 inch wheel makes a full revolution in 100 milliseconds at 64 mph, totally negating ripple in a 100 millisecond average wheel force. A single instantaneous measurement is rarely sought and any filtering has a mitigating influence on ripple.

5.4 Load Point Sensitivity

A comparison of load point sensitivity between vertical and lateral bridges in Figure 5.5 indicates that the effect on vertical bridges in greater than expected of simply the change in hub movement due to a load point change. The failure of the tread to transmit the moment due to load point offset uniformly into the wheelplate probably results in unusual changes to the local intense compressive strains in the wheelplate above the rail contact to which the vertical bridge is most sensitive. The high load point sensitivity of the 33 inch freight wheel which had the thinnest tread supports this hypothesis.

The effect of load point sensitivity on measurements taken with the FRA wheels was minimized in two ways. Taking as the load point for primary vertical sensitivity the wheel flange adjacent the rail, causes the heavier loaded high rail wheel to deviate little from the calibrated load point. The additional movement of load point toward the flange under heavy lateral loading was accounted for in the net lateral force crosstalk correction factor. The lesser effect of vertical load point variation on lateral force was also accounted for in its crosstalk correction factor. The residual effect of load point variation is that load transfer from low rail wheel to high rail wheel in high cant deficiency curving is over estimated by about 5% because the low rail wheel is loaded at a less sensitive point on the tread.

5.5 Thermal and Centrifugal Effects and Other Sources of Drift

The vertical and lateral bridges used on the FRA wheelsets are particularly immune to drift by virtue of strain gage location and instrumentation technique. Strains induced by thermal change and centrifugal force are radially symmetric on each side of the wheelplate. The lateral bridge consists

of eight gages at the same radius on the same side of the wheelplate positioned in the bridge so that four add and four subtract. A radially symmetric strain field is cancelled by the additions and subtractions. Similarly, the vertical bridges have four gages at the same radius on each side of the wheelplate. On each side two gages add and two subtract.

Each bridge generates a triangular or sinusoidal waveform as the wheel rotates under load. High pass filtering of the amplified bridge signals at .2 Hz does not attenuate the oscillating part of the signal but it forces the signal to oscillate about zero. High pass filtering eliminates gradual drift that could occur from thermal effects on the wheelset wiring and wheel to amplifier cabling and zero drift of the strain gage bridge amplifiers. It would also suppress thermal and centrifugal effects in bridges which do not self cancel them.

5.6 Sensitivity to Longitudinal Force

Longitudinal forces involved in braking and driving are extraneous influences on the vertical and lateral force measurement bridges. Brakes on instrumented wheelsets are usually disabled to avoid damage by overheating or flatspotting, but instrumented wheelsets on self propelled vehicles must cope with driving forces. Figure 5.6 shows the strain distribution in a driven wheel. The longitudinal force may be resolved into a torque about the axle and a horizontal force perpendicular to the axle. The similarity between this horizontal force component and the vertical force suggests an error source.

The vertical force measuring bridges on the fRA wheelsets are configured in such a way as to cancel the effect of longitudinal forces. Figure 5.6 shows the strain components at four gages positions on one side of the wheelplate due to vertical and driving forces. The bridge is shown in the vertical null output position. Gages at 180° spacing add together in their contribution to the bridge summation. The vertical, horizontal and shear components of strain are opposite in sense for gages spaced 180° apart and cancel each other out retaining the null bridge output. The longitudinal force does not create an intense local strain aligned with the sensitive

LONGITUDINAL FORCE STRAIN DISTRIBUTION

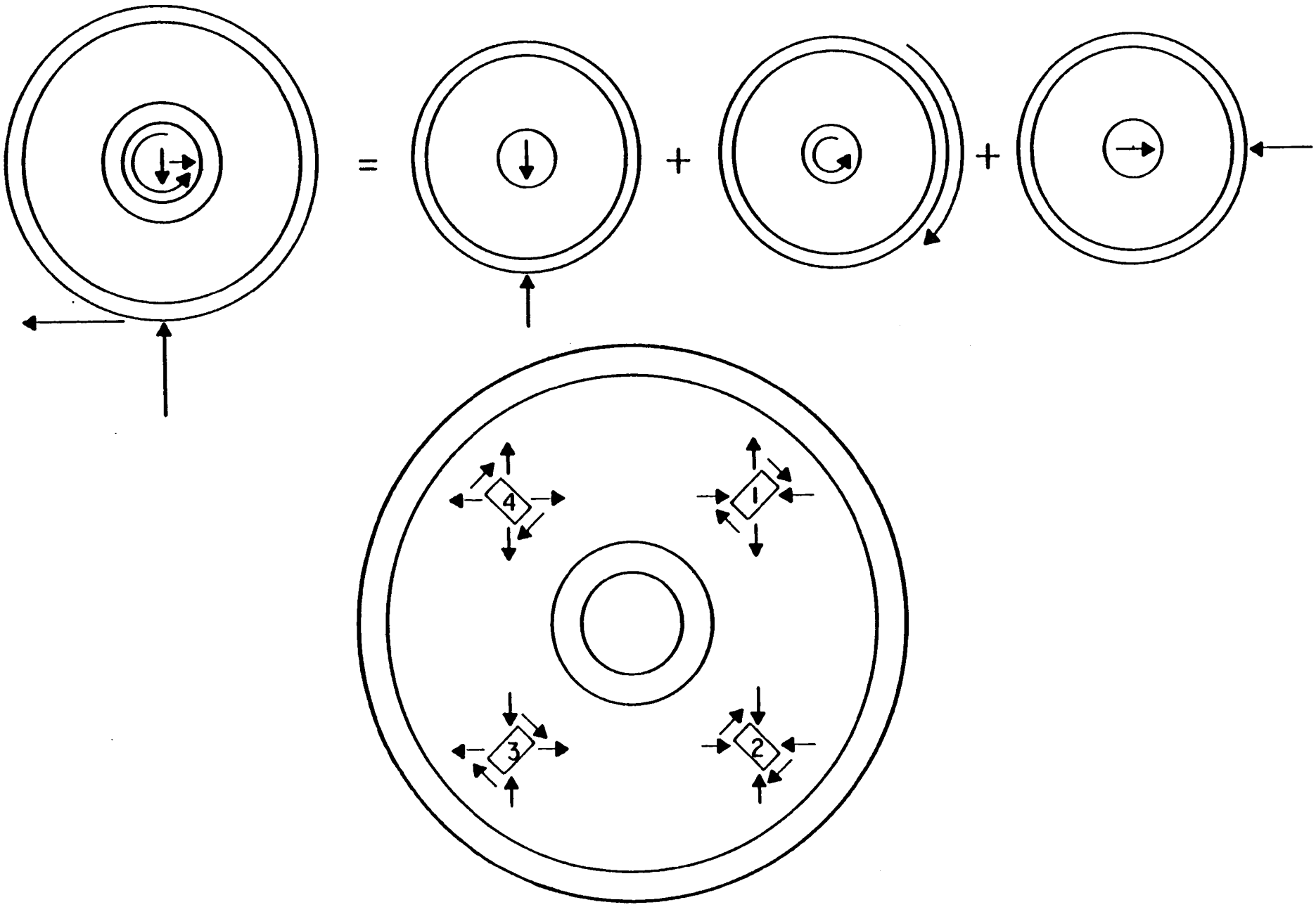

Figure 5.6

axis of a strain gage which stimulates the vertical bridge in any rotational position. The insensitivity of the vertical bridges to longitudinal force has also been verified experimentally.

The lateral bridges used on the FRA wheelset are also insensitive to longitudinal forces. The symmetric gage pattern limits the effect of the shear strains and the horizontal force has the effect of adding vectorially to the vertical force to produce crosstalk. Since the longitudinal force is limited by friction to about 1/4 the vertical load, the vector sum of forces is only about 3% higher than the vertical force alone. An increase in crosstalk of 3% of 4% or 0.12% is insignificant.

If the measurement of driving force is desired, torque sensing bridges can be added to the axle between each wheel and the drive gear.

CALIBRATION CHARACTERISTICS OF FORCE SENSING PATCO CAR WHEELSET AFTER RETRUEING AT WMATA

NOMENCLATURE

Wheel 1 is the gear side wheel. It is on the left side when the axle is leading.

Dimension d is the distance from the inside of the wheel flange to the gage side of the rail. It is about 1.25 inches when the flange is directly adjacent to the rail and greater when the flange is away from the rail.

Calibration loads are given in kips, with the vertical load first. For example 15-05 is a 15,000 lb vertical load with a 5,000 lb lateral load applied simultaneously.

Vertical channel outputs are normalized by the output at 15-00, d = 1.25. The vertical sensitivity is defined at the 15-00, d = 1.25 load.

The lateral sensitivity is defined by the difference between the lateral outputs at 15-10 and 15-00, d = 1.25 divided by 10 kips. The lateral outputs are normalized by the difference between the 15-10 and 15-00 lateral outputs.

The crosstalk reported in the following summary is the basis for the correction algorithm used by the real time processor. The strip chart recordings are free of crosstalk effect.

The following relationships are used in the determination of wheel forces from the measurement of wheel bridge strains.

where:

V_a = Strain measured by vertical bridge A

V_b = Strain measured by vertical bridge B

L_a = Strain measured by lateral bridge A

L_b = Strain measured by lateral bridge B

K = Scale factor to reduce vertical channel ripple

V = Vertical channel strain output

L = Lateral channel strain output

G_v = Average vertical channel (or bridge) sensitivity in με/kip units from (15-00) loading

G_l = Average lateral channel (or bridge) sensitivity in με/kip units from difference between the (15-10) and (15-00) loadings.

H_v = Increase in vertical force measurements as a ratio of applied lateral force (positive lat. force crosstalk)

H_l = Increase in lateral force measurements as a ratio of applied vertical force (positive vert. force crosstalk)

F_v = Vertical force indication uncorrected for lateral force crosstalk

F_v' = Vertical force indication corrected for lateral force crosstalk

F_l = Lateral force indication uncorrected for vertical force crosstalk

F_l' = Lateral force indication corrected for vertical force crosstalk

1. Vertical Channel Processing

$$K = \frac{(\text{minimum } |V_a| \text{ or } |V_b|) + (\text{maximum } |V_a| \text{ or } |V_b|)}{2\ (\text{maximum } |V_a| \text{ or } |V_b|)}$$

$$V = \text{Greatest of} \begin{matrix} |V_a| \\ |V_b| \\ K(|V_a| + |V_b|) \end{matrix}$$

2. Lateral Channel Processing

$$L = \sqrt{L_a^2 + L_b^2}$$

3. Sensitivity Determination

$$G_v = \frac{\text{V avg of all rotational positions}}{\text{15 kips}}$$

for (15-00) loading with flange adjacent to rail (d=1.25)

$$G_l = \frac{\text{L avg of all rotational positions for (15-10) loading minus (15-00) loading}}{\text{10 kips}}$$

4. Crosstalk Correction Factors

$$H_v = \frac{\text{V avg (15-10) loading - V avg (15-00) loading}}{G_v \times \text{10 kips}}$$

$$H_l = \frac{\text{L avg (15-00) loading}}{G_L \times \text{15 kip}}$$

5. Vertical Force Determination

$$F_v = \left(\frac{1}{G_v}\right) V$$

$$F_v' = \left(\frac{1}{G_v}\right) V - (H_v) F_l'$$

6. Lateral Force Determination

$$F_l = \left(\frac{1}{G_l}\right) L$$

$$F_l' = \left(\frac{1}{G_l}\right) L - (H_l) F_v'$$

Tables 1A and 2A summarize the calibration characteristics.

Tables 1A-1 to 1A-9 and 2A-1 to 2A-9 give the raw bridge calibration data along with the uncorrected channel outputs.

TABLE 1A

SUMMARY OF CHARACTERISTICS
PATCO WHEEL #1 (Gear Side)
(After Retrueing at WMATA)

Load		Vertical Output, με		Lateral Output, με	
15-00	d=1.25	89.94	(1.000)	142.7	(.227)
15-00	d=1.50	93.99	(1.046)	116.0	(.185)
15-00	d=1.75	95.82	(1.066)	99.5	(.158)
15-00	d=2.00	95.96	(1.068)	126.0	(.200)
15-00	d=2.25	97.98	(1.091)	70.5	(.112)
15-01		91.78	(1.021)	202.9	(.323)
15-02		93.00	(1.035)	264.7	(.421)
15-05		97.50	(1.085)	453.7	(.722)
15-10		104.50	(1.163)	771.3	(1.227)

$$G_V = \frac{89.84\,\mu\varepsilon}{15\ \text{kip}} = 5.99\ \mu\varepsilon/\text{kip}$$

$$H_V = \frac{104.5 - 89.84}{5.99 \times 10} = 24.5\%$$

$$\text{Vertical Force Load Point Variation} = \frac{1.091 - 1.000}{1\ \text{inch}} = 9.1\%/\text{inch}$$

$$G_L = \frac{771.3 - 142.7}{10} = 62.9\ \mu\varepsilon/\text{kip}$$

$$H_L = \frac{142.7}{62.9 \times 15} = 15.1\%$$

$$\text{Lateral Force Load Point Variation} = \frac{(.112 - .227)\ 10}{1\ \text{inch} \times 15} = \frac{-7.7\%\ \text{of Vertical Force}}{\text{inch}}$$

TABLE 2A
SUMMARY OF CHARACTERISTICS
PATCO WHEEL #2
(After Retrueing at WMATA)

Load		Vertical Output, με		Lateral Output, με	
15-00	d=1.25	90.4	(1.000)	138.1	(.22)
15-00	d=1.50	92.8	(1.027)	125.2	(.20)
15-00	d=1.75	95.8	(1.060)	105.8	(.17)
15-00	d=2.00	97.9	(1.084)	104.6	(.16)
15-00	d=2.25	98.6	(1.092)	90.4	(.14)
15-01		94.6	(1.025)	199.6	(.314)
15-02		93.2	(1.042)	261.7	(.412)
15-05		98.9	(1.095)	447.6	(.705)
15-10		105.7	(1.169)	773.0	(1.22)

$$G_V = \frac{90.4\ \mu\varepsilon}{15\ \text{kip}} = 6.03\ \mu\varepsilon/\text{kip}$$

$$H_V = \frac{105.7 - 90.4}{6.03 \times 10} = 25.3\%$$

$$\text{Vertical Force Load Point Variation} = \frac{1.092 - 1.000}{1\ \text{inch}} = 9.2\%/\text{inch}$$

$$G_L = \frac{773.0\ \mu\varepsilon - 138.1\ \mu\varepsilon}{10\ \text{kip}} = 63.5\ \ /\text{kip}$$

$$H_L = \frac{138.1}{63.5 \times 15} = 14.5\%$$

$$\text{Lateral Force Load Point Variation} = \frac{(.14 - .22)10}{1\ \text{inch} \times 15} = \frac{-5.3\%\ \text{of Vertical Force}}{\text{inch}}$$